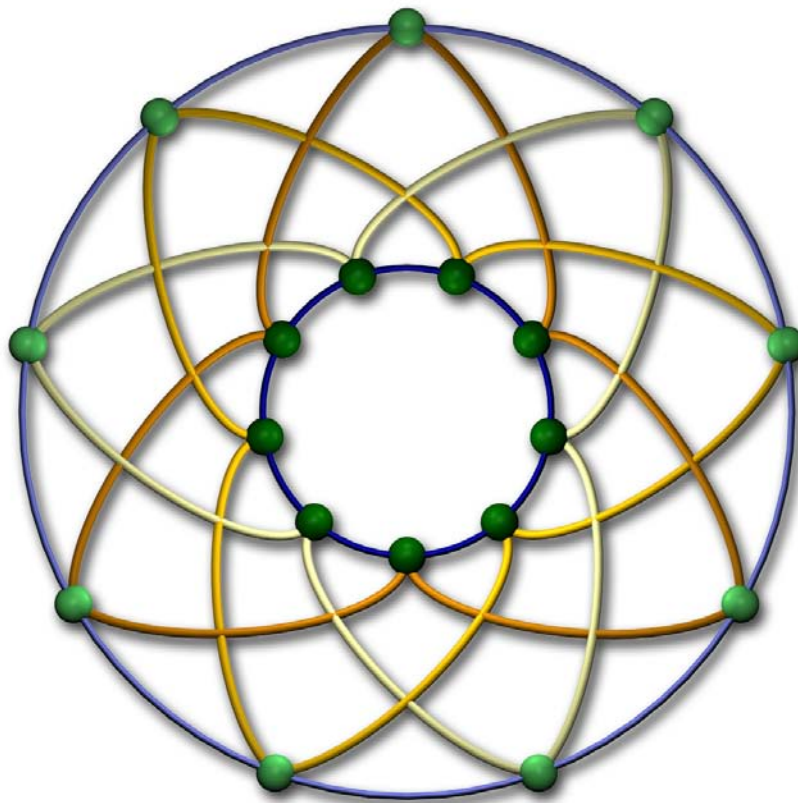


Development of Models to Implement low Dimensional Structures in Correlated Electronic Systems

Dissertation
zur Erlangung des Doktorgrades
der Mathematisch-Naturwissenschaftlichen Fakultät
der Universität Augsburg



vorgelegt von
Dipl. Phys. Christian Hackenberger
Augsburg
November 2006

Datum der Prüfung: 18 Dezember 2006

Erstgutachter: Prof. Thilo Kopp

Zweitgutachter: Prof. Ulrich Eckern

Drittgutachter: Prof. Roland Hayn (Université de Aix-Marseille III)

Viertgutachter: Prof. Raymond Frésard (ENSICAEN, Caen)

Acknowledgments

One famous part of a thesis is the page where one has to assure that the thesis was his or her work alone. In the juristic sense that is of course true for most thesis but in a less strict sense it is far from the reality. A work like this thesis is never the product of only one person's work. I had a lot of help in the process of writing this Ph. D. thesis. And I will gladly take the opportunity to say "thank you".

First and foremost I want to thank my wife Niki. Without her help this thesis would never have been possible. In the last weeks she was my connection to the real world, helping me not to get lost in the realms of physics. Without her I would definitely have starved to death before chapter three.

A special thanks goes to our lovely daughter Anna. She is a constant source of happiness. Whenever I felt She was always able to make me smile, even when I didn't feel like smiling.

This work wouldn't have been possible without my supervisors Thilo Kopp and Raymond Frésard. Thank you for all your help, for the discussions both about physics and the rest. I learned a lot from you. Thank you for all the administrative hassle you both had to take in order to make this joint theses happen.

I also want to thank Volker Eyert and Udo Schwingenschlögel for the many fruitful discussions about the physics of $\text{Ca}_3\text{Co}_2\text{O}_6$ and its brothers and sisters.

I had the great privilege to stay three month during my Ph. D. at the institute Crismat in Caen. I want to thank Bernard Raveau and Charles Simon, that they gave me the opportunity to work at their institute and take advantage of their profound knowledge of the $\text{Ca}_3\text{Co}_2\text{O}_6$ business.

When I have to deal with latex there are three sources of help that I can get. There are of course the books, the good ones and the not so good ones, there is the internet and if nothing else can help, there is German "the guy who knows the answers". Thanks for your help German.

A very special thanks goes to all of my colleagues at Experimentalphysik VI. It is a pleasure to work with you. It has been said many times, but it's true, the friendly atmosphere at this chair is a great gift.

Finally I want to thank Prof. Mannhart for his courage to "embed" theorists in his chair, for his support over all the years and for his infectious enthusiasm about physics and technology.

Contents

1	Introduction	7
1.1	Materials Properties and Technological Progress	7
1.2	A Very Special Compound – $\text{Ca}_3\text{Co}_2\text{O}_6$	10
2	A Closer Look at $\text{Ca}_3\text{Co}_2\text{O}_6$	15
2.1	Crystal Structure	15
2.2	Physical Properties	17
2.3	Theoretical Findings	24
3	High Order Perturbation Theory	29
3.1	Perturbative Treatment of Degenerate States in Second and Third Order	29
3.2	Nearly Degenerate States	31
3.3	Degeneracy in Fourth Order and Above	32
4	Magnetic Models	37
4.1	Superexchange	38
4.2	Hopping via Orthogonal Orbitals	42
4.3	Ring Exchange	44
5	Matrix Elements of the Coulomb Potential	47
5.1	Evaluation of the Matrix Elements	48
5.2	The Racah Parameters	50
6	Magnetic Chains	53
6.1	Coordinate Systems and Notation	53
6.2	Anisotropic Spin Chains – Models	56
6.3	Anisotropic Spin Chains – Results	58
6.4	Interacting Chains	62
7	Microscopic Ferromagnetic Coupling	71

Contents

7.1	Perturbative Treatment	71
7.2	Determination of the Parameter Space	73
7.3	Results for the Effective Coupling	73
8	Summary and Outlook	77
	Bibliography	81

“And one day it will be possible, by exploiting the power of nature, to create instruments of navigation by which ships will proceed unico homine regente, and far more rapid than those propelled by sails or oars; and there will be self-propelled wagons ‘and flying apparatuses of such form that a man seated in them, by turning a device, can flap artificial wings, ad modum avis volantis.’ And tiny machines will lift huge weights and vehicles will allow travel on the bottom of the sea.”

Umberto Eco, *The Name of the Rose*

1 Introduction

1.1 Materials Properties and Technological Progress

In the last 50 years, life in western countries changed dramatically. It took less than a generation to turn our lives digital. There is hardly any business left, that doesn't use computers in some way. There is no science anymore without computers. Nearly everyone owns a computer personally and works on one in his or her job. Professions with long traditions like type-setting lost their importance because of the new possibilities that came with the computers. The invention of computer games brought the new machines into our childrens playrooms. Teenagers and students all over the world spend their spare time in new social networks like myspace, which are built in the artificial parallel universe called world wide web.

Looking back only 60 years, none of these developments were to be foreseen. The state of the art computer was the ENIAC which came to life in 1946 and started the computing revolution in science [1]. But ENIAC was of course nothing modern people would consider a computer. It was 30 m long, occupied an area of 167 m², weighed 27 t, and consumed 150 kW of power. This enormous dimensions and energy hunger was in large parts due to the more than 17.000 vacuum tubes ENIAC was made of [2,3]. A computer like this would never have become a mainstream device. The invention that changed everything in this field was the development of the point contact transistor by Bardeen, Brattain and Schockley in December of 1947 [4]. These new transistors and their successors eventually replaced all the vacuum tubes in computers. This was the initial step to the still ongoing miniaturization in the electronic business and the beginning of the digital age.

Bardeen and Brattain used germanium to realize the first transistor. The understanding of the physical properties of germanium and other semiconductors was the prerequisite for building this impressive device. The ingenious application of materials properties made it possible to fabricate a tiny little novel device that eventually changed the lives of billions of people.

1 Introduction

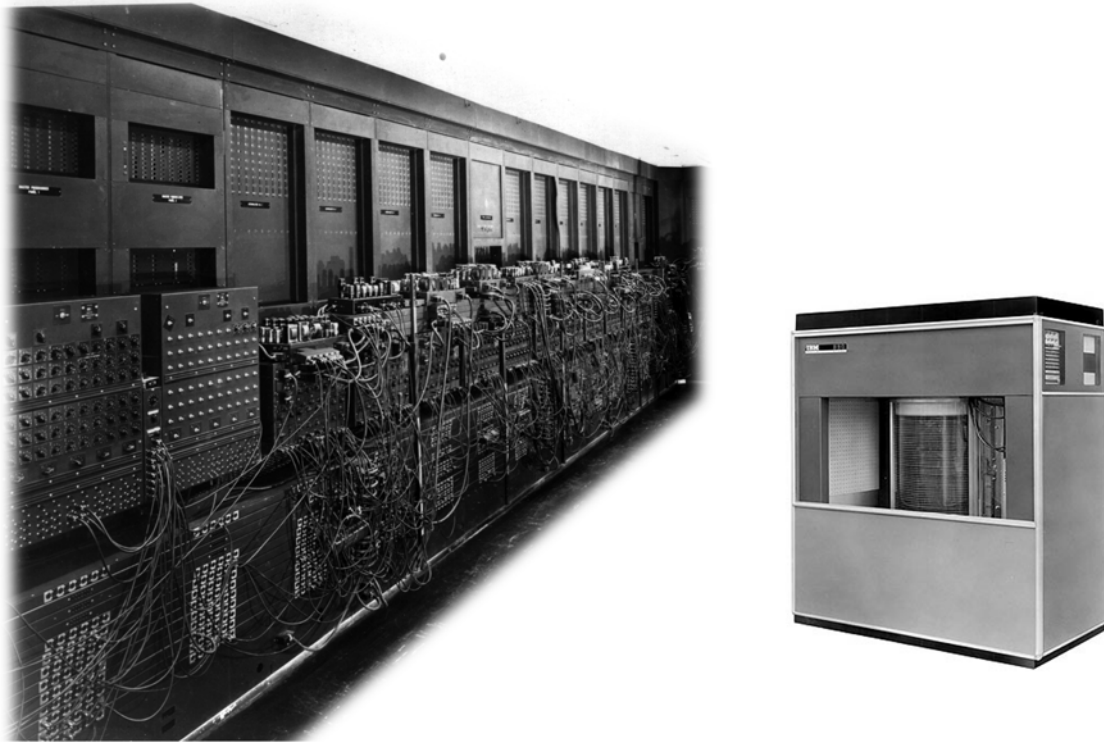


Fig. 1.1: On the left is depicted a photograph of the ENIAC (or parts of it), a high performance computer of 1946 using vacuum tube technology. With a weight of 27 tons an area of 167 m^2 and a power consumption of 150 kW it is not the kind of machine we are used to nowadays. On the right an image of the first commercially available hard drive of 1956, the IBM 350, which had about the size of a closet and was able to store 5 MB of data.

One of the most amazing facts about the digital revolution is the almost unbelievable rate of progress. Over decades the silicon based technology has followed the famous Moore's law [5]. In the original version of 1965 it made a forecast for the next ten years and predicted a doubling of the "complexity" of chips about every 24 month (without specifying what "complexity" means in this context). But Moore's law is still valid and in today's version it expects that modern chips double the number of transistors every 18 month, even faster than the original prediction. The truth might be somewhere in between, but nevertheless it is very impressive that it was possible to more or less follow an exponential law over four decades. And this kind of long term exponential growth is not restricted to microchips.

The information density of magnetic hard drives is another field that has seen enormous growth rates over the years. The first commercially available hard drive was introduced in 1956. It was called the IBM 350 and was introduced as part of a new vacuum tube based computer, the 305 RAMAC. The IBM 350 was about the size of a closet, weighed a ton, had a power consumption of 12 kW, and a capacity of 5 MB [6]. The areal bit density was about 0.002 Mb/in.^2 [7]. Of course there were many issues to be solved to get to nowadays hard drives. But one of the most important fields of innovation was the usage of new materials, which suits the engineering needs. The constant progress that was made with new materials

allowed in 1981 for hard disks with areal bit densities higher than 12 Mb/in.^2 [7], in 2000 we were already at densities of about 10^4 Mb/in.^2 [8] and the latest offerings of the industry work with densities around 10^5 Mb/in.^2 [9]. In the same time the price for hard disk memory dropped immensely. While it was not even possible to buy the IBM 350 (one could only have it leased for 3.500 dollars per month), in 1980 one could buy a megabyte of hard disk storage for about 200 dollars. The same amount of storage was sold for 1 cent in 2000 [8] and today we buy hard disk storage at rates of about 40 cents per gigabyte. This fantastic progress over the years makes it now possible to build amazing, very small mobile devices which hold ten thousands of songs or pictures or several complete movies, to watch or listen to on the go.

By scaling down the dimensions of the area that defines a bit, it is unavoidable that the magnetic signal of one bit is becoming smaller. One needs a read head that is as sensitive to spatial changes in the magnetic field of the medium as possible. Beginning with the IBM 350, until 1994 inductive pick-up read heads were used in hard drives. This technique worked fine all the years but would not operate cost effective beyond several hundreds of Mb/in.^2 . The need for a new read head technology was solved by using the anisotropic magneto-resistance effect (AMR) [10]. In materials that exploit the AMR effect one finds that the difference between the resistivity along the applied magnetic field and perpendicular to the magnetic field changes with the absolute value of the field. In permalloy, which used to be the material of choice in hard drives, this change is about 4% at room temperature [11, 12] and can be used to electrically detect magnetic fields. In 1988 a giant magneto resistance effect (GMR) was found in multilayers of magnetic and nonmagnetic metals. In the original work a drop of 50% in resistivity is reported [13]. With this huge resistivity changes these materials are of course promising candidates for hard disk read heads. And indeed, modern read heads are made of multilayered GMR materials. Equally high magneto resistance effects are found in manganites and other perovskite related materials [14] which have an intrinsically layered structure. To distinguish these materials from the GMR superlattice materials, they are called colossal magneto resistance (CMR) materials. Of course CMR materials would also be good candidates for future hard disk read heads.

The development of high performance silicon based electronics and the amazing growth of storage density on magnetic storage devices are only two examples of the enormous technological influence of materials properties. From these two examples it becomes clear that modern technological development is driven by the creation, investigation, and understanding of new materials and the exploration of their properties. This is of course nothing new, every technology, even the most primitive, is based on the special properties of certain materials, e.g., wood, stone, metals, or glass. But today we have the tools and the knowledge to explore a much broader range of compounds than ever before. With every newly found and understood material the space for future, yet unknown applications is becoming richer and more promising.

1.2 A Very Special Compound – $\text{Ca}_3\text{Co}_2\text{O}_6$

Although first synthesized already in 1969 [15], $\text{Ca}_3\text{Co}_2\text{O}_6$ was not investigated further at that time. Since it became obvious in the 1980's that some perovskite materials show extraordinary physical properties, this class of oxides has been in the center of physical and chemical interest. With this revival of the perovskites, $\text{Ca}_3\text{Co}_2\text{O}_6$ was rediscovered in 1996 by Fjellvåg and Aasland [16,17], 27 years after its first appearance in literature.

$\text{Ca}_3\text{Co}_2\text{O}_6$ is a hexagonal perovskite oxide, it is a member of a family of compounds with the same or similar structure. A large number of members of this family have been experimentally investigated [18], but the most investigated compound is $\text{Ca}_3\text{Co}_2\text{O}_6$. The interest in this compound is due to its unusual magnetic and electric properties and spans the range from basic research to actual applications.

From the point of view of basic research the most striking feature of $\text{Ca}_3\text{Co}_2\text{O}_6$ is its highly complex magnetic response. The magnetic susceptibility above about 150 K is that of a ferromagnet with a Curie temperature of 28 to 80 K, depending on the experiment. This simple Curie picture breaks down at low temperatures. At around 24 K the susceptibility shows a steep increase pointing to a ferromagnetic transition [19]. Together with other experimental results and the fact that $\text{Ca}_3\text{Co}_2\text{O}_6$ is built of Co- O_3 chains on a hexagonal lattice (see chapter 2), this points to the formation of ferromagnetically ordered chains. Assuming the validity of the results of Mermin and Wagner [20] and Bruno [21] in this case, there cannot be long range ferromagnetic order at finite temperatures along the chains. Nevertheless experimental data clearly state the existence of long range order around 24 K, which is then only possible if we include correlations between the chains. Measurements suggest that the corresponding interactions are rather of the antiferromagnetic type [17]. In this temperature range the magnetic properties of $\text{Ca}_3\text{Co}_2\text{O}_6$ seem to be controlled by a close competition of ferromagnetic interactions along the chains and weaker antiferromagnetic interactions between the chains.

Cooling down to temperatures below 10 to 12 K reveals another phase transition into a short range ordered state with several properties of conventional spin glasses. But again $\text{Ca}_3\text{Co}_2\text{O}_6$ does not perfectly match this picture as an unusually strong frequency dependence of the ac-susceptibility has been observed. In this temperature regime the field dependence of the magnetization also changes drastically. Above 12 K there exists a very pronounced step in the magnetization with a height of about $\frac{1}{3}$ of the saturation magnetization without any hysteresis. Going to lower temperatures more and more steps in the magnetization curve are observable and a hysteresis starts to be visible, becoming more and more distinct with lower temperatures. The magnetic response is very anisotropic and generally higher along the chains. This anisotropy is also observed in the resistivity data. The resistance is, by a factor of 10^4 , higher perpendicular to the chains than along the chains. The temperature dependence of the resistance is that of an insulator but the absolute value of the resistance is not very high, especially along the chains.

The large number of experimental results make this compound also very attractive for theoretical investigations, particularly because some of the results appear to be ambiguous and lack theoretical interpretation. Although the experimental data are not always conclusive many properties of $\text{Ca}_3\text{Co}_2\text{O}_6$ seem to be settled:

- The crystal structure is built by Co-O chains on a triangular two dimensional lattice.
- The chains are made of alternating, face sharing trigonal prisms and octahedra of oxygen atoms with a Co atom in their centers.
- The Ca atoms are found to have no significant influence on the system but act mainly as spacers between the chains.
- Both Co atoms are in the oxidation state 3+. The Co atom centered in the octahedron is in a low spin configuration with a total spin of 0. The other Co atom is in a high spin configuration with a total spin of 2.
- The magnetic moments on the high spin Co atoms couple ferromagnetically along the chain.
- Between the chains an antiferromagnetic coupling is present. It is weaker than the ferromagnetic intrachain coupling.
- The magnetic and the electric response is highly anisotropic.
- The system is a Mott insulator.
- Below 24 K the field dependence of the magnetization shows steps. Between 24 K and about 12 K only a step at $\frac{1}{3}$ of the saturation magnetization is observed. Below this temperature range more steps are visible, the lower the temperature the more steps can be resolved. Below 12 K the steps are accompanied by a hysteresis.
- The spin relaxation time below 12 K is very slow but becomes faster at magnetic fields in the vicinity of the magnetization steps.

The above list is far from being complete. A much more detailed look into the known properties of $\text{Ca}_3\text{Co}_2\text{O}_6$ can be found in chapter 2. Nonetheless the presented facts about $\text{Ca}_3\text{Co}_2\text{O}_6$ already raise some very interesting theoretical questions:

How can the steps in the magnetization be explained?

Two very different attempts have already been made to resolve this issue, both making severe simplification and exploring the problem from opposite limiting cases. One approach considers the system as a two-dimensional triangular lattice of antiferromagnetically coupled Ising spins, emphasizing the frustration effects on a triangular lattice. This formulation assumes, that the ferromagnetic coupling along the chains is much stronger than the antiferromagnetic coupling between the chains [22]. The other approach starts with uncoupled anisotropic magnetic moments and explains the magnetization steps with quantum tunneling of the magnetization [23] in analogy to the situation in molecular magnets [24, 25]. If this latter interpretation is correct, it would make $\text{Ca}_3\text{Co}_2\text{O}_6$ the first known realization of this physics on the microscopic scale. Both ideas shown above are based on strong approx-

imations, but the complexity of the compound might demand more realistic models. This immediately leads to the next question.

How would an approximate Heisenberg or Ising Hamiltonian, which describes the low energy physics of the system, look like?

Of course we know that an isotropic Hamiltonian would not be appropriate. Nevertheless, it is not clear what kind of anisotropic Hamiltonian would be the right choice. Most of the arguments found in literature are in favor of a perfect Ising anisotropy. But the validity of this assumption is a matter of ongoing discussion.

What is the origin of the ferromagnetic intrachain coupling?

Ferromagnetism is an extraordinary phenomenon. Materials showing spontaneous magnetization have been known for more than 2500 years. Despite its long history this phenomenon has withstood a thorough understanding for more than two millennia. Only with the advent of modern physics at the beginning of the last century the understanding of ferromagnetism made a major leap forward. The reason why ferromagnetism was so hard to conceive is that the modern physical theories are essential for an understanding. It is a relativistic, quantum mechanical, many-body phenomenon. Even nowadays ferromagnetism has not lost its fascination, as it is still not completely understood. That is because ferromagnetic behavior is ruled by an interplay of the Coulomb interaction of the electrons and the Pauli principle, as was already pointed out by Heisenberg in 1928 [26]. So electron correlations are at the heart of ferromagnetism, making it a topic of interest in current research. One of the simplest models including electron-electron interactions is the Hubbard model [27]. This model is indeed able to explain ferromagnetism under certain conditions, both in metals [28–30] and insulators [31–33]. The assumption of a sufficiently strong on-site interaction U leads to the formation of an insulating phase, that otherwise could not be understood. Such insulators are denoted as Mott insulators. How this transition occurs is the topic of many theoretical works in solid state physics (several excellent reviews on Mott insulators are available [34–37]). Recent investigation extends the scope of the abstract one band Hubbard model towards real systems [38–40]. In the case of insulating materials like $\text{Ca}_3\text{Co}_2\text{O}_6$ there are only a few situations known that lead to ferromagnetic coupling. The most prominent of these situations is described by one of the so called Goodenough-Kanamori-Anderson (GKA) rules. Using these rules in the case of $\text{Ca}_3\text{Co}_2\text{O}_6$ predicts antiferromagnetic coupling along the chain, which is in disagreement with the experimental results. As the electronic configuration in $\text{Ca}_3\text{Co}_2\text{O}_6$ is much more complicated than assumed in the formulation of the GKA rules a deeper investigation is needed to understand this issue.

From a theoretical perspective, as is visible from the above considerations, $\text{Ca}_3\text{Co}_2\text{O}_6$ is a very fruitful and possibly unique field of research. But it is even more than that, some of its properties make it a potentially useful compound for certain applications. As discussed in section 1.1 a very interesting material property is the dependence of the resistance on the magnetic field. A strong dependence of the conductivity on the magnetic field could be used to build a sensitive electrical sensor for magnetic fields, which is, for example, needed as read

heads in hard drives. Several perovskite oxides, e.g., some manganites [41] are known to show an extremely strong variation of the resistance with an applied magnetic field. $\text{Ca}_3\text{Co}_2\text{O}_6$ shows a similar behavior at low temperatures. At about 2 K the resistivity drops nearly 80% at a field of 20 T [42, 43]. $\text{Ca}_3\text{Co}_2\text{O}_6$ could therefore be used to build special low temperature magnetic field sensors.

Another promising area of application for $\text{Ca}_3\text{Co}_2\text{O}_6$ is the transformation of thermal into electrical energy. A crucial topic for the future development of our societies is the production and use of energy. As nowadays energy generation is primarily based on finite resources it is obvious that sooner or later these resources will be exhausted. A way to save energy is to use the present resources as effectively as possible. A lot of energy is used to drive combustion engines, most prominent examples are of course the millions or even billions of cars on our streets. One idea to make better use of the burned fuel in a car engine is to use the temperature difference of the hot exhaust fumes and the colder environment. A device that could be used to meet this goal has to fulfill some preconditions. It has to transfer heat into an easily storable or usable energy form, most preferably electricity, and it has to do it as efficiently as possible. It must be able to operate at relatively high temperatures. And of course it has to be cheaply producible in a mass production process. The state of the art thermoelectric materials like Bi_2Te_3 cannot be used under these circumstances, because they are neither stable nor efficient at the operating temperatures in an exhaust pipe. $\text{Ca}_3\text{Co}_2\text{O}_6$ on the other hand is a very promising candidate for this kind of application. It is stable in air up to more than 1300 K [15] and most importantly has a high Seebeck coefficient combined with a low thermal- and a high electric conductivity [44–47]. These three physical values namely the Seebeck coefficient S , the thermal conductivity κ and the electrical resistivity ρ are combined to a key figure $Z = S^2/\rho\kappa$, called the figure of merit, which characterizes the efficiency of the transformation of heat into electric energy. This figure of merit, already high for $\text{Ca}_3\text{Co}_2\text{O}_6$, can even be enlarged by doping with rare earth atoms [48].

The main concern of the present thesis is to clarify some of the theoretical questions, that are yet unanswered for $\text{Ca}_3\text{Co}_2\text{O}_6$. In chapter 2 we review the current knowledge of the compounds properties. Our particular interest is in explaining the ferromagnetic coupling between the cobalt moments along the chains. In order to investigate this issue we performed a perturbation calculation up to fifth order. Technically there are two major challenges in this calculation. One is the sheer amount of possible perturbation paths in the rigorous treatment. A reduction of the complexity can be achieved by utilizing the symmetry of the problem. Another technical issue is the treatment of degenerate or nearly degenerate states in higher order of perturbation theory. This question will be discussed in detail in section 3. The high order is necessary to include both the superexchange terms in fourth order and cyclic terms, that are evolving in the fifth order. The basic ideas behind superexchange and cyclic exchange are examined in chapter 4. In order to investigate the puzzling magnetic properties of $\text{Ca}_3\text{Co}_2\text{O}_6$ we developed several effective models. The definition of the models and a analysis of the corresponding physical properties is given in chapter 6. The perturbative analysis of the microscopic ferromagnetic interaction is presented in chapter 7.

“A normal family down here has as much as fifty tablets of land.”

“How much is a tablet?”

“Four square trabucchi, of course.”

“Square trabucchi? How much are they?”

“Thirty-six square feet is a square trabuccho. Or, if you prefer, eight hundred linear trabucchi make a Piedmont mile.”

Umberto Eco, *The Name of the Rose*

2 A Closer Look at $\text{Ca}_3\text{Co}_2\text{O}_6$

In order to provide a starting point for the investigation of the oxides of trivalent Co, Woermann and Muan synthesized in 1969 two stable phases of CaO – CoO. These two phases are $\text{Ca}_3\text{Co}_2\text{O}_6$ and $\text{Ca}_3\text{Co}_4\text{O}_9$, which are stable in air up to 1026 °C and 926 °C respectively [15]. Since Bednorz and Müller found high temperature superconductivity in the perovskite compound $\text{BaLa}_4\text{Cu}_3\text{O}_{5(3-y)}$ in 1986 [49], a big effort has been made in the physical and chemical community to investigate perovskites and perovskite related compounds. On the basis of these efforts Fjellvåg and Aasland again investigated the hexagonal perovskite oxide $\text{Ca}_3\text{Co}_2\text{O}_6$ in 1996 and 1997. They characterized for the first time the structure [16] of this compound and investigated the magnetic properties [17]. This work initiated considerable experimental and theoretical interest in $\text{Ca}_3\text{Co}_2\text{O}_6$ and isostructural compounds like $\text{Ca}_3\text{CoRhO}_6$ and $\text{Ca}_3\text{FeRhO}_6$.

2.1 Crystal Structure

$\text{Ca}_3\text{Co}_2\text{O}_6$ is a member of a whole family of oxides with hexagonal 2H-perovskite structure and the general formula $\text{A}_{3n+3m}\text{A}'_n\text{B}_{3m+n}\text{O}_{9m+6n}$ (A = alkaline earth, A', B = metallic ions). A prominent feature of this structure is the presence of chains in *c*-direction with face sharing octahedra and trigonal prisms. The ratio of octahedral coordinated B cations and A' cations, which are surrounded by a trigonal prism of oxygen atoms, is $\frac{n}{3m+n}$ [18]. By far the most investigated subclass of this family is the one with $m = 0$ and $n = 1$ resulting in the general formula $\text{A}_3\text{A}'\text{BO}_6$. An impressive list of known and investigated compounds can be found in [18]. In this class of compounds the ratio of octahedral to trigonal prismatic sites is 1:1 and the chains are built from alternating face sharing octahedra and trigonal prisms (see e.g. [16, 19, 50–52]). $\text{Ca}_3\text{Co}_2\text{O}_6$ belongs to this subclass and is the only known member thereof with identical atoms on the octahedral and the trigonal prismatic coordinated sites. Although A' and B sites are both occupied by Co the different local environments require a differentiation of the two. It is common to call the Co atom on the B sites Co1 and the Co atom the A' sites Co2.

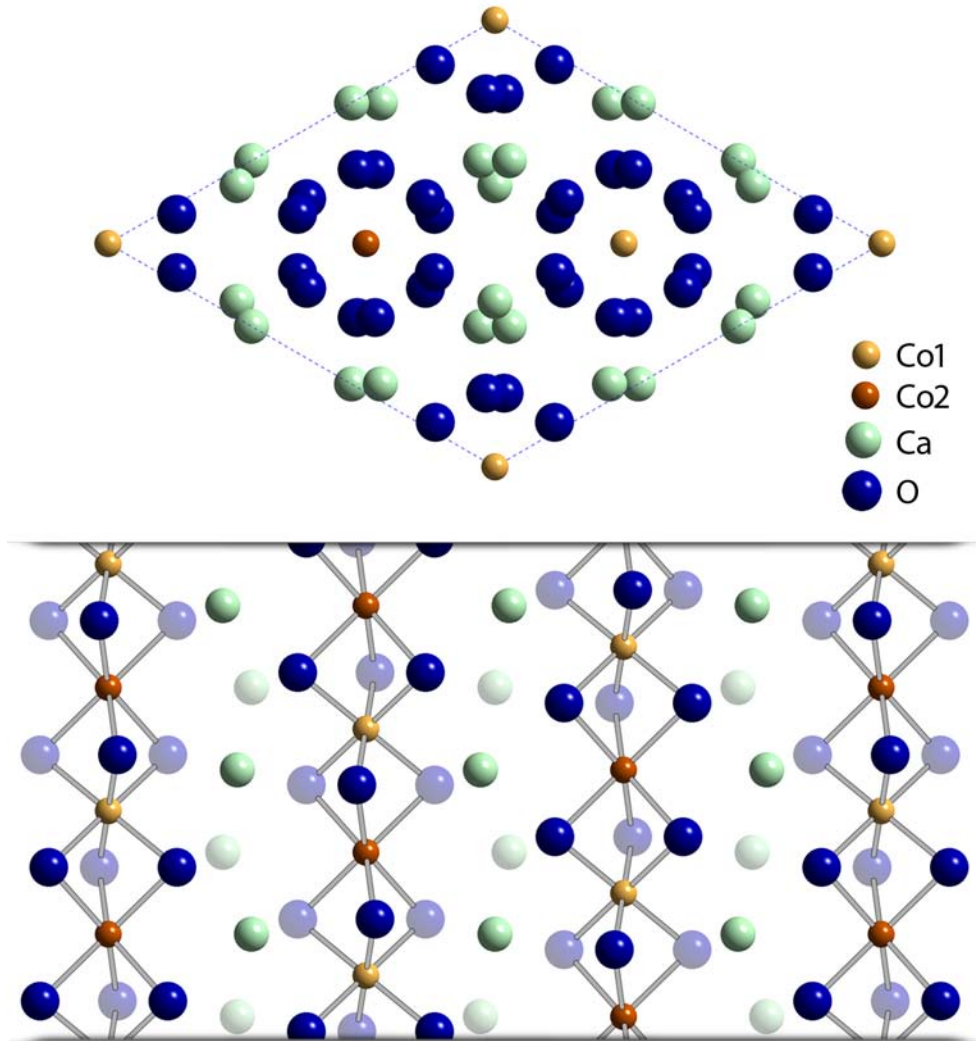


Fig. 2.1: Structure of $\text{Ca}_3\text{Co}_2\text{O}_6$. The upper part of the figure shows a view on the ab -plane of $\text{Ca}_3\text{Co}_2\text{O}_6$. The yellow and red spheres are Co1 and Co2 atoms. Together with the blue spheres, which denote the oxygen atoms, they build chains running along the c -axis. The chains are arranged in a hexagonal lattice. The non-connected spheres show calcium atoms that act as spacers between the chains. The lower part of the figure shows a cut along a row of chains. All cobalt atoms are exactly on the cut plane. The dark colored oxygen and calcium atoms are nearer to the viewer, the light colored ones are further away.

The structure of $\text{Ca}_3\text{Co}_2\text{O}_6$ was determined by powder neutron diffraction for temperatures of 298 K [16] and 10 K [17]. The space group of the structure is $R\bar{3}c$. Looking at the ab -plane in figure 2.1 we can see that the cobalt atoms align perfectly along the c -axis and build the center of a circular arrangement of oxygen atoms, that seems to have six-fold symmetry. We see 12 oxygen atoms projected onto the ab -plane per CoO -chain. If we would have a chain of perfect prisms and octahedra we would only see 6 oxygen atoms. But neither the prisms nor the octahedra are perfect. The two triangles that build a prism are rotated by about 13.9° against each other. In the octahedra the angles between the Co-O bonds differ by about 4.1° from the perfect 90° of a real octahedron. Despite these imperfections there are

still some properties that remain ideal. First and foremost the chain as a whole is still perfectly three-fold symmetric about the cobalt axis. Both oxygen environments remain D_3 symmetric and the not quite octahedral environment in addition retains the inversion symmetry.

The CoO chains are arranged in a hexagonal lattice. A unit cell contains three chains. The height of a unit cell is exactly four Co-Co distances along the chain. That is because each two consecutive Co1 environments are rotated against each other by 180° . Parallel to the c -axis rows of Ca atoms fill the space between the Co-O chains. Using the low temperature data [17] we find a distance between the chains of about 5.23 \AA . The distance from one Co2 to another one of the six nearest chains is at least 5.51 \AA . The difference is best explained by the lower part of figure 2.1, which shows a row of chains. One finds that two equivalent Co atoms on neighboring chains are shifted against each other along the c -axis by one third of the height of the unit cell. The shortest Co-Co distance between to Co atoms on next neighbor chains is 5.30 \AA , whereas the Co1-Co2 distance along the chains is 2.59 \AA [17], which is close to the atomic radius of Co of 2.51 \AA . The interchain distance is more than twice the Co-Co distance along the c -direction. This emphasizes the quasi one-dimensional nature of the compound. The Co1-O bond length is 1.91 \AA and thus shorter than the bond length of Co2-O of about 2.06 \AA . This suggests a stronger crystal field splitting on Co1 than on Co2. A single chain together with some of the intrachain distances is shown in figure 2.2.

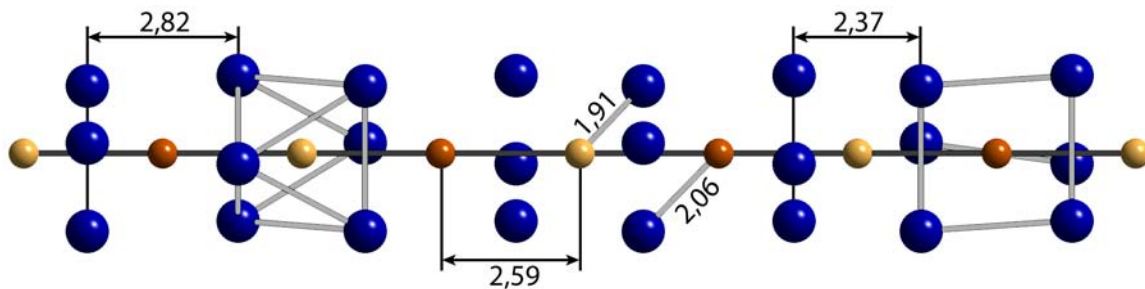


Fig. 2.2: Single CoO chain. Some distances are emphasized. All distances are calculated using the low temperature neutron diffraction results measured by Aasland et al. [17]. They are given in Ångstroem. The color code of figure 2.1 is used. Both the octahedral and the prismatic environments are highlighted by drawing in the O-O bonds. The distortion in the trigonal prism is clearly visible.

2.2 Physical Properties

The physical properties of $\text{Ca}_3\text{Co}_2\text{O}_6$ have been the focus of considerable experimental and theoretical effort since 1997. The quasi one-dimensional structure together with the hexagonal lattice of chains leads to very interesting and non trivial properties. These include such intriguing features as frustration, spin glass behavior, colossal magneto resistance, correlation physics, very high figure of merit, and possible quantum tunneling of magnetization. A

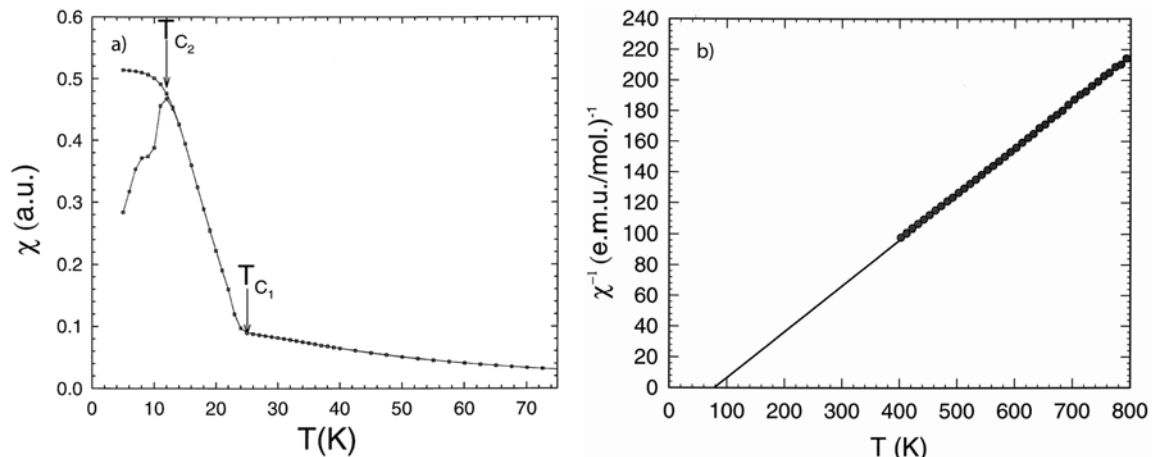


Fig. 2.3: Magnetic susceptibility: a) magnetic susceptibility with two prominent features. A steep increase at 25 K (T_{c1}) and a bifurcation of zero field cooled (zfc) and field cooled (fc) data, with a saturation for fc and a maximum at 10 K for zfc data. b) Inverse susceptibility shows good agreement with the Curie-Weiss law above 150 K. Both plots are taken from [19].

great deal of the research efforts are going into the exploration and theoretical explanation of the complex and fascinating magnetic properties of $\text{Ca}_3\text{Co}_2\text{O}_6$.

Measurements of the static magnetic susceptibility both in powders [17, 53, 54] and single crystal samples [19, 23] reveal Curie-Weiss behavior down to 150 K (see fig. 2.3). Fitting the Curie-Weiss law $\chi(T) = \frac{C}{T-\theta}$ one finds a relatively broad range of values for both θ and the effective magnetization μ_{eff} . The values for θ range from 28 K [17] to 80 K [19]. The effective magnetization μ_{eff} was found to be between $2.85 \mu_B$ per Co [17] and $3.88 \mu_B$ per Co [19, 53]. Kageyama *et al.* pointed out that the discrepancy in the values is due to differences of the powder samples. That is why we rather focus on the values given for the single crystal analysis by Maignan *et al.* [19] which give a value of θ of about 80 K and μ_{eff} of $3.88 \mu_B$ per Co. All authors report a positive Curie temperature which points towards a ferromagnetic ordering.

Below 150 K the magnetic susceptibility begins to deviate from the Curie-Weiss behavior. At about 25 K a steep increase in the susceptibility arises, another indicator for the existence of ferromagnetic order. This feature of the susceptibility was interpreted as a signature of ferromagnetic ordering along the chains. Specific heat measurements on the other hand revealed a pronounced peak at 25 K, a clear signal for the transition to long range order [55]. This result implies that the ordering process has to involve three dimensions as long range order is suppressed at finite temperatures in lower dimensions due to strong quantum fluctuations. Indications for 1D short range order were already found at temperatures of about 100 K. The 25 K peak in the specific heat vanishes for magnetic fields larger than 5 T, which is again consistent with ferromagnetic order. The latter result could not be verified by Sampathkumaran *et al.*, who also performed specific heat measurements but in higher fields [56]. Instead they found a pronounced peak even in fields up to 14 T. Aasland *et al.* reported the occurrence of neutron diffraction Bragg peaks that indicate antiferromagnetic order at temperatures below

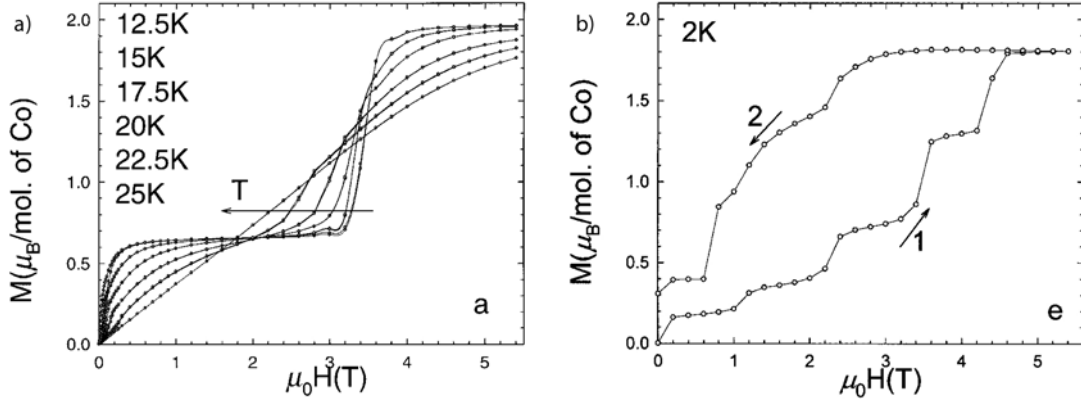


Fig. 2.4: Magnetization data: a) Above 25 K a linear dependence on the field is found. Below T_{c1} a step with a height of $\frac{1}{3}$ of the saturation magnetization develops. b) Going to temperatures below 10 K reveals hysteretic behavior and the existence of several additional steps in the magnetization. The plots are taken from [19].

25 K [17]. All these results are consistent with the existence of a long range ordered phase below 25 K; we will call this temperature T_{c1} . Above T_{c1} short range ferromagnetic order seems to be present in the chains until at 100 to 150 K the pure Curie-Weiss behavior is observed.

Additional information is provided by magnetization measurements. Above T_{c1} the magnetization is a linear function of field (when sufficiently lower than the saturation field). The situation changes below T_{c1} . There is a steep increase of the magnetization for low fields followed by a pronounced plateau at $\frac{1}{3}$ of the saturation magnetization M_{sat} , that finally evolves into another step increase up to M_{sat} [17, 19, 23, 53] (see fig. 2.3 a)). This step becomes more and more prominent from 25 K down to about 10 K (T_{c2}). In the temperature range between T_{c1} and T_{c2} no hysteresis is observed. Below T_{c2} the magnetization gets more and more hysteretic and the $\frac{1}{3}$ step vanishes in favor of several other more or less equally spaced steps as shown in fig. 2.3 b) [19, 23]. A magnetization step of $\frac{1}{3}$ in the intermediate temperature range can easily be understood in terms of a triangular two-dimensional lattice formed of Ising spins. A first approximation to the ground state of this scenario is a partially disordered antiferromagnetic (PDA) state. In a PDA state $\frac{2}{3}$ of the sites are antiferromagnetically ordered in a honeycomb lattice, $\frac{1}{3}$ of the sites are centered in the honeycomb hexagons and have arbitrary spin projections. The total energy of the lattice is independent of the spin projections of the spins on the centers of the honeycomb lattice. Therefore any small magnetic field orders the honeycomb centers along the field resulting in a magnetization of $\frac{1}{3}$ of M_{sat} . This scenario has been investigated lately both analytically [22] and numerically [57] finding not only the $\frac{1}{3}$ step in the magnetization but also other step structures for lower temperatures. These latter steps are also observed experimentally. The measured magnetization in the intermediate temperature range between T_{c1} and T_{c2} points towards a situation where we basically have giant Ising-like spins in ferromagnetically ordered chains, which themselves are antiferromagnetically ordered on a hexagonal 2D lattice. This modeling of a two-dimensional antiferromagnetic interaction finds further confirmation by muon spin rotation and relax-

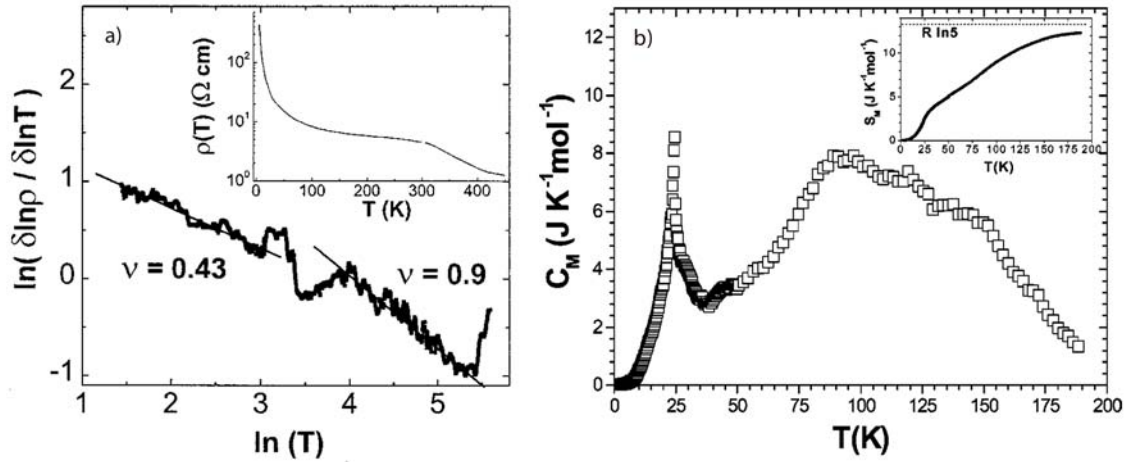


Fig. 2.5: Conductivity and specific heat: a) Conductivity measurements [42] showing a negative slope and two different exponents for the exponential variable range hopping fit. b) Specific heat measurements [55] with a clear λ like peak at T_{c1} and a broad feature above this temperature.

ation measurements [58]. The authors also found evidence for the onset of the intrachain short range ferromagnetic ordering already at temperatures as high as 200 K.

This picture involves a strongly anisotropic magnetic coupling. It is supported by experimental work on oriented powders and single crystals [19, 53], which show strong anisotropic magnetic behavior (see fig 2.6). The analysis of neutron diffraction data revealed that the magnetic moments in $\text{Ca}_3\text{Co}_2\text{O}_6$ are nearly exclusively located on Co2 and are parallel to the c -axis [17]. Strong anisotropy was also found in the conductivity data [42, 43]. These conductivity measurements identify $\text{Ca}_3\text{Co}_2\text{O}_6$ to be an insulator. The conductivity can be described at temperatures below T_{c1} with one-dimensional variable range hopping (VHR) [59]. It was found that the exponent is consistent with a gap due to Coulomb interaction between the localized electrons [60]. At temperatures above 70 to 80 K the conductivity behavior is still insulating and of the VHR type, but the exponent changes to reflect the 3D nature of the paramagnetic phase.

Going to temperatures lower than T_{c2} reveals a difference in the dc susceptibility for field cooled (fc) and zero field cooled (zfc) samples. In the case of fc samples the susceptibility seems to saturate reaching a constant value towards lower temperatures, zfc samples instead show a pronounced maximum at T_{c2} [19]. This behavior is typical for spin glass phases and is frequently called a frozen spin phase. Such a spin glass phase is characterized by slow spin response, which is indeed found in ac-susceptibility measurements [19, 23, 61, 62]. But $\text{Ca}_3\text{Co}_2\text{O}_6$ seems to be a very unusual spin glass material as the peak position in the real part of the temperature-dependent ac-susceptibility curve varies strongly with the frequency [19, 23, 61] which is not observed in usual spin glass materials. A spin glass phase has no long range order which is again consistent with the absence of any particular feature in the specific heat for temperatures close to T_{c2} [55, 56]. As already mentioned the magnetization also shows unusual behavior in the low temperature regime. It was argued that the equally spaced step

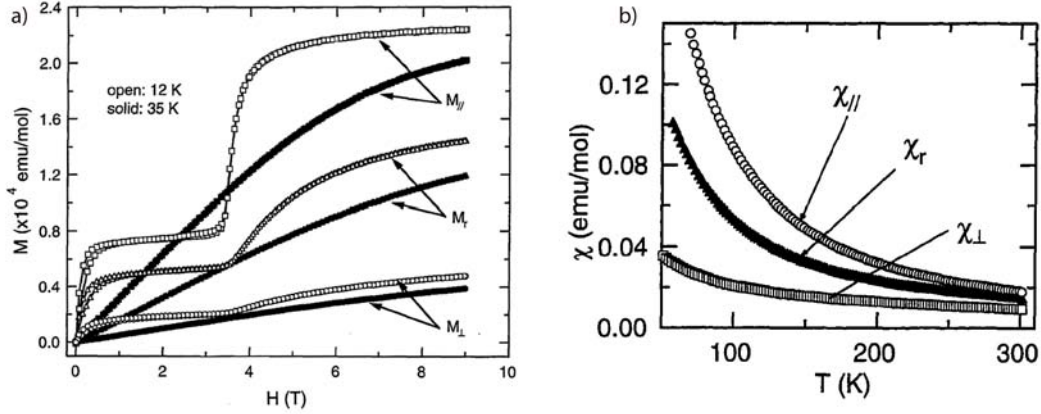


Fig. 2.6: Anisotropic magnetic properties: a) Magnetization data taken from oriented powder samples [53] show a clear difference between the directions \parallel and \perp to the c -axis. The curve M_r was measured for an intermediate direction. b) The same effect is also seen in the susceptibility data.

structure of the magnetization could be due to quantum tunneling of the magnetization [23, 62]. Other theoretical approaches try to explain the phenomenon with antiferromagnetic 2D Ising like models [22, 57]. This is still an area of intense discussion.

Another topic of controversy were the oxidation states of the Co atoms together with their magnetic configuration. The formal average oxidation state of Co in $\text{Ca}_3\text{Co}_2\text{O}_6$ is 3+ but this could be realized either with one Co^{2+} and another Co^{4+} or both Co atoms in the oxidation state 3+. susceptibility and magnetization measurements were not able to sort this out. Several DFT calculations were in favor of the 3+ scenario [63–65], but others claimed to have evidence for 2+/4+ [66]. The Co^{3+} arrangement is also supported by NMR measurements, at least at temperatures below 10 K [67]. We therefore regard this topic as settled and use Co^{3+} in our calculations.

In the 3+ oxidation state Co can be found in three spin states, namely a high spin state (HS) with a total spin of 2, an intermediate spin state with a total spin of 1, and a low spin state (LS) with a total spin of 0. From the magnetic and structural measurements it was not clear what spin states the cobalt atoms are in. Aasland *et al.* found by means of neutron diffraction a magnetic moment of about $3 \mu_B$ on Co2 and a nearly vanishing moment on Co1 [17]. As already mentioned, by fitting high temperature susceptibility data to the Curie-Weiss behavior, $\text{Ca}_3\text{Co}_2\text{O}_6$ was found to have effective moments per formula unit of 5.7 to $7.8 \mu_B$ [17, 19, 53]. Early reports on magnetization measurements revealed saturation magnetizations of about $4 \mu_B$ [17, 19]. But from recent measurements going to higher fields up to 9 T the saturation magnetization seems to be much more likely in the region of $4.8 \mu_B$ [23]. Altogether this gives no simple picture for the spin states. Theoretical work suggests [64, 65, 68] the spin states to be HS on Co2 sites and LS on Co1 sites.

Several other quantities have been investigated. Pressure effects on the magnetic properties have been explored by Martinez, Hernando, and Goko [69–71]. It is found, that both T_{c1} and

2 A Closer Look at $\text{Ca}_3\text{Co}_2\text{O}_6$

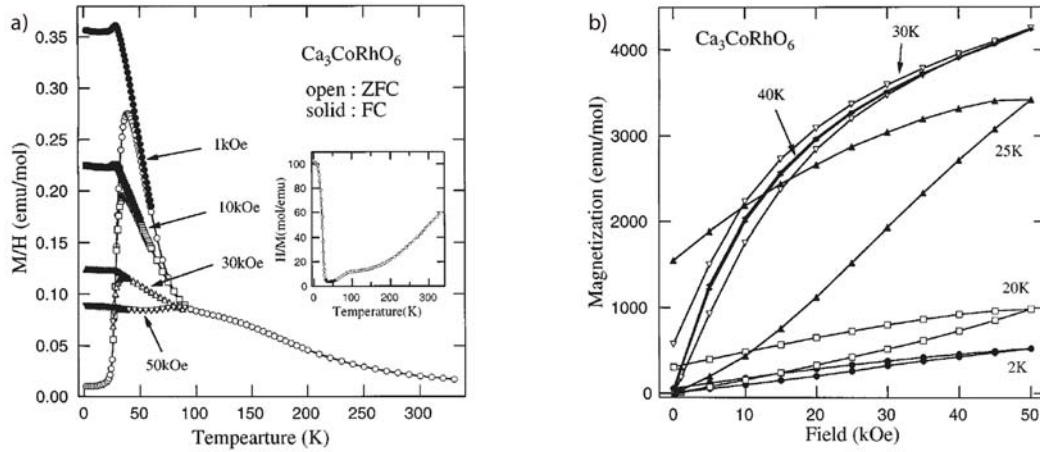


Fig. 2.7: Magnetic properties of $\text{Ca}_3\text{CoRhO}_6$: a) Magnetic susceptibility versus temperature; The data show a steep increase below 90 K. Zero field cooled (zfc) and field cooled (fc) samples behave differently below 35 K. The inset shows the inverse susceptibility, which is almost linear in T above 200 K. b) Magnetization versus field: No steps are found at any temperature (figures are taken from [50]).

the spin flip field H_{SF} above T_{c2} increases with the pressure. H_{SF} above T_{c2} is defined as the field strength necessary to overcome the $\frac{1}{3}$ step in the magnetization bringing the system towards M_{sat} . These effects are explained by the authors with interchain bond length compression. Conductivity measurements at temperatures below T_{c2} revealed a strong dependence of the conductance on the magnetic field. At 2 K the resistance is lowered by 80%. These effects nearly disappear above T_{c1} [42, 43].

A property that is very promising for applications is a high figure of merit, meaning a strong Seebeck effect combined with a small resistance. $\text{Ca}_3\text{Co}_2\text{O}_6$ was investigated in that respect and a strong Seebeck effect was indeed found [44]. Due to quality issues with the single crystal samples the measured resistance was two orders of magnitude too high. The high absolute value of the resistance would reduce the figure of merit, which is inversely proportional to the resistance. This would disqualify $\text{Ca}_3\text{Co}_2\text{O}_6$ for real world applications. Redoing the resistance measurements on better single crystal samples yields absolute values of the resistance that make $\text{Ca}_3\text{Co}_2\text{O}_6$ a very promising candidate for high temperature applications [45–47], due to its high thermal stability [15]. The already very good values for the figure of merit of $\text{Ca}_3\text{Co}_2\text{O}_6$ could even be improved by rare earth doping [48].

The influence of doping has also been investigated by several groups. In principle there are three different approaches in doping $\text{Ca}_3\text{Co}_2\text{O}_6$. The first one consists in substituting Ca by a trivalent cation, in order to obtain a metallic compound. Unfortunately, at the moment, none of the attempts in this direction have been successful [72]. The second one would be to replace parts of the Ca by another divalent cation. This has been done with Y as substituent in $\text{Ca}_{3-x}\text{Y}_x\text{Co}_2\text{O}_6$ [73]. By raising the content of Y the lattice elongates mostly along the direction parallel to the chains. This should mainly suppress the ferromagnetic coupling along the chains. The experimental outcome is a downshift of both transition temperatures

T_{c1} and T_{c2} , another sign that the increasing susceptibility at T_{c1} is connected to the one-dimensional inter-chain interaction. Another interesting result is that the Y substitution significantly changes the behavior of the conductivity at low temperatures, namely from the 1D to the 3D variable-range hopping type.

Another doping scheme replaces Co with transition metals. This has been done, e.g., with Ru, Ir [52], Mn [74, 75], Cr [76] and Fe [77, 78] as substituent. For Ru and Ir it is possible to synthesize a whole series $\text{Ca}_3\text{Co}_{1-x}\text{M}_{1-x}\text{O}_6$ ($\text{M} = \text{Ru}, \text{Ir}$), with $0 \leq x \leq 1$. At $x = 0$ both compounds behave very differently from $\text{Ca}_3\text{Co}_2\text{O}_6$. In $\text{Ca}_3\text{CoIrO}_6$ the Ir-ions seem to occupy the trigonal prismatic sites but the oxidation states are most likely Ir^{+4} and Co^{+2} . The high temperature behavior of the susceptibility points towards ferromagnetic inter-chain interactions. No long range order can be established and no magnetization steps exist at low temperatures. The missing long range order as well as the divergence of the zfc and fc susceptibilities below 30 K, and the dc susceptibility data show clear signs of a spin glass transition [61]. Nevertheless, in the case of $\text{Ca}_3\text{CoIrO}_6$ it is difficult to draw final conclusions due to material problems, as there seems to be a sizeable fraction of vacancies in the Ir site, which is hardly documented in the literature [79]. $\text{Ca}_3\text{CoRuO}_6$ on the other hand behaves completely differently, as its magnetic properties are consistent with conventional antiferromagnetic behavior [77]. For $0 < x < 1$ in both of the series the magnetic properties pretty much interpolate between the $x = 0$ compounds and $\text{Ca}_3\text{Co}_2\text{O}_6$.

Doping with Mn drives the $\text{Ca}_3\text{Co}_2\text{O}_6$ system into a long-range antiferromagnetic order, which is surprising as one would expect more pronounced spin glass behavior due to the additional disorder from the substituted Mn atoms [75]. The Mn atoms occupy the octahedral positions. The compound $\text{Ca}_3\text{CoMnO}_6$ shows no steps in the magnetization and much weaker spin glass behavior at low temperatures. The antiferromagnetic order temperature is about 13 K [74]. In the case of Cr doped $\text{Ca}_3\text{Co}_2\text{O}_6$, it is not possible to synthesize a whole series of compounds, as the solubility of Cr in $\text{Ca}_3\text{Co}_2\text{O}_6$ is very limited. Cr seems to prefer the octahedral positions as Cr^{3+} . This means that Co^{3+} with total spin $S = 0$ is replaced by Cr^{3+} with $S = 3/2$. The ferromagnetic coupling is weakened by the Cr atoms and the susceptibility is suppressed below the antiferromagnetic ordering temperature even by very small Cr doping [76].

The investigations of doping $\text{Ca}_3\text{Co}_2\text{O}_6$ with Fe are somewhat special because ^{57}Fe can be used for Mössbauer spectroscopy. The Fe cations could be identified as Fe^{3+} in the high spin state, which most likely occupy the trigonal prismatic sites of the lattice. For temperatures lower than T_{c1} it is possible to resolve the hyperfine structure of $^{57}\text{Fe}^{3+}$. This is attributed to the different character of Heisenberg-like Fe spins and strongly anisotropic Co spins [77, 78, 80]. These measurements again support the assumption of a strong anisotropic nature of the Co2 spins.

The unusual magnetic properties of $\text{Ca}_3\text{Co}_2\text{O}_6$ motivated a whole bunch of experimental and theoretical work on isostructural compounds [44, 50, 52, 63, 81–89]. Two prominent examples are $\text{Ca}_3\text{CoRhO}_6$ and $\text{Ca}_3\text{FeRhO}_6$. In both cases Rh occupies the octahedral sites

whereas Fe and Co are on the trigonal prismatic sites, respectively. Especially interesting is $\text{Ca}_3\text{CoRhO}_6$ because here not only the structure is similar to $\text{Ca}_3\text{Co}_2\text{O}_6$ but also the magnetic moments are distributed in the same way. Co stays in the oxidation state 3+ and in the high spin state on the trigonal prismatic sites and Rh is also 3+ and in the low spin state with $S = 0$ [90]. The magnetic condition is equivalent to the one in $\text{Ca}_3\text{Co}_2\text{O}_6$. So it is not surprising that both share similarities in the magnetic response. The susceptibility of $\text{Ca}_3\text{CoRhO}_6$ shows pretty much the same features as the susceptibility data of $\text{Ca}_3\text{Co}_2\text{O}_6$. A positive Curie temperature, a steep increase of the susceptibility below 90 K, zfc samples showing a sudden drop in the susceptibility below 35 K whereas fc samples converge to a constant susceptibility at this temperature [50] (fig. 2.7 a)). But in $\text{Ca}_3\text{CoRhO}_6$ magnetization steps do not appear clearly. Still, the derivative $\partial M/\partial H$ shows a strong magnetic field dependence in the temperature range of 30-70 K, which is reminiscent of the behavior of $\text{Ca}_3\text{Co}_2\text{O}_6$ below T_{c1} . In contrast to $\text{Ca}_3\text{Co}_2\text{O}_6$ and $\text{Ca}_3\text{CoRhO}_6$ the compound $\text{Ca}_3\text{FeRhO}_6$ is found to be a 3D anti-ferromagnet [84].

The whole class of compounds shows a rich variety of physical properties. Nevertheless $\text{Ca}_3\text{Co}_2\text{O}_6$ is in some respects a special member of this class. With the competition of ferromagnetic order along the chains and antiferromagnetic order perpendicular to the chains, the complicated step structure of the magnetization versus field curves at low temperatures, the spin glass behavior below T_{c2} , and the unusual dynamical susceptibility it is sort of the most complex compound in the tribe. Hardy *et al.* found only recently, that at low temperature $\text{Sr}_3\text{HoCrO}_6$ shows a behavior very similar to $\text{Ca}_3\text{Co}_2\text{O}_6$ [88].

2.3 Theoretical Findings

The experimental investigation of $\text{Ca}_3\text{Co}_2\text{O}_6$ raised some interesting questions for theoretical considerations. The interplay of anisotropy, correlations, low dimensionality and complex structure is responsible for some remarkable physical properties. In order to gain theoretical insight into the physics of such a complex material, it is necessary to perform density functional theory (DFT) calculations as a first step [63, 64, 66, 91]. The hexagonal unit cell of $\text{Ca}_3\text{Co}_2\text{O}_6$ contains six formula units in the form of three chains that are built from two formula units respectively. In total this sums up to 66 atoms in the hexagonal unit cell. This unit cell can become even bigger, when one considers magnetic unit cells. That is why all calculations are done for simple magnetic order not altering the size of the unit cell. Whangbo's group took a totally ferromagnetically ordered unit cell for its spin polarized DFT calculations [63]. Using this configuration helps to reduce the complexity of the unit cell tremendously, as it is possible to use the trigonal unit cell with only 22 atoms in this case. They found Co in the 3+ oxidation state to be in a high spin configuration on the trigonal sites. For the octahedral sites the calculation yields an oxidation state 3+ and a low spin configuration on the Co. This result is in good agreement with experimental findings [17, 67]. The local spin density approximation (LSDA) in this case fails to predict the insulating behavior as it finds

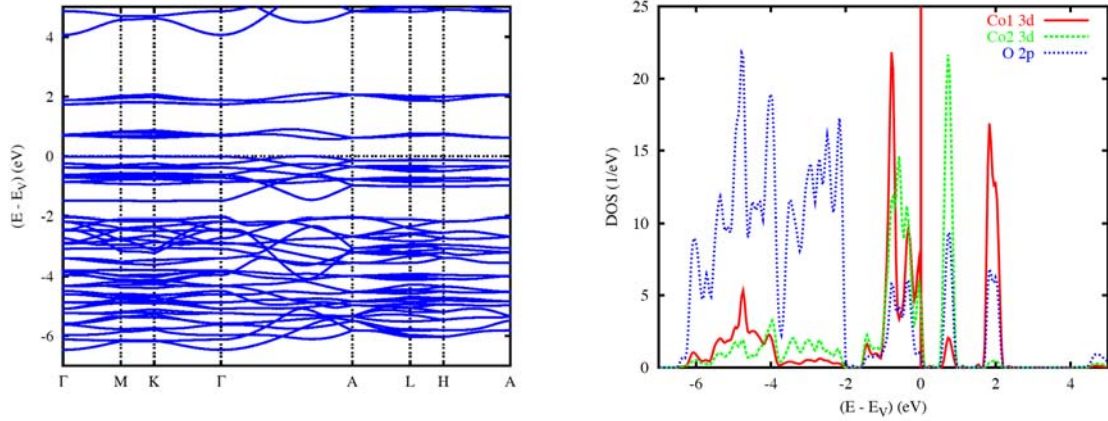


Fig. 2.8: Spin degenerate LDA: a) Band structure depicted in the hexagonal unit cell. The dispersion is strongest along Γ - A, indicating the one-dimensionality of the compound. b) Corresponding total density of states. (figures taken from [64]).

$\text{Ca}_3\text{Co}_2\text{O}_6$ to be a half metal. It is a well known shortcoming of the DFT in conjunction with the LSDA that it underestimates the optical band gap. The reason for this systematic failure is the incomplete treatment of electron-electron correlations [92] in the LSDA.

Eyert in cooperation with Kopp, Frésard and myself also performed an LSDA calculation [64], extending the scope of the work of Whangbo. We also found $\text{Ca}_3\text{Co}_2\text{O}_6$ to be half metallic, which is a strong indicator for the importance of electron-electron correlations. In many cases the strongest effect of the correlations is the increase of the band gap size. If one is aware of this central problem LSDA gives still valuable insight into the physics of the compound. The afore mentioned group performed three calculations for $\text{Ca}_3\text{Co}_2\text{O}_6$ [64]. In the first one spin degeneracy is enforced. The second one, similar to Whangbo, uses the trigonal unit cell, effectively assuming total ferromagnetic order. A third calculation actually applies the hexagonal unit cell in the ferrimagnetic order, where the magnetic moments of two chains point in c direction and the third chain has a magnetic moment in opposite direction.

The spin degenerate calculation reflects clearly the one-dimensionality of the compound. The bands show the most distinct dispersion along the chains. The chain direction corresponds to the part of the band structure between the Γ - and the A-point in figure 2.8 a). Another finding of this calculation is a clearly identifiable crystal field splitting in the partial DOS for Co1 and Co2 (see fig. 2.9 a and b). The labelling of the orbitals is relative to a global coordinate system with the z -axis along the chain direction. For this reason, the crystal field split bands are not formed from the d_{xy} , d_{xz} , d_{yz} and $d_{x^2-y^2}$, $d_{3z^2-r^2}$ orbitals, respectively, as they would be in the standard orientation with the Cartesian axes pointing along the metal-ligand bonds but rather from admixtures of these orbitals. Only after a transformation into a symmetry adapted coordinate system for Co1, a nearly perfect t_{2g} - e_g splitting can be seen.

Performing the LSDA calculation for a lattice of ferromagnetically ordered chains confirms the low-spin and high-spin states for Co1 and Co2, respectively, and magnetizations close to

measured values [17]. It is found that the oxygen atoms carry almost $1 \mu_B$ per unit cell. This is due to a rather strong hybridization between Co1 d-states and O p-states. The magnetic moments are still localized but spread on the oxygens of the prism. Such a situation has been previously observed in copper oxides. It is known as extended moment formation [93, 94]. Along the chains a strong metal-metal overlap is found, mostly of $d_{z^2-r^2}$ orbitals of Co1 and Co2. Extending the calculation to ferrimagnetic order does not change the results significantly. All qualitative findings remain unchanged [64].

The strong anisotropy of the magnetic response found in the experiments [54] suggests, that spin-orbit coupling is an important interaction in this material. Spin-orbit coupling can be treated in the LSDA framework which has been done for $\text{Ca}_3\text{Co}_2\text{O}_6$ [66, 91]. These calculations predict the insulating character of $\text{Ca}_3\text{Co}_2\text{O}_6$ correctly. But both of these calculations have problems of their own. The group of An [91] *et al.* found, e.g., that the mobility of the electrons in $\text{Ca}_3\text{Co}_2\text{O}_6$ is much lower along the chains than perpendicular to the chains, in marked contrast to experimental results [43]. The group of Vidya predicts in its calculations

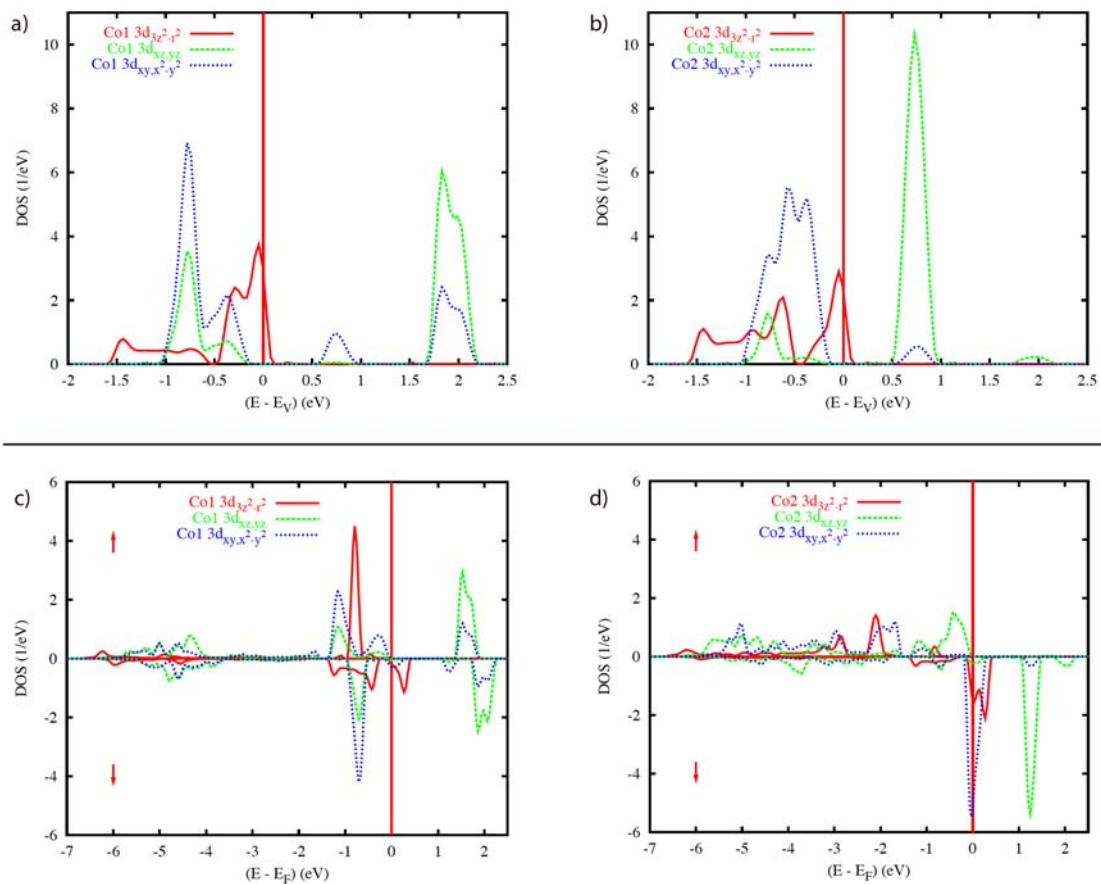


Fig. 2.9: Partial density of states: a) and b) spin degenerate results for Co1 and Co2, respectively. The crystal field splitting is in both cases clearly visible. In the Co1 case it is necessary to transform the data into the ‘natural’ coordinate system defined by the octahedral environment to observe the $t_{2g} - e_g$ splitting. c) and d) shows the corresponding data in the spin resolved ferromagnetic case.

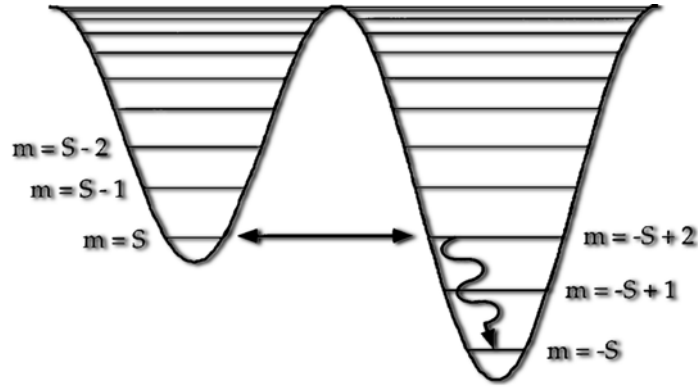


Fig. 2.10: Illustration of quantum tunneling: the system is in the metastable state $m = S$. If the magnetic field is tuned such that the system state is degenerate with an excited state on the other side of the barrier $m = -S + n$, the system can overcome the barrier by tunneling into the state $m = -S + n$. The tunneling is then followed by a rapid relaxation into the ground state [25].)

that cobalt should be 2+ and 4+, which can not be confirmed by experimental findings [67] and is in contradiction to several other theoretical works [63–65, 68].

The failure of the LSDA calculations to produce the experimental gap is most likely due to electron-electron correlations in $\text{Ca}_3\text{Co}_2\text{O}_6$. A way to introduce local electron interactions in a LDA like calculation is provided by the LSDA + U scheme. Wu *et al.* performed such calculations for $\text{Ca}_3\text{Co}_2\text{O}_6$, also including spin-orbit coupling [65]. The incorporation of local electron interactions indeed leads to an insulating ground state. The system becomes insulating for any reasonable value of U . This result suggests that $\text{Ca}_3\text{Co}_2\text{O}_6$ is a Mott insulator, which emphasizes the importance of correlations in the compound. The addition of spin-orbit coupling together with the unusual crystal field splitting of the local energy levels on the trigonal prismatic sites serves as an explanation for the strong anisotropy. The above calculation also supports the assumption of Co being in a 3+ oxidation state on both the octahedral and prismatic sites.

An interesting question, which is outside the scope of LSDA in this system, is the occurrence of a series of steps in the magnetization at temperatures below T_{c2} . Two explanations are proposed by different groups. Kudasov [22] maps the structure of $\text{Ca}_3\text{Co}_2\text{O}_6$ on a 2D triangular lattice being formed of Ising spins. One chain is represented by one Ising spin in this formulation. Starting from a partially disordered antiferromagnetic (PDA) state it is possible to analytically construct a sequence of excited states approaching the ground state of the system [95, 96]. Any of these states results in a different set of magnetization steps. Assuming that the system is going through these states during the cooling process, this sequence of states could explain the observed steps in the magnetization curve.

The basis for the mapping of the magnetic structure of $\text{Ca}_3\text{Co}_2\text{O}_6$ onto a triangular lattice of Ising spins is the assumption of rigid, ferromagnetically coupled chains. A complementary idea is that the steps are related to a quantum tunneling effect phenomenon [23, 62]. In this formulation the Ising like spins on the Co_2 atoms are in a first approximation not

coupled to each other. The steps in the magnetization come from resonant tunneling effects. The phenomenon of quantum tunneling is widely discussed in the context of molecular magnets [25, 97]. The magnetic properties of these systems are dominated by large, highly anisotropic magnetic moments, that are relatively far apart and therefore only weakly coupled to each other. The large moments are typically formed by mesoscopic ferromagnetic particles or molecular clusters, e.g., Mn₁₂ [24, 98]. Several observations support the idea of quantum tunneling in Ca₃Co₂O₆: first of all the strong anisotropy of the magnetic response, which is a crucial precondition. A second finding, that supports this picture is that the magnetization steps occur at constant magnetic field intervals, independent of the sweep rate of the field. Along with the measurements of faster magnetic relaxation in the vicinity of the steps [23, 62], this behavior is consistent with the results in molecular magnets [25]. Nevertheless the situation in Ca₃Co₂O₆ is much more complex, as the coupling of the magnetic moments cannot be neglected. Therefore it might not be unexpected that the agreement with findings in molecular magnets are far from perfect. One striking difference is that the steps in Mn₁₂ only occur during the up sweep of the field towards saturation. On the back sweep to zero field no steps are visible, but in Ca₃Co₂O₆ steps are clearly visible in both directions. Another unclear matter is the appearance and freezing of steps dependent on sweep rate and temperature, where additional experiments might bring new insights. Whether the differences between the magnetic features of Ca₃Co₂O₆ and molecular magnets are a consequence of the spin-spin interactions or of an inadequate analogy is still heavily discussed.

“As we came closer, we realized that the quadrangular form included, at each of its corners, a heptagonal tower, five sides of which were visible on the outside - four of the eight sides, then, of the greater octagon producing four minor heptagons, which from the outside appeared as pentagons.”

Umberto Eco, *The Name of the Rose*

3 High Order Perturbation Theory

For $\text{Ca}_3\text{Co}_2\text{O}_6$ experimental and theoretical investigations find a Mott-Hubbard gap at low temperatures [42, 65]. We will therefore assume that the local Coulomb interactions dominate the low energy physics in this system. Using perturbation expansion in the hopping terms should give at least a qualitatively correct description of the system. It should be possible to find a reasonably good approximation to the lowest eigenstate within a few orders of perturbation theory. The problem we are discussing demands perturbation theory to fourth and fifth order.

We divide the Hamiltonian \mathbf{H} into one part \mathbf{H}_0 , which we assume to define a solvable or already solved problem, and another part \mathbf{H}_1 , the perturbation, with $\mathbf{H} = \mathbf{H}_0 + \mathbf{H}_1$. Using the reasoning described in quantum mechanics books (e.g., [99]) it is tedious but straightforward to derive the formulae for higher orders in the Rayleigh-Schrödinger formalism. Table 3.1 lists all expressions up to fifth order. Especially the higher order corrections are quite complicated. The formulae become much simpler if the first order correction $E_n^{(1)}$ vanishes. For a typical hopping Hamiltonian it is usually possible to choose a basis such that the perturbation Hamilton matrix contains only off diagonal elements.

3.1 Perturbative Treatment of Degenerate States in Second and Third Order

The formulae in table 3.1 are valid only if the following condition is fulfilled:

$$|\langle n | \mathbf{H}_1 | \mu \rangle| \ll |\Delta E_\mu| = |E_n - E_\mu|. \quad (3.1)$$

In a zeroth order estimation the value of $H^{n\mu}$ is typically of the order of the hopping energy t , and the energy difference of two eigenstates of the Hubbard Hamiltonian is of the order of U . In the weak coupling limit we have indeed $t \ll U$. But with a multi-orbital Hamiltonian, U is not the only energy scale. We cannot be *a priori* sure that we actually meet the criterion 3.1

3 High Order Perturbation Theory

$E_n^{(1)} = \langle n \mathbf{H}_1 n \rangle = H^{nn}$
$E_n^{(2)} = \sum_{\mu} \frac{H^{n\mu} H^{\mu n}}{\Delta E_{\mu}}$
$E_n^{(3)} = \sum_{\mu\nu} \frac{H^{n\mu} H^{\mu\nu} H^{\nu n}}{\Delta E_{\mu} \Delta E_{\nu}} - E_n^{(1)} \sum_{\mu} \frac{H^{n\mu} H^{\mu n}}{(\Delta E_{\mu})^2}$
$E_n^{(4)} = \sum_{\mu\nu\lambda} \frac{H^{n\mu} H^{\mu\nu} H^{\nu\lambda} H^{\lambda n}}{\Delta E_{\mu} \Delta E_{\nu} \Delta E_{\lambda}} - E_n^{(2)} \sum_{\mu} \frac{H^{n\mu} H^{\mu n}}{(\Delta E_{\mu})^2}$ $- E_n^{(1)} \sum_{\mu\nu} \frac{H^{n\mu} H^{\mu\nu} H^{\nu n}}{\Delta E_{\mu} \Delta E_{\nu}} \left(\frac{1}{\Delta E_{\mu}} + \frac{1}{\Delta E_{\nu}} \right) + (E_n^{(1)})^2 \sum_{\mu} \frac{H^{n\mu} H^{\mu n}}{(\Delta E_{\mu})^3}$
$E_n^{(5)} = \sum_{\mu\nu\lambda\delta} \frac{H^{n\mu} H^{\mu\nu} H^{\nu\lambda} H^{\lambda\delta} H^{\delta n}}{\Delta E_{\mu} \Delta E_{\nu} \Delta E_{\lambda} \Delta E_{\delta}} - \sum_{\mu\nu\lambda} \frac{H^{n\mu} H^{\mu\nu} H^{\nu n} H^{n\lambda} H^{\lambda n}}{\Delta E_{\mu} \Delta E_{\nu} \Delta E_{\lambda}} \left(\frac{1}{\Delta E_{\mu}} + \frac{1}{\Delta E_{\nu}} + \frac{1}{\Delta E_{\lambda}} \right)$ $- E_n^{(1)} \sum_{\mu\nu\lambda} \frac{H^{n\mu} H^{\mu\nu} H^{\nu\lambda} H^{\lambda n}}{\Delta E_{\mu} \Delta E_{\nu} \Delta E_{\lambda}} \left(\frac{1}{\Delta E_{\mu}} + \frac{1}{\Delta E_{\nu}} + \frac{1}{\Delta E_{\lambda}} \right)$ $+ E_n^{(1)} \sum_{\mu\nu} \frac{H^{n\mu} H^{\mu n} H^{n\nu} H^{\nu n}}{\Delta E_{\mu} \Delta E_{\nu}} \left(\frac{1}{(\Delta E_{\mu})^2} + \frac{1}{\Delta E_{\mu} \Delta E_{\nu}} + \frac{1}{(\Delta E_{\nu})^2} \right)$ $+ (E_n^{(1)})^2 \sum_{\mu\nu} \frac{H^{n\mu} H^{\mu\nu} H^{\nu n}}{\Delta E_{\mu} \Delta E_{\nu}} \left(\frac{1}{(\Delta E_{\mu})^2} + \frac{1}{\Delta E_{\mu} \Delta E_{\nu}} + \frac{1}{(\Delta E_{\nu})^2} \right) - (E_n^{(1)})^3 \sum_{\mu} \frac{H^{n\mu} H^{\mu n}}{(\Delta E_{\mu})^4}$

Table 3.1: Energy corrections up to fifth order of perturbation theory for non degenerate states. The unperturbed states are labeled μ , ν , λ , and σ . A state μ is eigenstate of the unperturbed Hamiltonian \mathbf{H}_0 with the eigenvalue $E_{\mu}^{(0)}$. The energy corrections are calculated for the state n , that is excluded in all summations. We use the abbreviations $\Delta E_{\mu} = E_n^{(0)} - E_{\mu}^{(0)}$ and $H^{\mu\nu} = \langle \mu | \mathbf{H}_1 | \nu \rangle$, where \mathbf{H}_1 is the Hamiltonian of the perturbation.

in any case. Further problems arise for unperturbed states that are degenerate with state $|n\rangle$. In case of degenerate states the inequality 3.1 breaks down completely.

To avoid problems with troublesome intermediate states we have to make sure that there is no way to reach such a state in the considered order of the perturbation. That is already the basic idea for the necessary modifications for degenerate perturbation theory. First let us focus on all states that are exactly degenerate with the state n . These unperturbed states span a subspace \mathbb{D} of the total Hilbert space \mathbb{H} . Furthermore we define a projector $\mathbf{P} = \sum_{n \in \mathbb{D}} |n\rangle\langle n|$, which performs a projection into \mathbb{D} . As all $n \in \mathbb{D}$ are eigenstates to the same eigenvalue of \mathbf{H}_0 , we can choose any linear combination of these states as the basis of the perturbation expansion. In particular we can choose them to be eigenstates of $\mathbf{P} \mathbf{H}_1 \mathbf{P}$. We will call these new states n' , they are still eigenstates of \mathbf{H}_0 . But for two states m' and n' the matrix element $\langle m' | \mathbf{H}_1 | n' \rangle$ now vanishes. There is no hopping matrix element between these two states up to

first order. With this property we can correct the energy up to third order without running into degeneracy problems.

3.2 Nearly Degenerate States

For nearly degenerate states the basic idea is the same, but we have to treat the problem a little bit more formal. The subspace \mathbb{D} is now spanned by both degenerate and nearly degenerate states with respect to the state n . In this situation an additional problem arises. If we simply diagonalize $\mathbf{P} \mathbf{H}_1 \mathbf{P}$ the resulting states will no longer be eigenstates of \mathbf{H}_0 , which is a precondition of the perturbation theory that lead us to the formulae of table 3.1. In order to solve this issue we will transform the original Hamiltonian. This transformation has to be done in a way, that we are able to put the problematic terms in that part of the Hamiltonian that can be diagonalized exactly, leaving the rest of the Hamiltonian for the now unproblematic perturbative treatment. To achieve this goal we introduce an additional projection operator $\mathbf{Q} = \mathbf{1} - \mathbf{P}$, which projects a general state into the complement of \mathbb{D} . A ket state $|\mu\rangle$ can then be written as:

$$|\mu\rangle = \mathbf{P} |\mu\rangle + \mathbf{Q} |\mu\rangle . \quad (3.2)$$

We can also rewrite the Hamiltonian:

$$\mathbf{H} = \mathbf{H}_0 + (\mathbf{P} + \mathbf{Q}) \mathbf{H}_1 (\mathbf{P} + \mathbf{Q}) = \mathbf{H}_0 + \mathbf{P} \mathbf{H}_1 \mathbf{P} + \mathbf{Q} \mathbf{H}_1 \mathbf{P} + \mathbf{P} \mathbf{H}_1 \mathbf{Q} + \mathbf{Q} \mathbf{H}_1 \mathbf{Q} . \quad (3.3)$$

At this point we will simply redefine the unperturbed part of the Hamiltonian and the perturbation. With the definitions:

$$\begin{aligned} \mathbf{H}'_0 &\equiv \mathbf{H}_0 + \mathbf{P} \mathbf{H}_1 \mathbf{P} , \\ \mathbf{H}'_1 &\equiv \mathbf{P} \mathbf{H}_1 \mathbf{Q} + \mathbf{Q} \mathbf{H}_1 \mathbf{P} + \mathbf{Q} \mathbf{H}_1 \mathbf{Q} , \end{aligned} \quad (3.4)$$

the perturbative problem is restated in an adequate fashion. Now we have to diagonalize \mathbf{H}'_0 resulting in new eigenstates $|\mu'\rangle$ and formulate the perturbation theory with \mathbf{H}'_1 and the states $|\mu'\rangle$. This looks like we would have to redo the diagonalization completely but actually the eigenstates of \mathbf{H}_0 that are not in \mathbb{D} are unaltered because the Hamiltonian has not changed in the complement of \mathbb{D} . The diagonalization can be limited to the subspace \mathbb{D} . This reformulation of the problem has two beneficial effects. First, the additional term in \mathbf{H}'_0 typically lifts the degeneracy at least partly. Second, even if there are still degenerate states left, they will not harm, because terms comprising these states in second order vanish. All matrix elements of \mathbf{H}'_1 connecting two states in \mathbb{D} are zero by construction, therefore only states in the complement \mathbb{H}/\mathbb{D} can be intermediate states in the perturbation expansion. A benefit of this construction is that we can use the formulae of the non degenerate perturbation theory and simply use the new perturbation Hamiltonian \mathbf{H}'_1 . Using the formula in 3.1 we calculate the first order energy correction for a state $n' \in \mathbb{D}$:

$$E_{n'}^{(1)} = \langle n' | \mathbf{H}'_1 | n' \rangle = \langle n' | \mathbf{P H}_1 \mathbf{Q} + \mathbf{Q H}_1 \mathbf{P} + \mathbf{Q H}_1 \mathbf{Q} | n' \rangle = 0. \quad (3.5)$$

The first order energy correction vanishes for the state n' . The first order correction is obviously already included by the way the nearly degenerate states are treated. If the energy degeneracy is lifted by this procedure we are done and can calculate the higher order energy correction accordingly. Unfortunately this is not the case in our problem, because in our hopping expansion the first order corrections vanish already from the beginning. The degeneracy can therefore not be lifted by the above technique. If the degeneracy is not lifted one can easily see from table 3.1 that it is nevertheless save to calculate energy corrections up to third order.

3.3 Degeneracy in Fourth Order and Above

Beginning with the fourth order we are again faced with problems due to degenerate or nearly degenerate states. This originates in the fact that the above treatment eliminates only direct matrix elements of two degenerate states with the perturbation Hamiltonian. The fourth order energy correction contains terms that lead to indirect matrix elements between two degenerate states. We assume the state $n' \in \mathbb{D}$ to be already corrected with the above illustrated method. One of the terms of the energy correction in fourth order looks like this:

$$\delta E_{n'}^{(4)} = \frac{\langle n' | \mathbf{P H}_1 \mathbf{Q} | \mu' \rangle \langle \mu' | \mathbf{Q H}_1 \mathbf{P} + \mathbf{Q H}_1 \mathbf{Q} | \nu' \rangle}{(E_{n'}^{(0)} - E_{\mu'}^{(0)})(E_{n'}^{(0)} - E_{\nu'}^{(0)})} \quad (3.6)$$

$$\begin{aligned} & \times \frac{\langle \nu' | \mathbf{P H}_1 \mathbf{Q} + \mathbf{Q H}_1 \mathbf{Q} | \gamma' \rangle \langle \gamma' | \mathbf{Q H}_1 \mathbf{P} | n' \rangle}{(E_{n'}^{(0)} - E_{\gamma'}^{(0)})} \\ & = \frac{\langle n' | \mathbf{P H}_1 \mathbf{Q} | \mu' \rangle \langle \mu' | \mathbf{Q H}_1 \mathbf{Q} | \nu' \rangle \langle \nu' | \mathbf{Q H}_1 \mathbf{Q} | \gamma' \rangle \langle \gamma' | \mathbf{Q H}_1 \mathbf{P} | n' \rangle}{(E_{n'}^{(0)} - E_{\mu'}^{(0)})(E_{n'}^{(0)} - E_{\nu'}^{(0)})(E_{n'}^{(0)} - E_{\gamma'}^{(0)})} \quad (3.7) \\ & + \frac{\langle n' | \mathbf{P H}_1 \mathbf{Q} | \mu' \rangle \langle \mu' | \mathbf{Q H}_1 \mathbf{P} | \nu' \rangle \langle \nu' | \mathbf{P H}_1 \mathbf{Q} | \gamma' \rangle \langle \gamma' | \mathbf{Q H}_1 \mathbf{P} | n' \rangle}{(E_{n'}^{(0)} - E_{\mu'}^{(0)})(E_{n'}^{(0)} - E_{\nu'}^{(0)})(E_{n'}^{(0)} - E_{\gamma'}^{(0)})} \end{aligned}$$

The numerator of the second term of equation 3.7 has a finite value if the states ν' are degenerate or nearly degenerate with the state n' . With an energy denominator that is zero or close to zero this whole term will cause the perturbation expansion to break down. In order to deal with such terms up to fifth order we introduce the following operators:

$$\begin{aligned} \mathbf{V}_L : \langle l' | \mathbf{V}_L &= \sum_{\mu'} \frac{\langle l' | \mathbf{P} \mathbf{H}_1 \mathbf{Q} | \mu' \rangle \langle \mu' | \mathbf{Q} \mathbf{H}_1 \mathbf{P}}{E_{l'}^{(0)} - E_{\mu'}^{(0)}} \\ &+ \sum_{\mu' \nu'} \frac{\langle l' | \mathbf{P} \mathbf{H}_1 \mathbf{Q} | \mu' \rangle \langle \mu' | \mathbf{Q} \mathbf{H}_1 \mathbf{Q} | \nu' \rangle \langle \nu' | \mathbf{Q} \mathbf{H}_1 \mathbf{P}}{(E_{l'}^{(0)} - E_{\mu'}^{(0)}) (E_{n'}^{(0)} - E_{\mu'}^{(0)})}, \end{aligned} \quad (3.8)$$

$$\begin{aligned} \mathbf{V}_R : \mathbf{V}_R | l' \rangle &= \sum_{\mu'} \frac{\mathbf{P} \mathbf{H}_1 \mathbf{Q} | \mu' \rangle \langle \mu' | \mathbf{Q} \mathbf{H}_1 \mathbf{P} | l' \rangle}{E_{l'}^{(0)} - E_{\mu'}^{(0)}} \\ &+ \sum_{\mu' \nu'} \frac{\mathbf{P} \mathbf{H}_1 \mathbf{Q} | \mu' \rangle \langle \mu' | \mathbf{Q} \mathbf{H}_1 \mathbf{Q} | \nu' \rangle \langle \nu' | \mathbf{Q} \mathbf{H}_1 \mathbf{P} | l' \rangle}{(E_{l'}^{(0)} - E_{\mu'}^{(0)}) (E_{n'}^{(0)} - E_{\mu'}^{(0)})}. \end{aligned} \quad (3.9)$$

This definition uses states $l' \in \mathbb{D}$ and the reference state n' which we want to correct. The operator \mathbf{V}_L is defined in the dual space whereas \mathbf{V}_R is acting on ket vectors. Generally both operators are not hermitian but in spaces of energetically degenerate states they are hermitian. In the latter case they have the same matrix representation. In general one is the adjoint operator of the other, $\mathbf{V}_L^\dagger = \mathbf{V}_R$. We want to investigate the case of nearly degenerate states. In a similar way as before we want to redefine the perturbation problem. We can neither use \mathbf{V}_L nor \mathbf{V}_R for this task, because they do not represent observables due to their non hermitian nature. Nevertheless we can define hermitian and antihermitian combinations of the two operators:

$$\mathbf{V}_+ \equiv \frac{1}{2} (\mathbf{V}_L + \mathbf{V}_R), \quad (3.10)$$

$$\mathbf{V}_- \equiv \frac{1}{2} (\mathbf{V}_L - \mathbf{V}_R). \quad (3.11)$$

From these definitions we get of course the inverse relations $\mathbf{V}_L = \mathbf{V}_+ + \mathbf{V}_-$ and $\mathbf{V}_R = \mathbf{V}_+ - \mathbf{V}_-$. Now we are able to restate the original problem in the following form:

$$\mathbf{H} = \mathbf{H}_0 + \mathbf{P} \mathbf{H}_1 \mathbf{P} + \mathbf{V}_+ + \mathbf{Q} \mathbf{H}_1 \mathbf{P} + \mathbf{P} \mathbf{H}_1 \mathbf{Q} + \mathbf{Q} \mathbf{H}_1 \mathbf{Q} - \mathbf{V}_-. \quad (3.12)$$

From the definition of \mathbf{V}_L and \mathbf{V}_R it is obvious that these two operators are in second and third order in \mathbf{H}_1 and so is \mathbf{V}_+ . Moreover \mathbf{V}_+ has only finite matrix elements for states in \mathbb{D} . Like before we define a modified unperturbed Hamiltonian $\tilde{\mathbf{H}}_0$. The new perturbation term can be split into a term which is first order and another which is second and third order in \mathbf{H}_1 :

$$\mathbf{H} = \tilde{\mathbf{H}}_0 + \tilde{\mathbf{H}}_1 + \tilde{\mathbf{H}}_2 \quad (3.13)$$

3 High Order Perturbation Theory

with

$$\tilde{\mathbf{H}}_0 = \mathbf{H}_0 + \mathbf{P} \mathbf{H}_1 \mathbf{P} + \mathbf{V}_+, \quad (3.14)$$

$$\tilde{\mathbf{H}}_1 = \mathbf{Q} \mathbf{H}_1 \mathbf{P} + \mathbf{P} \mathbf{H}_1 \mathbf{Q} + \mathbf{Q} \mathbf{H}_1 \mathbf{Q}, \quad (3.15)$$

$$\tilde{\mathbf{H}}_2 = -\mathbf{V}_+. \quad (3.16)$$

We now perform the diagonalization of $\tilde{\mathbf{H}}_0$. As $\tilde{\mathbf{H}}_0$ is not different from \mathbf{H}_0 outside of \mathbb{D} all states of the complement \mathbb{H}/\mathbb{D} are still eigenstates and stay unaltered. Only the states in \mathbb{D} have to be diagonalized again with the new Hamiltonian. A state \tilde{n} is an eigenstate of $\tilde{\mathbf{H}}_0$ with the eigenvalue $\tilde{E}_{\tilde{n}}^{(0)}$. To calculate the energy corrections we can still use the formulae in table 3.1 but with some caution. Due to the fact that we have to deal with a perturbation that already contains higher order terms we have to rearrange the terms according to their order in \mathbf{H}_1 . Therefore we distinguish between the energy corrections given by the formulae for the unperturbed case $E_{\tilde{n}}^{(i)}$ in order i with respect to perturbation $\tilde{H}_1 + \tilde{H}_2$ and energy corrections $\tilde{E}_{\tilde{n}}^{(i)}$ in order i with respect to the perturbation H'_1 for the states \tilde{n} . To illustrate this procedure, we perform the first order energy correction to a state \tilde{n} :

$$E_{\tilde{n}}^{(1)} = \langle \tilde{n} | \tilde{\mathbf{H}}_1 + \tilde{\mathbf{H}}_2 | \tilde{n} \rangle = \langle \tilde{n} | \tilde{\mathbf{H}}_1 | \tilde{n} \rangle - \langle \tilde{n} | \mathbf{V}_+ | \tilde{n} \rangle. \quad (3.17)$$

The term $\langle \tilde{n} | \mathbf{V}_+ | \tilde{n} \rangle$ is already at least of second order and does not belong to a first order correction. But this term has to be taken into account for the second order energy correction. This means:

$$\tilde{E}_{\tilde{n}}^{(1)} = \langle \tilde{n} | \tilde{\mathbf{H}}_1 | \tilde{n} \rangle = \langle \tilde{n} | \mathbf{H}'_1 | \tilde{n} \rangle = 0. \quad (3.18)$$

The chosen construction of $\tilde{\mathbf{H}}_0$ does still lead to a vanishing first order correction. Bringing together all second order terms shows that $\tilde{E}_{\tilde{n}}^{(2)}$ is also vanishes by construction and the same is true for $\tilde{E}_{\tilde{n}}^{(3)}$.

All energy corrections up to fifth order are shown in table 3.2. It appears that there are still terms in 3.2 that have very small or even vanishing denominators. These terms include factors of \mathbf{V}_- . So let us have a closer look on \mathbf{V}_- in second order, with the states $\tilde{n}, \tilde{m} \in \mathbb{D}$:

$$\langle \tilde{n} | \mathbf{V}_- | \tilde{m} \rangle = \sum_{\tilde{\mu}} \frac{\langle \tilde{n} | \mathbf{P} \mathbf{H}_1 \mathbf{Q} | \tilde{\mu} \rangle \langle \tilde{\mu} | \mathbf{Q} \mathbf{H}_1 \mathbf{P} | \tilde{m} \rangle}{2(E_{\tilde{n}}^{(0)} - E_{\tilde{\mu}}^{(0)})} - \sum_{\tilde{\mu}} \frac{\langle \tilde{n} | \mathbf{P} \mathbf{H}_1 \mathbf{Q} | \tilde{\mu} \rangle \langle \tilde{\mu} | \mathbf{Q} \mathbf{H}_1 \mathbf{P} | \tilde{m} \rangle}{2(E_{\tilde{m}}^{(0)} - E_{\tilde{\mu}}^{(0)})} \quad (3.19)$$

$$= \sum_{\tilde{\mu}} \langle \tilde{n} | \mathbf{P} \mathbf{H}_1 \mathbf{Q} | \tilde{\mu} \rangle \langle \tilde{\mu} | \mathbf{Q} \mathbf{H}_1 \mathbf{P} | \tilde{m} \rangle \left(\frac{E_{\tilde{m}}^{(0)} - E_{\tilde{n}}^{(0)}}{(E_{\tilde{n}}^{(0)} - E_{\tilde{\mu}}^{(0)})(E_{\tilde{m}}^{(0)} - E_{\tilde{\mu}}^{(0)})} \right) \quad (3.20)$$

The matrix elements $\langle \tilde{n} | \mathbf{V}_- | \tilde{m} \rangle$ are proportional to the energy difference of the states \tilde{m} and \tilde{n} . This same energy difference also enters the denominator of the energy correction

$\tilde{E}_{\tilde{n}}^{(1)} = \tilde{E}_{\tilde{n}}^{(2)} = 0$
$\tilde{E}_{\tilde{n}}^{(3)} = 0$
$\tilde{E}_{\tilde{n}}^{(4)} + \tilde{E}_{\tilde{n}}^{(5)} = - \sum_{\tilde{\mu} \in \mathbb{D}} \frac{\langle \tilde{n} \mathbf{V}_- \tilde{\mu} \rangle \langle \tilde{\mu} \mathbf{V}_- \tilde{n} \rangle}{\Delta E_{\tilde{\mu}}}$

Table 3.2: Energy corrections up to fifth order of perturbation theory for degenerate states. The eigenstates of $\tilde{\mathbf{H}}_0$ are labelled $\tilde{\mu}$. The state $\tilde{n} \in \mathbb{D}$ is eigenstate of $\tilde{\mathbf{H}}_0$ with eigenvalue $E_{\tilde{n}}^{(0)}$. \mathbb{D} is the linear space that is spanned by all states that are degenerate or nearly degenerate with the state n , an eigenstate to \mathbf{H}_0 . The operator \mathbf{P} projects in \mathbb{D} and \mathbf{Q} into the complement of \mathbb{D} in the total Hilbert space \mathbb{H} . We use the abbreviation $\Delta E_{\tilde{\mu}} = E_{\tilde{n}}^{(0)} - E_{\tilde{\mu}}^{(0)}$. Compare with table 3.1.

terms that contain matrix elements of \mathbf{V}_- . Exactly this energy difference causes the problems because it is an energy difference of states in \mathbb{D} . But as both numerator and denominator contain these differences they cancel out and the fraction stays finite. The matrix elements of the third order parts of \mathbf{V}_- can be evaluated correspondingly.

If the states are exactly degenerate, then the above treatment is not necessary. In this case a much simpler standard treatment exists. We already noted that in a degenerate subspace \mathbf{V}_L equals \mathbf{V}_R and both are hermitian. So the construction of \mathbf{V}_+ and \mathbf{V}_- is not needed. Furthermore it is possible to diagonalize an hermitian operator in a degenerate subspace of another hermitian operator without losing the diagonality of the latter operator. This means that we can diagonalize \mathbf{V}_L in the degenerate subspace and the resulting eigenstates of \mathbf{V}_L are still eigenstates of \mathbf{H}_0 . Using these states for the perturbation expansion assures that the nominator in the expansion stays finite.

“Therefore you don’t have a single answer to your questions?”
“Adso, if I did I would teach theology in Paris.”
“In Paris do they always have the true answer?”
“Never”, William said, “but they are very sure of their errors.”

Umberto Eco, *The Name of the Rose*

4 Magnetic Models

One challenge of this work is to obtain an explanation for the ferromagnetic coupling between the Co2 sites in $\text{Ca}_3\text{Co}_2\text{O}_6$. Since $\text{Ca}_3\text{Co}_2\text{O}_6$ is not a metal [42, 65], it is unlikely that the magnetic coupling is due to itinerant magnetism. Therefore we favor a local explanation for the ferromagnetic coupling. Such local interactions arise in many cases from direct exchange [26,100] or superexchange [101–104]. In our case superexchange, involving the non-magnetic Co1 sites, is what we would expect to be the most important contribution. Direct exchange should be very small because the direct overlap of the Co2 wavefunctions is strongly suppressed due to the long distance between the sites. Using the well known Goodenough-Kanamori-Anderson rules (GKA) in this situation tells us that we should rather find antiferromagnetic coupling [28, 33, 103]. While this is the case for some isostructural compounds like $\text{Ca}_3\text{FeRhO}_6$, experiments reveal ferromagnetic intrachain coupling for $\text{Ca}_3\text{Co}_2\text{O}_6$ and $\text{Ca}_3\text{CoRhO}_6$ [17, 50, 81]. In many cases the GKA rules yield results in agreement with the experiments. But they are not applicable in certain distinct cases [105]. One example is the two-band Hubbard model at quarter-filling, where strong coupling and weak coupling approaches yield contradicting answers, resulting into a rich phase diagram [106–108]. Nevertheless, assuming that GKA provides the correct qualitative signature of the superexchange, there has to be a competing mechanism favoring ferromagnetic interaction. One of the potential competing interactions is the cyclic exchange interaction [109–111]. Cyclic exchange is possible in $\text{Ca}_3\text{Co}_2\text{O}_6$ by paths involving oxygen states. As we will see, cyclic exchange leads to ferromagnetic coupling under certain preconditions and for this reason it could explain the ferromagnetic coupling observed in $\text{Ca}_3\text{Co}_2\text{O}_6$.

Exchange models are often sufficient to describe magnetism in systems with localized electrons. These models are based on a perturbative treatment of the Hubbard model with the assumption of a local electron-electron interaction that is much larger than the kinetic overlap between the sites. This picture is particularly successful for transition metals in the insulating phase. There the d-orbitals are typically strongly localized, making the Coulomb repulsion an important energy scale of the system. In many cases there will be no direct overlap between the magnetic sites, instead the transition metal ions will be separated by anions

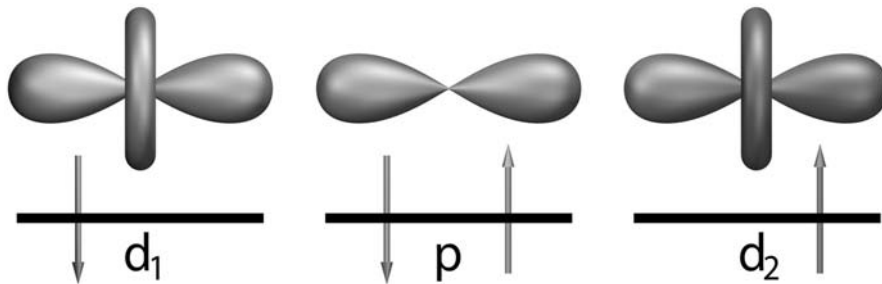


Fig. 4.1: Toy model for superexchange: Two d -sites are connected over one p -site. In this simple model we have only one orbital per site. The ground state for this configuration is a singlet state.

like oxygen. Perturbation theory to fourth order results in an effective coupling between the transition metal sites known as superexchange [101–103]. This effective coupling can either be ferromagnetic or antiferromagnetic depending on the symmetry relations between the orbitals that mediate the interaction [31, 33]. Another exchange mechanism possibly leading to ferromagnetic coupling is the ring exchange, where the electrons are moving on a cyclic path [111–113]. It can lead to both ferromagnetic and antiferromagnetic coupling depending on the sign of the hopping parameter that closes the cycle by directly connecting the magnetic sites.

4.1 Superexchange

We will discuss two simple albeit instructive examples to illustrate the possible exchange mechanisms leading to ferromagnetic or antiferromagnetic coupling. First let us consider two transition metal sites with one $3z^2 - r^2$ -orbital on each site, which are connected to an oxygen site through a p_z orbital (see figure 4.1). We will denote the oxygen p -state with spin σ by $|p_\sigma\rangle$. The corresponding energy level and Hubbard energy are denoted ϵ_p and U_p , respectively. The d -states are labelled $|d_{1/2\sigma}\rangle$ with energy ϵ_d and Coulomb repulsion U_d . An electron is created in the state $|p_\sigma\rangle$ with the operator $\mathbf{p}_\sigma^\dagger$ and in a d -state with $\mathbf{d}_{1/2\sigma}^\dagger$. The number operators \mathbf{n} are indexed accordingly. With these conventions we have the Hamiltonian:

$$\mathbf{H}_S = \sum_{\sigma} (\epsilon_p \mathbf{n}_{p\sigma} + \epsilon_d \mathbf{n}_{d1\sigma} + \epsilon_d \mathbf{n}_{d2\sigma}) + U_p \mathbf{n}_{p\uparrow} \mathbf{n}_{p\downarrow} + U_d \mathbf{n}_{d1\uparrow} \mathbf{n}_{d1\downarrow} + U_d \mathbf{n}_{d2\uparrow} \mathbf{n}_{d2\downarrow}, \quad (4.1)$$

$$-t \sum_{\sigma} (\mathbf{c}_{p\sigma}^\dagger \mathbf{c}_{d1\sigma} + \mathbf{c}_{p\sigma}^\dagger \mathbf{c}_{d2\sigma} + \mathbf{c}_{d1\sigma}^\dagger \mathbf{c}_{p\sigma} + \mathbf{c}_{d2\sigma}^\dagger \mathbf{c}_{p\sigma}).$$

To simplify this Hamiltonian we will use the freedom to choose a zero point for the energy scale and set ϵ_d to zero. The largest energy scale in the problem is U_d , therefore we will mea-

sure all energies in units of U_d and denote all quantities using this energy scale with a hat. Using this convention with $\hat{\mathbf{H}}_S = \mathbf{H}_S/U_d$, $\hat{\epsilon} = \epsilon_p/U_d$, $\hat{U} = U_p/U_d$, and $\hat{t} = t/U_d$ we have:

$$\begin{aligned} \hat{\mathbf{H}}_S &= \sum_{\sigma} \hat{\epsilon} \mathbf{n}_{p\sigma} + \hat{U} \mathbf{n}_{p\uparrow} \mathbf{n}_{p\downarrow} + \mathbf{n}_{d1\uparrow} \mathbf{n}_{d1\downarrow} + \mathbf{n}_{d2\uparrow} \mathbf{n}_{d2\downarrow}, \\ &\quad - \hat{t} \sum_{\sigma} (\mathbf{c}_{p\sigma}^{\dagger} \mathbf{c}_{d1\sigma} + \mathbf{c}_{p\sigma}^{\dagger} \mathbf{c}_{d2\sigma} + \mathbf{c}_{d1\sigma}^{\dagger} \mathbf{c}_{p\sigma} + \mathbf{c}_{d2\sigma}^{\dagger} \mathbf{c}_{p\sigma}). \end{aligned} \quad (4.2)$$

In particular this Hamiltonian conserves the particle number and the z -component of the total spin m_z . Thus it is possible to work in subspaces with a fixed number of particles per spin direction. Suppose we wish to calculate the energy difference between an ‘‘antiferromagnetic state’’ ($m_z = 0$) and the corresponding ‘‘ferromagnetic state’’ ($m_z = 1$) with the same total number of particles. To that aim we choose the antiferromagnetic state to have two up spins and two down spins, the ferromagnetic state has three up spins and one down spin. In the regime of $\hat{t} \ll 1$ we can treat the problem with perturbation theory, where we call the local part of the Hamiltonian $\hat{\mathbf{H}}_{\text{loc}}^D$ and the perturbative hopping part $\hat{\mathbf{H}}_{\text{hop}}^D$, with $\hat{\mathbf{H}}_D = \hat{\mathbf{H}}_{\text{loc}}^D + \hat{\mathbf{H}}_{\text{hop}}^D$ and:

$$\hat{\mathbf{H}}_{\text{loc}}^D = \sum_{\sigma} \hat{\epsilon} \mathbf{n}_{p\sigma} + \hat{U} \mathbf{n}_{p\uparrow} \mathbf{n}_{p\downarrow} + \mathbf{n}_{d1\uparrow} \mathbf{n}_{d1\downarrow} + \mathbf{n}_{d2\uparrow} \mathbf{n}_{d2\downarrow}, \quad (4.3)$$

$$\hat{\mathbf{H}}_{\text{hop}}^D = -\hat{t} \sum_{\sigma} (\mathbf{c}_{p\sigma}^{\dagger} \mathbf{c}_{d1\sigma} + \mathbf{c}_{p\sigma}^{\dagger} \mathbf{c}_{d2\sigma} + \mathbf{c}_{d1\sigma}^{\dagger} \mathbf{c}_{p\sigma} + \mathbf{c}_{d2\sigma}^{\dagger} \mathbf{c}_{p\sigma}). \quad (4.4)$$

As we are only interested in the question which spin configuration has the lowest energy we have to regard the lowest order in \hat{t} that makes a difference between the configurations. To second order there is no difference between the ferromagnetic and the antiferromagnetic configuration. The lowest order that contributes to an energy difference is the fourth order. Therefore we have to calculate the fourth order terms of the perturbation expansion in \hat{t} . With only one orbital on each site no explicit diagonalization of $\hat{\mathbf{H}}_{\text{loc}}^D$ is necessary.

The Hilbert space of the antiferromagnetic configuration is spanned by nine basis vectors. Table 4.1 shows all eigenvectors of $\hat{\mathbf{H}}_{\text{loc}}^D$ together with the notation and the eigenvalues. In the strong coupling regime, $\hat{\epsilon} + \hat{U} < 1$, the ground states are $|\uparrow\downarrow\downarrow\rangle$ and $|\downarrow\uparrow\uparrow\rangle$; they build a twofold degenerate subspace. All eigenstates are distributed over four energy subspaces, three of which have a dimension higher than one. The reason for the degenerate eigenstates is that the Hamiltonian $\hat{\mathbf{H}}_{\text{loc}}^D$ is invariant under two symmetry operations, namely the spin flip of the z -component of the total spin and the permutation of the sites d_1 and d_2 . To make use of the symmetries we introduce the symmetry adapted eigenstates of $\hat{\mathbf{H}}_{\text{loc}}^D$, meaning the respective symmetric and antisymmetric combinations (see table 4.1). For the definition of symmetric and antisymmetric states one has to be careful to get the right phase due to the anticommutation of the fermionic operators. Although the lowest energy states are degenerate we are allowed to proceed with standard perturbation theory. This has two reasons: First, there are no corrections in second order degenerate perturbation theory, because all hopping matrix element between the degenerate ground states are zero. Second, none of the excited states has a finite hopping amplitude with both of the degenerate ground states, a fact that as-

sures the validity of the fourth order expansion (for a discussion of high-order perturbation theory see section 3).

With the use of the symmetrized eigenstates of $\hat{\mathbf{H}}_{\text{loc}}^{\text{D}}$, the hopping matrix $H^{mn} = \langle m | \hat{\mathbf{H}}_{\text{hop}}^{\text{D}} | n \rangle$ is significantly simplified. It is now block diagonal (see table 4.2) and we can use the sub blocks that contain the degenerate ground states to build the corresponding fourth order expansion. Using the formulae derived in section 3 and the tables 4.1 and 4.2 we get:

$$\hat{E}_{\text{D},1'_f}^{(4)} = \frac{4\hat{t}^4}{(\hat{\epsilon} + \hat{U} - 1)^2} \left(\frac{2}{2(\hat{\epsilon} - 1) + \hat{U}} - 1 \right), \quad (4.5)$$

$$\hat{E}_{\text{D},2'_f}^{(4)} = 0. \quad (4.6)$$

A detailed analysis of the perturbation expansion shows that there is an additional term for both energy corrections. It originates from the repetition of second order processes, and is not considered as a genuine fourth order process. In the calculation for the ferromagnetic states we will again find the same term, which allows us to omit this term, as it does not contribute to an energy difference. For the state $|2'_a\rangle$ there is no genuine fourth order process. We assumed $\epsilon + U < 1$ which means that the fourth order energy correction to the state $|1'_a\rangle$ is negative and therefore $|1'_a\rangle$ is the lowest state in the antiferromagnetic case.

The calculation for the ferromagnetic case is equivalent, so we do not describe it in detail. Only three states span the Hilbert space in this case, making the evaluation much easier. Performing the same steps as above we find that the lowest state $|1_f\rangle$ has the same unperturbed energy and the same second order corrections as $|1'_a\rangle$. The abovementioned non-genuine

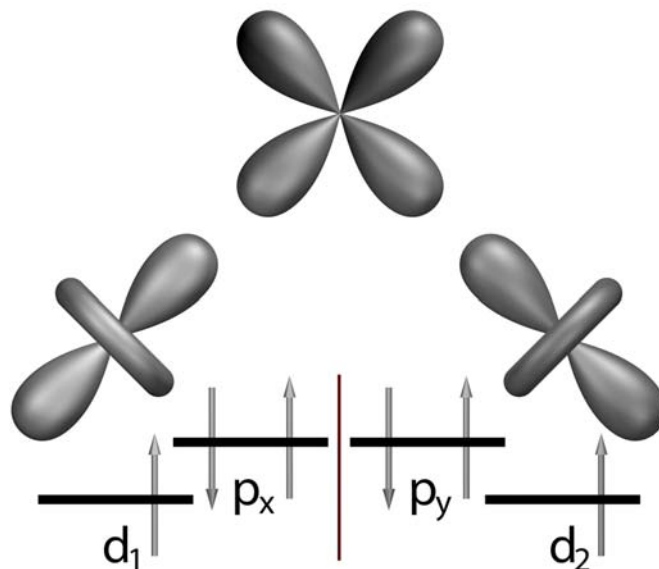


Fig. 4.2: Orthogonal superexchange: Two d -sites are connected over two orthogonal p -orbitals. The hopping Hamiltonian does not couple the two d -sites in any order of perturbation theory. The energy difference between singlet and triplet is due to Hund's rule on the p -site. Then the ferromagnetic state is the ground state.

Direct Superexchange: Definition of Antiferromagnetic Eigenstates and Ket Notation									
\mathbf{d}_1		\mathbf{p}		\mathbf{d}_2		eigenval. units: U_d	ket notation		symmetric eigenstates definition
\uparrow	\downarrow	\uparrow	\downarrow	\uparrow	\downarrow		nr	symbolic	
\times	$-$	\times	\times	$-$	\times	$2\hat{e} + \hat{U}$	$ 1_a\rangle$	$ \uparrow- \uparrow\downarrow -\downarrow\rangle$	$ 1'_a\rangle = \frac{1}{\sqrt{2}}(1_a\rangle - 2_a\rangle)$
$-$	\times	\times	\times	\times	$-$	$2\hat{e} + \hat{U}$	$ 2_a\rangle$	$ \downarrow- \uparrow\downarrow \uparrow-\rangle$	$ 2'_a\rangle = \frac{1}{\sqrt{2}}(1_a\rangle + 2_a\rangle)$
\times	\times	$-$	\times	\times	$-$	$\hat{e} + 1$	$ 3_a\rangle$	$ \uparrow\downarrow -\downarrow \uparrow-\rangle$	$ 3'_a\rangle = \frac{1}{2}(3_a\rangle - 4_a\rangle + 5_a\rangle - 6_a\rangle)$
\times	\times	\times	$-$	$-$	\times	$\hat{e} + 1$	$ 4_a\rangle$	$ \uparrow\downarrow \uparrow- -\downarrow\rangle$	$ 4'_a\rangle = \frac{1}{2}(3_a\rangle + 4_a\rangle + 5_a\rangle + 6_a\rangle)$
$-$	\times	\times	$-$	\times	\times	$\hat{e} + 1$	$ 5_a\rangle$	$ \downarrow- \uparrow- \uparrow\downarrow\rangle$	$ 5'_a\rangle = \frac{1}{2}(3_a\rangle - 4_a\rangle - 5_a\rangle + 6_a\rangle)$
\times	$-$	$-$	\times	\times	\times	$\hat{e} + 1$	$ 6_a\rangle$	$ \uparrow- -\downarrow \uparrow\downarrow\rangle$	$ 6'_a\rangle = \frac{1}{2}(3_a\rangle + 4_a\rangle - 5_a\rangle - 6_a\rangle)$
\times	\times	\times	\times	$-$	$-$	$2\hat{e} + \hat{U} + 1$	$ 7_a\rangle$	$ \uparrow\downarrow \uparrow\downarrow --\rangle$	$ 7'_a\rangle = \frac{1}{\sqrt{2}}(7_a\rangle + 8_a\rangle)$
$-$	$-$	\times	\times	\times	\times	$2\hat{e} + \hat{U} + 1$	$ 8_a\rangle$	$ -- \uparrow\downarrow \uparrow\downarrow\rangle$	$ 8'_a\rangle = \frac{1}{\sqrt{2}}(7_a\rangle - 8_a\rangle)$
\times	\times	$-$	$-$	\times	\times	2	$ 9_a\rangle$	$ \uparrow\downarrow -- \uparrow\downarrow\rangle$	$ 9'_a\rangle = 9_a\rangle$
Direct Superexchange: Definition of Ferromagnetic Eigenstates and Ket Notation									
\mathbf{d}_1		\mathbf{p}		\mathbf{d}_2		eigenval. units: U_d	ket notation		symmetric eigenstates definition
\uparrow	\downarrow	\uparrow	\downarrow	\uparrow	\downarrow		nr	symbolic	
\times	$-$	\times	\times	\times	$-$	$2\hat{e} + \hat{U}$	$ 1_f\rangle$	$ \uparrow- \uparrow\downarrow \uparrow-\rangle$	$ 1'_f\rangle = 1_f\rangle$
\times	\times	\times	$-$	\times	$-$	$\hat{e} + 1$	$ 2_f\rangle$	$ \uparrow\downarrow \uparrow- \uparrow-\rangle$	$ 2'_f\rangle = \frac{1}{\sqrt{2}}(2_f\rangle - 3_f\rangle)$
\times	$-$	\times	$-$	\times	\times	$\hat{e} + 1$	$ 3_f\rangle$	$ \uparrow- \uparrow- \uparrow\downarrow\rangle$	$ 3'_f\rangle = \frac{1}{\sqrt{2}}(2_f\rangle + 3_f\rangle)$

Table 4.1: Direct superexchange: all nine eigenstates of \hat{H}_{loc}^D with $S_z = 0$ and the three eigenstates with $S_z = 1$. The eigenvalues are given in units of U_d with $\epsilon_d = 0$. The column “ket notation” presents the nomenclature we use in the text. The symmetry adapted eigenstates are defined in the last column. For $\hat{e} + \hat{U} < 1$ the ground states are $|1_a\rangle$, $|2_a\rangle$, and $|1_f\rangle$ or alternatively $|1'_a\rangle$, $|2'_a\rangle$, and $|1'_f\rangle$.

fourth order term is obviously also the same for $|1'_a\rangle$ and $|1_f\rangle$. A genuine fourth order term, which correlates d_1 and d_2 does not exist, in contrary to the case of $|2'_a\rangle$. This makes the singlet state $|1'_a\rangle$ the ground state and the energy difference between singlet and the triplet states is:

$$\Delta\hat{E}_D = E_{\text{singlet}} - E_{\text{triplet}} = \frac{4\hat{t}^4}{(\hat{e} + \hat{U} - 1)^2} \left(\frac{2}{2(\hat{e} - 1) + \hat{U}} - 1 \right) < 0. \quad (4.7)$$

If we assume $\hat{e}, \hat{U} \ll 1$ and rewrite the result in standard energy units we get: $\Delta E_D = -8t^4/U_d^3$. If hopping is mediated over a single orbital, the Pauli principle imposes strong restrictions on possible hopping paths in the ferromagnetic arrangement. This ultimately leads to an effective antiferromagnetic coupling.

Direct Superexchange: Evaluation of $\hat{\mathbf{H}}_{\text{hop}}^{\text{D}}$ in the Antiferromagnetic Hilbert Space

$\hat{\mathbf{H}}_{\text{hop}}^{\text{D}} 1_a\rangle = \hat{t} 4_a\rangle + \hat{t} 6_a\rangle$	$\hat{\mathbf{H}}_{\text{hop}}^{\text{D}} 1'_a\rangle = -\sqrt{2} \hat{t} 3'_a\rangle$
$\hat{\mathbf{H}}_{\text{hop}}^{\text{D}} 2_a\rangle = \hat{t} 3_a\rangle + \hat{t} 5_a\rangle$	$\hat{\mathbf{H}}_{\text{hop}}^{\text{D}} 3'_a\rangle = \sqrt{2} \hat{t} (- 1'_a\rangle + 7'_a\rangle + 9'_a\rangle)$
$\hat{\mathbf{H}}_{\text{hop}}^{\text{D}} 3_a\rangle = \hat{t} 2_a\rangle + \hat{t} 7_a\rangle + \hat{t} 9_a\rangle$	$\hat{\mathbf{H}}_{\text{hop}}^{\text{D}} 7'_a\rangle = \sqrt{2} \hat{t} 3'_a\rangle$
$\hat{\mathbf{H}}_{\text{hop}}^{\text{D}} 4_a\rangle = \hat{t} 1_a\rangle - \hat{t} 7_a\rangle - \hat{t} 9_a\rangle$	$\hat{\mathbf{H}}_{\text{hop}}^{\text{D}} 9'_a\rangle = \sqrt{2} \hat{t} 3'_a\rangle$
$\hat{\mathbf{H}}_{\text{hop}}^{\text{D}} 5_a\rangle = \hat{t} 2_a\rangle + \hat{t} 8_a\rangle + \hat{t} 9_a\rangle$	$\hat{\mathbf{H}}_{\text{hop}}^{\text{D}} 2'_a\rangle = \sqrt{2} \hat{t} 4'_a\rangle$
$\hat{\mathbf{H}}_{\text{hop}}^{\text{D}} 6_a\rangle = \hat{t} 1_a\rangle - \hat{t} 8_a\rangle - \hat{t} 9_a\rangle$	$\hat{\mathbf{H}}_{\text{hop}}^{\text{D}} 4'_a\rangle = \sqrt{2} \hat{t} 2'_a\rangle$
$\hat{\mathbf{H}}_{\text{hop}}^{\text{D}} 7_a\rangle = \hat{t} 3_a\rangle - \hat{t} 4_a\rangle$	$\hat{\mathbf{H}}_{\text{hop}}^{\text{D}} 5'_a\rangle = \sqrt{2} \hat{t} 8'_a\rangle$
$\hat{\mathbf{H}}_{\text{hop}}^{\text{D}} 8_a\rangle = \hat{t} 5_a\rangle - \hat{t} 6_a\rangle$	$\hat{\mathbf{H}}_{\text{hop}}^{\text{D}} 8'_a\rangle = \sqrt{2} \hat{t} 5'_a\rangle$
$\hat{\mathbf{H}}_{\text{hop}}^{\text{D}} 9_a\rangle = \hat{t} 3_a\rangle - \hat{t} 4_a\rangle + \hat{t} 5_a\rangle - \hat{t} 6_a\rangle$	$\hat{\mathbf{H}}_{\text{hop}}^{\text{D}} 6'_a\rangle = 0$

 Direct Superexchange: Evaluation of $\hat{\mathbf{H}}_{\text{hop}}^{\text{D}}$ in the Ferromagnetic Hilbert Space

$\hat{\mathbf{H}}_{\text{hop}}^{\text{D}} 1_f\rangle = \hat{t} 2_f\rangle + \hat{t} 2_f\rangle$	$\hat{\mathbf{H}}_{\text{hop}}^{\text{D}} 1'_f\rangle = \sqrt{2} \hat{t} 3'_f\rangle$
$\hat{\mathbf{H}}_{\text{hop}}^{\text{D}} 2_f\rangle = \hat{t} 1_f\rangle$	$\hat{\mathbf{H}}_{\text{hop}}^{\text{D}} 3'_f\rangle = \sqrt{2} \hat{t} 1'_f\rangle$
$\hat{\mathbf{H}}_{\text{hop}}^{\text{D}} 3_f\rangle = \hat{t} 1_f\rangle$	$\hat{\mathbf{H}}_{\text{hop}}^{\text{D}} 2'_f\rangle = 0$

Table 4.2: Direct superexchange: $\hat{\mathbf{H}}_{\text{hop}}^{\text{D}}$ acting on Hilbert space vectors. The left column shows the results for the usual direct product states whereas in the right column the results for the symmetry adapted eigenstates of $\hat{\mathbf{H}}_{\text{loc}}^{\text{D}}$ are listed. Definitions of the states can be found in table 4.1. The hopping matrix for the symmetry adapted states decomposes in four subspaces, they are indicated by the horizontal lines in the right column.

4.2 Hopping via Orthogonal Orbitals

A completely different situation arises if we introduce two p-orbitals on the central atom, as is depicted in figure 4.2. The main difference in this setup is that one of the central orbitals is only accessible by the electrons on d_1 and the other one only by electrons on d_2 . There is no hopping path for an electron from d_1 to d_2 . In this configuration the singlet state is not favored by a higher number of accessible paths, in contrast to the previous example. Indeed, in the border case $U_d = 0$, singlet and triplet states are degenerate. Another two-particle energy scale plays an important role for p-orbitals, namely the Hund's coupling J . This local interaction couples electrons on different orbitals on the same site. It lowers the energy of high spin states of an atom, favoring the formation of a magnetic moment. A thorough investigation shows that generically the ferromagnetic coupling, that results from orthogonal superexchange is significantly weaker than the antiferromagnetic coupling due to direct superexchange. The modified Hamiltonian for the orthogonal superexchange is of the following form:

Orthogonal Superexchange: Definition of Antiferromagnetic Eigenstates										
\mathbf{d}_1		\mathbf{p}_x		\mathbf{p}_y		\mathbf{d}_2		eigenvalues	ket notation	
\uparrow	\downarrow	\uparrow	\downarrow	\uparrow	\downarrow	\uparrow	\downarrow	in units of U_d	nr	symbolic
\times	$-$	\times	\times	\times	\times	$-$	\times	$4\hat{\epsilon} + 2(\hat{U} + \hat{J})$	$ 1_a\rangle$	$ \uparrow\downarrow\uparrow\downarrow\rangle$
$-$	\times	\times	\times	\times	\times	\times	$-$	$4\hat{\epsilon} + 2(\hat{U} + \hat{J})$	$ 2_a\rangle$	$ \downarrow\uparrow\downarrow\uparrow\rangle$
\times	\times	\times	$-$	\times	\times	$-$	\times	$3\hat{\epsilon} + \hat{U} + \hat{J} + 1$	$ 3_a\rangle$	$ \uparrow\downarrow\uparrow\downarrow\rangle$
\times	\times	$-$	\times	\times	\times	\times	$-$	$3\hat{\epsilon} + \hat{U} + \hat{J} + 1$	$ 4_a\rangle$	$ \uparrow\downarrow\downarrow\uparrow\rangle$
\times	$-$	\times	\times	$-$	\times	\times	\times	$3\hat{\epsilon} + \hat{U} + \hat{J} + 1$	$ 5_a\rangle$	$ \uparrow\downarrow\downarrow\uparrow\rangle$
$-$	\times	\times	\times	\times	$-$	\times	\times	$3\hat{\epsilon} + \hat{U} + \hat{J} + 1$	$ 6_a\rangle$	$ \downarrow\uparrow\downarrow\uparrow\rangle$
\times	\times	\times	$-$	$-$	\times	\times	\times	$2\hat{\epsilon} + \hat{J} + 2$	$ 7_a\rangle$	$ \uparrow\downarrow\uparrow\downarrow\rangle$
\times	\times	$-$	\times	\times	$-$	\times	\times	$2\hat{\epsilon} + \hat{J} + 2$	$ 8_a\rangle$	$ \uparrow\downarrow\downarrow\uparrow\rangle$
Orthogonal Superexchange: Definition of Ferromagnetic Eigenstates										
\mathbf{d}_1		\mathbf{p}_x		\mathbf{p}_y		\mathbf{d}_2		eigenvalues	ket notation	
\uparrow	\downarrow	\uparrow	\downarrow	\uparrow	\downarrow	\uparrow	\downarrow	in units of U_d	nr	symbolic
\times	$-$	\times	\times	\times	\times	\times	$-$	$4\hat{\epsilon} + 2(\hat{U} + \hat{J})$	$ 1_f\rangle$	$ \uparrow\downarrow\uparrow\downarrow\rangle$
\times	\times	\times	$-$	\times	\times	\times	$-$	$3\hat{\epsilon} + \hat{U} + \hat{J} + 1$	$ 2_f\rangle$	$ \uparrow\downarrow\uparrow\downarrow\rangle$
\times	$-$	\times	\times	\times	$-$	\times	\times	$3\hat{\epsilon} + \hat{U} + \hat{J} + 1$	$ 3_f\rangle$	$ \uparrow\downarrow\uparrow\downarrow\rangle$
\times	\times	\times	$-$	\times	$-$	\times	\times	$2\hat{\epsilon} + 2$	$ 4_f\rangle$	$ \uparrow\downarrow\uparrow\downarrow\rangle$

Table 4.3: Orthogonal superexchange: all eigenstates of $\hat{H}_{\text{loc}}^{\text{O}}$ with $S_z = 0$ and $S_z = 1$ are listed. The eigenvalues are given in units of U_d with $\epsilon_d = 0$. The column “ket notation” presents the nomenclature we use in the text. The symmetry adapted eigenstates are defined in analogy to the definitions given in table 4.1.

$$\hat{H}_{\text{O}} = \hat{H}_{\text{loc}}^{\text{O}} + \hat{H}_{\text{hop}}^{\text{O}} \quad (4.8)$$

with

$$\begin{aligned} \hat{H}_{\text{loc}}^{\text{O}} = & \hat{\epsilon} \sum_{\sigma} (\mathbf{n}_{\text{p}_y \sigma} + \mathbf{n}_{\text{p}_x \sigma}) + \hat{U} (\mathbf{n}_{\text{p}_x \uparrow} \mathbf{n}_{\text{p}_x \downarrow} + \mathbf{n}_{\text{p}_y \uparrow} \mathbf{n}_{\text{p}_y \downarrow}) \\ & + \hat{J} \sum_{\sigma} \mathbf{c}_{\text{p}_y \sigma}^{\dagger} \mathbf{c}_{\text{p}_x \bar{\sigma}}^{\dagger} \mathbf{c}_{\text{p}_y \bar{\sigma}} \mathbf{c}_{\text{p}_x \sigma} + \mathbf{n}_{\text{d}1 \uparrow} \mathbf{n}_{\text{d}1 \downarrow} + \mathbf{n}_{\text{d}2 \uparrow} \mathbf{n}_{\text{d}2 \downarrow}, \end{aligned} \quad (4.9)$$

$$\hat{H}_{\text{hop}}^{\text{O}} = -\hat{t} \sum_{\sigma} (\mathbf{c}_{\text{p}_x \sigma}^{\dagger} \mathbf{c}_{\text{d}1 \sigma} + \mathbf{c}_{\text{p}_y \sigma}^{\dagger} \mathbf{c}_{\text{d}2 \sigma} + \mathbf{c}_{\text{d}1 \sigma}^{\dagger} \mathbf{c}_{\text{p}_x \sigma} + \mathbf{c}_{\text{d}2 \sigma}^{\dagger} \mathbf{c}_{\text{p}_y \sigma}). \quad (4.10)$$

We chose the same conventions as in table 4.2, where all energies are measured with respect to ϵ_d and in units of U_d . The Hund’s coupling $\hat{J} = J/U_d$ is a positive real number, which usually fulfills the condition $\hat{J} \ll 1$. The calculation is again equivalent to the one for the

antiferromagnetic direct superexchange, so we will not discuss the details of the calculation. A definition of the states we used is given in table 4.3. Under the condition $\hat{\epsilon} + \hat{U} + \hat{J} < 1$ the result is:

$$\Delta \hat{E}_O = \hat{E}_{\text{singlet}} - E_{\text{triplet}} = \frac{2\hat{t}^4}{(\hat{\epsilon} + \hat{U} + \hat{J} - 1)^3} \frac{\hat{J}}{(2(\hat{\epsilon} + \hat{U} + \hat{J} - 1) - \hat{J})} > 0. \quad (4.11)$$

If we again assume $1 \gg \hat{J}, \hat{U}$, and $\hat{\epsilon}$, and reintroduce the standard units, we get: $\Delta E_O = J t^4 / U_d^4$. We can compare this to the equivalently approximated result for ΔE_D and find:

$$\lim_{\hat{\epsilon}, \hat{J}, \hat{U} \rightarrow 0} \left| \frac{\Delta E_D}{\Delta E_O} \right| \rightarrow \frac{8U_d}{J} \gg 1. \quad (4.12)$$

In $\text{Ca}_3\text{Co}_2\text{O}_6$ the intermediate states are not p-states, but d-states. Therefore \hat{U} can not be neglected, as it is comparable to 1. We will now assume that it is exactly 1. Under these circumstances the energy corrections in fourth order become:

$$\lim_{\hat{U} \rightarrow 1} \Delta \hat{E}_D \rightarrow -\frac{4\hat{t}^4(3 - 2\hat{\epsilon})}{\hat{\epsilon}^2(1 - 2\hat{\epsilon})}, \quad (4.13)$$

$$\lim_{\hat{U} \rightarrow 1} \Delta \hat{E}_O \rightarrow \frac{2\hat{t}^4\hat{J}}{(\hat{\epsilon} + \hat{J})^3(2(\hat{\epsilon} + \hat{J}) - \hat{J})}. \quad (4.14)$$

In order to develop a more realistic model one would have to introduce more than one level on the sites d_1 and d_2 . But the simplest model already shows the trend: direct superexchange favors antiferromagnetic coupling and orthogonal superexchange brings an energy advantage for the ferromagnetic case. These results are known in the literature as the Goodenough-Kanamori-Anderson rules [31, 33]. These rules are not strict. Nevertheless in many cases they give at least a qualitatively correct description. But there are examples when these rules fail, e.g., due to the suppression of the antiferromagnetic paths as a consequence of quantum interference effects [105, 114].

4.3 Ring Exchange

In the previous discussion only even orders of perturbation theory contributed to the effective interaction between the total spins on the sites d_1 and d_2 . This is a consequence of the fact that the Hamiltonian did not support cyclic paths. Let us now investigate a very simple situation which, to a large extent, is equivalent to the problem we already discussed as direct superexchange. The only difference to the direct superexchange is that the hopping part of the Hamiltonian contains additional terms allowing an electron to hop directly from d_1 to d_2 and vice versa. Again we write the total Hamiltonian as a sum of a local and a hopping contributions:

$$\hat{\mathbf{H}}_C = \hat{\mathbf{H}}_{\text{loc}}^C + \hat{\mathbf{H}}_{\text{hop}}^C \quad (4.15)$$

with

$$\hat{\mathbf{H}}_{\text{loc}}^C = \hat{\mathbf{H}}_{\text{loc}}^D = \sum_{\sigma} \hat{\epsilon} \mathbf{n}_{p\sigma} + \hat{U} \mathbf{n}_{p\uparrow} \mathbf{n}_{p\downarrow} + \mathbf{n}_{d1\uparrow} \mathbf{n}_{d1\downarrow} + \mathbf{n}_{d2\uparrow} \mathbf{n}_{d2\downarrow}, \quad (4.16)$$

$$\begin{aligned} \hat{\mathbf{H}}_{\text{hop}}^C &= -\hat{t}_1 \sum_{\sigma} (\mathbf{c}_{p\sigma}^{\dagger} \mathbf{c}_{d1\sigma} + \mathbf{c}_{p\sigma}^{\dagger} \mathbf{c}_{d2\sigma} + \mathbf{c}_{d1\sigma}^{\dagger} \mathbf{c}_{p\sigma} + \mathbf{c}_{d2\sigma}^{\dagger} \mathbf{c}_{p\sigma}) \\ &\quad -\hat{t}_2 \sum_{\sigma} (\mathbf{c}_{d1\sigma}^{\dagger} \mathbf{c}_{d2\sigma} + \mathbf{c}_{d2\sigma}^{\dagger} \mathbf{c}_{d1\sigma}). \end{aligned} \quad (4.17)$$

We want to discuss an example with a four-electron occupation. Because the local Hamiltonian is the same as in the case of direct superexchange and also the occupation is identical we can use the results of table 4.1. The evaluation of the hopping Hamiltonian is straight forward and similar to previous results. A difference is that the hopping is now governed by two different hopping parameters \hat{t}_1 and \hat{t}_2 . In contrast to the situations in the previous perturbation expansions, there exists now a finite third order term. Due to the direct overlap between the sites d_1 and d_2 there is also an important second order contribution. Again we assume the condition $\hat{U} + \hat{\epsilon} < 1$ that makes the singlet and triplet states the degenerate ground states of the unperturbed problem. The expansion yields the following energy corrections for singlet and triplet states:

$$E_{C,\text{singlet}}^{(2)} = \frac{2\hat{t}_1^2}{\hat{\epsilon} + \hat{U} - 1} - 4\hat{t}_2^2, \quad (4.18)$$

$$E_{C,\text{singlet}}^{(3)} = \frac{2\hat{t}_1^2 \hat{t}_2}{(\hat{\epsilon} + \hat{U} - 1)^2} - \frac{8\hat{t}_1^2 \hat{t}_2}{\hat{\epsilon} + \hat{U} - 1}, \quad (4.19)$$

$$E_{C,\text{triplet}}^{(2)} = \frac{2\hat{t}_1^2}{\hat{\epsilon} + \hat{U} - 1}, \quad (4.20)$$

$$E_{C,\text{triplet}}^{(3)} = \frac{-2\hat{t}_1^2 \hat{t}_2}{(\hat{\epsilon} + \hat{U} - 1)^2}. \quad (4.21)$$

These corrections lift the degeneracy of singlet and triplet states. The energy splitting is:

$$\Delta E_C^{(2)} = E_{C,\text{singlet}}^{(2)} - E_{C,\text{triplet}}^{(2)} = -4\hat{t}_2^2 < 0, \quad (4.22)$$

$$\Delta E_C^{(3)} = E_{C,\text{singlet}}^{(3)} - E_{C,\text{triplet}}^{(3)} = \frac{4\hat{t}_1^2 \hat{t}_2}{\hat{\epsilon} + \hat{U} - 1} \left(\frac{1}{\hat{\epsilon} + \hat{U} - 1} - 2 \right). \quad (4.23)$$

The second order energy splitting is independent of \hat{t}_1 and unambiguously negative, favoring the singlet state. The sign of the third order splitting depends on the sign of \hat{t}_2 . If \hat{t}_2 is positive, the third order correction lowers the energy of the triplet compared to the singlet. The nature of the ground state in the case $\hat{t}_2 > 0$, is the result of a competition between second and third order terms. Indeed a ferromagnetic ground state is stable within a finite param-

4 *Magnetic Models*

eter regime [109–111]. A more detailed discussion of cyclic exchange is given in Fazekas' book [115]. The important point of this discussion for our calculation is that cyclic paths are able to stabilize a ferromagnetic ground state. In the compound $\text{Ca}_3\text{Co}_2\text{O}_6$ the competition between ferro- and antiferromagnetic order is more complicated, because many more orbitals are involved. In $\text{Ca}_3\text{Co}_2\text{O}_6$ the third order processes exist but will not make a difference for ferro- and antiferromagnetic order. The first cyclic paths involving both magnetic Co2 sites occur in the fifth order. So the ground state is the result of the competition between fourth and fifth order in that case. The complex structure of $\text{Ca}_3\text{Co}_2\text{O}_6$ results in many possible hopping paths and therefore quantum interference plays an important role [105] in the theoretical understanding of this material.

5 Matrix Elements of the Coulomb Potential

The standard textbook Hubbard model deals with one orbital per site. If this orbital is doubly occupied the two electrons “feel” each other because of the Coulomb repulsion between the two negative electric charges. For a second electron on the orbital the system has to pay an extra energy U , the Hubbard on-site interaction U . In the more realistic case of three or five orbitals the situation becomes more involved. With exactly the same reasoning as before one would of course expect that there is also an interaction between electrons on different orbitals on the same site. This interaction is usually called U' . At first sight it looks like one will have to deal with many parameters to handle all the different interactions between the electrons in the various orbitals. Writing the problem in second quantization, one gets the following expression for a general two particle interaction:

$$\mathbf{H}_{\text{two}} = \sum_{\alpha\beta\gamma\delta} \langle \Psi_\alpha \Psi_\beta | \mathbf{V}(\vec{r}, \vec{r}') | \Psi_\gamma \Psi_\delta \rangle \mathbf{c}_\alpha^\dagger \mathbf{c}_\beta^\dagger \mathbf{c}_\delta \mathbf{c}_\gamma. \quad (5.1)$$

Here \mathbf{H}_{two} is used to indicate a two particle contribution to the Hamiltonian. Greek symbols number the single particle states involved in the problem. Ψ_α denotes a wave function for a specific state α , which includes spatial and spin degrees of freedom. $|\Psi_\alpha \Psi_\beta\rangle$ is a simple direct product of the wave function Ψ_α for particle one and Ψ_β for particle two. All the different interaction energies in the multiband Hubbard model are now given by the two-particle matrix elements of the Coulomb potential.

5.1 Evaluation of the Matrix Elements

In the following we focus on the cases where there either are only electrons in a d-shell or only in a p-shell. The matrix elements to evaluate have the form:

$$\begin{aligned} V_{vl,\sigma\sigma'\rho\rho'}^{mm'nn'} &= \langle \Psi_{vl,\sigma}^m \Psi_{vl,\sigma'}^{m'} | \frac{e^2}{4\pi\epsilon_0|\vec{r}-\vec{r}'|} | \Psi_{vl,\rho}^n \Psi_{vl,\rho'}^{n'} \rangle, \\ &= \langle R_\nu(r)Y_l^m(\Omega)R_\nu(r')Y_l^{m'}(\Omega') | \frac{e^2}{4\pi\epsilon_0|\vec{r}-\vec{r}'|} | R_\nu(r)Y_l^n(\Omega)R_\nu(r')Y_l^{n'}(\Omega') \rangle \\ &\quad \times \langle \sigma\sigma' | \rho\rho' \rangle. \end{aligned} \quad (5.2)$$

In this equation l is the angular momentum, and ν the main quantum number of the orbitals. The values n and m refer to the z -projection of l , σ and ρ denote spin degrees of freedom, and Ω is the solid angle. Primed variables are related to the second electron whereas non primed variables refer to the first electron (we can differentiate between the two electrons because we explicitly evaluate a non symmetrized matrix element). The Coulomb potential does not operate on the spin degrees of freedom. The scalar product of the orthonormalized spin vectors then gives Kronecker deltas. Now we concentrate on the spatial part of the above equation

$$V_{vl,\sigma\sigma'\rho\rho'}^{mm'nn'} = V_{vl}^{mm'nn'} \delta_{\sigma\rho} \delta_{\sigma'\rho'}, \quad (5.4)$$

where

$$V_{vl}^{mm'nn'} = \langle R_\nu(r)Y_l^m(\Omega)R_\nu(r')Y_l^{m'}(\Omega') | \frac{e^2}{4\pi\epsilon_0|\vec{r}-\vec{r}'|} | R_\nu(r)Y_l^n(\Omega)R_\nu(r')Y_l^{n'}(\Omega') \rangle. \quad (5.5)$$

The wave functions are written in spherical coordinates. It is also possible to express the Coulomb potential in spherical coordinates:

$$\frac{e^2}{4\pi\epsilon_0|\vec{r}-\vec{r}'|} = \frac{e^2}{\epsilon_0} \sum_{l=0}^{\infty} \sum_{m=-l}^l \frac{r_{<}^l}{(2l+1)r_{>}^{l+1}} Y_l^{m*}(\Omega') Y_l^m(\Omega). \quad (5.6)$$

With $r_{<} = \min(r,r')$ and $r_{>} = \max(r,r')$. In the following formulae we use the abbreviation $\nu_l(r,r') = r_{<}^l \cdot (2l+1)^{-1} r_{>}^{-l-1}$. Inserting the expansion in the expression for the matrix elements yields:

$$\begin{aligned} V_{vl}^{mm'nn'} &= \frac{e^2}{\epsilon_0} \sum_{k=0}^{\infty} \sum_{m_k=-k}^k \left(\int dr \int dr' \nu_k(r,r') |R_\nu(r)|^2 |R_\nu(r')|^2 r^2 r'^2 \right) \\ &\quad \times \int d\Omega Y_k^{m_k}(\Omega) Y_l^{m*}(\Omega) Y_l^n(\Omega) \int d\Omega' Y_k^{m_k*}(\Omega') Y_l^{m'*}(\Omega') Y_l^{n'}(\Omega'). \end{aligned} \quad (5.7)$$

The integration over r and r' gives a number that is only dependent on the main quantum number ν and the angular momentum k . We will call this number a_k , dropping ν because it is a fixed number for a given atom in our problem and it is of no further relevance in the

following considerations. Given the simple exponential form of the azimuthal dependence in the spherical harmonics we can perform the azimuth integration of the remaining integrals at once. This integration yields a product of Kronecker functions $\delta_{m_k-m+n} \delta_{m_k-n'+m'}$, which immediately leads to the condition $m + m' = n + n'$. At this point we are left with

$$V_l^{mm'nn'} = \frac{e^2}{\epsilon_0 4\pi} \sum_{k=0}^{\infty} a_k \sum_{m_k=-k}^k \delta_{m_k, n-m} \delta_{m_k, m'-n'} C_{lkm_k}^{mm'nn'} \quad (5.8)$$

$$\times \int_{-1}^1 d\xi P_k^{m_k}(\xi) P_l^m(\xi) P_l^n(\xi) \int_{-1}^1 d\xi' P_k^{m_k}(\xi') P_l^{m'}(\xi') P_l^{n'}(\xi'),$$

where

$$C_{lkm_k}^{mm'nn'} = (2l+1)^2 (2k+1) \frac{(k-m_k)!}{(k+m_k)!} \sqrt{\frac{(l-m)!}{(l+m)!} \cdot \frac{(l-n)!}{(l+n)!} \cdot \frac{(l-m')!}{(l+m')!} \cdot \frac{(l-n')!}{(l+n')!}} \quad (5.9)$$

We made the common substitution $\cos(\theta) = \xi$. For further simplifications we can use some properties of the associated Legendre functions $P_l^m(\xi)$. The first fact we notice is that the integrand of both integrals has odd parity for odd k , which means that both integrals vanish in this case. It can easily be proven by using the relation $P_l^m(-\xi) = (-1)^l P_l^m(\xi)$. Next we focus on one of the integrals in equation 5.8

$$I_{lkm_k}^{mn} = \int_{-1}^1 d\xi P_k^{m_k}(\xi) P_l^m(\xi) P_l^n(\xi). \quad (5.10)$$

We can restrict ourselves to the cases with $m_k = m - n$, which is the condition of the Kronecker delta in equation 5.8. From the condition it follows in particular that m_k and the sum $m + n$ are always either both odd or both even. If $m + n$ is a multiple of two, the product $P_l^m(\xi) P_l^n(\xi)$ is a polynomial $p_{2l}(\xi)$ of degree $2l$. In this case the $P_s^{m_k}(\xi)$ build a complete set of orthogonal polynomials. Now we can expand $p_{2l}(\xi)$ in terms of the $P_s^{m_k}(\xi)$, which yield a series with the highest order term $P_{2l}^{m_k}(\xi)$. We analyze the integral using this expansion and the orthogonality relation

$$\int_{-1}^1 d\xi P_k^{m_k}(\xi) P_s^{m_k}(\xi) = \frac{2(k+m_k)!}{(2k+1)(k-m_k)!} \delta_{ks}. \quad (5.11)$$

In the case of $m + n$ being odd we follow the exact same reasoning but the details are slightly different because then $P_l^m(\xi) P_l^n(\xi)$ is no longer a polynomial but a product of a polynomial of degree $2l - 1$ and a factor $\sqrt{1 - \xi^2}$. As the same structure applies to $P_s^{m_k}(\xi)$ we can again expand the product of associated Legendre functions in the same way as above. Now we again apply equation 5.11 and find for all possible values of $n + m$ that $I_{lkm_k}^{mn}$ vanishes for $k > 2l$.

5.2 The Racah Parameters

The most important result of the last section is that we were able to reduce the number of parameters which are needed to describe the multiorbital Hamiltonian. In the case of d-orbitals we can construct all matrix elements with only three parameters, namely a_0 , a_2 , and a_4 . For p-orbitals only the first two of them are finite. The rest is now simply a matter of convention. We introduce the abbreviations

$$\eta = e^2/4\pi\epsilon_0 \quad (5.12)$$

and

$$\text{p-wave:} \quad F_0 = a_0, \quad F_2 = \frac{1}{5}a_2, \quad (5.13)$$

$$\text{d-wave:} \quad F_0 = a_0, \quad F_2 = \frac{5}{49}a_2, \quad F_4 = \frac{1}{49}a_4. \quad (5.14)$$

Using the fact that all matrix elements $V_l^{mm'nn'}$ are real numbers and the equation

$$P_l^{-1}(\xi) = (-1)^m \frac{(l-m)!}{(l+m)!} P_l^m(\xi), \quad (5.15)$$

it is easy to verify the following relations:

$$V_l^{mm'nn'} = V_l^{nn'mm'} = V_l^{-m-m'-n-n'} = (-1)^{m+n} V_l^{-nm'-mn'} = V_l^{m'n'n}. \quad (5.16)$$

It is therefore sufficient to calculate only a small number of matrix components and construct the remaining elements with equations 5.16. In table 5.1 all relevant matrix elements for p- and d-orbitals are listed. We can rewrite the matrix elements in terms of the so called Racah parameters [116, 117], they are defined in the following way:

$$\text{p-wave:} \quad A = F_0 + F_2, \quad B = 3F_2, \quad (5.17)$$

$$\text{d-wave:} \quad A = F_0 - 49F_4, \quad B = F_2 - 5F_4, \quad C = 35F_4. \quad (5.18)$$

In table 5.1 the matrix elements are written in both parameter systems. We can distinguish several classes of matrix elements:

- U_m : Matrix elements only involving one orbital in the form V_l^{mmmmm} . These terms give the Coulomb energy due to the Coulomb repulsion of two electrons in the orbital m .
- U'_{mn} : Matrix elements involving two orbitals in the form V_l^{mnnmm} . These terms represent the Coulomb energy due to the Coulomb repulsion of one electron in the orbital m and the other in the orbital n . They are called direct terms.
- J_{mn} : Matrix elements involving two orbitals in the form V_l^{mnnmm} . These terms give the energy needed to exchange two particles in the orbitals m and n . They are called exchange terms.

m	m'	n	n'	$V_1^{mm'mn}/\eta$		$V_1^{mm'mn'}/\eta$		
0	0	0	0	$F_0 + 4F_2$	$A + B$	$F_0 + 4F_2 + 36F_4$	$A + 4B + 3C$	U_m
1	1	1	1	$F_0 + F_2$	A	$F_0 + F_2 + 16F_4$	$A + B + 2C$	
2	2	2	2	—	—	$F_0 - 4F_2 + F_4$	$A - 4B + 2C$	
1	0	1	0	$F_0 - 2F_2$	$A - B$	$F_0 - 2F_2 - 24F_4$	$A - 2B + C$	U'_{mn}
2	0	2	0	—	—	$F_0 - 4F_2 + 6F_4$	$A - 4B + C$	
2	1	2	1	—	—	$F_0 - 2F_2 - 4F_4$	$A - 2B + C$	
-2	2	2	-2	—	—	$70F_4$	$2C$	J_{mn}
-1	1	1	-1	$6F_2$	$2B$	$6F_2 + 40F_4$	$6B + 2C$	
-1	2	2	-1	—	—	$35F_4$	C	
1	0	0	1	$3F_2$	B	$F_2 + 30F_4$	$B + C$	
2	0	0	2	—	—	$4F_2 + 15F_4$	$4B + C$	
2	1	1	2	—	—	$6F_2 + 5F_4$	$6B + C$	
0	1	2	-1	—	—	$2\sqrt{6}F_2 - 10\sqrt{6}F_4$	$2\sqrt{6}B$	
2	0	1	1	—	—	$\sqrt{6}F_2 - 5\sqrt{6}F_4$	$\sqrt{6}B$	

Table 5.1: Matrix elements of the Coulomb potential for p - and d -orbitals. All other components either vanish or can be constructed from equations 5.16. The matrix elements are expressed by the parameters F_0 , F_2 , F_4 and the Racah parameters A , B , C .

The presented form of the matrix elements is completely rotational invariant, meaning that we are free to rotate our reference system without changing the values for the Coulomb matrix elements. Values for the Racah parameters are discussed in the literature [118–122]. They are typically taken from a comparison of experimentally obtained photoemission spectra and theoretical results. By fitting the parameters to experimental data they do no longer describe the pure electromagnetic repulsion of two electrons, but rather incorporate screening effects by the remaining electrons. The whole treatment of the Coulomb matrix elements relies exclusively on the symmetry of the Coulomb interaction. If we can assume that screening effects do not alter this symmetry, as we will do, this treatment does not imply any further approximation.

6 Magnetic Chains

The fascinating magnetic properties of $\text{Ca}_3\text{Co}_2\text{O}_6$ and the desire to find their explanation inspired and drove this work. Especially two questions are at the center of this thesis: What is the reason for the ferromagnetic intrachain coupling, and how can a proper effective magnetic model be designed for this compound? To answer the second question we started to investigate the smallest characteristic entity of $\text{Ca}_3\text{Co}_2\text{O}_6$, namely the Co – O₃ chains. In order to account for the observed anisotropy, two approaches will be discussed: first, Ising anisotropy, which is assumed in most experimental works on $\text{Ca}_3\text{Co}_2\text{O}_6$. The second approach using a Heisenberg interaction with an on site anisotropy term will enable us to discuss the magnetic properties with varying anisotropy strength. A next step is to include the antiferromagnetic coupling between the chains. This is done by exploring models, which describe a triangle of chains. The basis for the complex magnetic response in $\text{Ca}_3\text{Co}_2\text{O}_6$ is the existence of two competing magnetic interactions together with a geometric frustration due to the triangular structure and the strong anisotropy. The ferromagnetic coupling of Co²⁺ moments along the chains plays a crucial role in this scenario. To clarify the origin of this interaction, the effective coupling of two Co²⁺ moments is examined by means of perturbation theory.

6.1 Coordinate Systems and Notation

We have already seen the rather complicated structure of the unit cell of $\text{Ca}_3\text{Co}_2\text{O}_6$. In the following discussion we first focus on a few sites on one chain. The only atoms of interest for the rest of this chapter are two neighboring Co²⁺-atoms, the Co¹-atom in between, and the six O-atoms, which build the octahedral environment of the Co¹-site, see fig. 6.1. This adds up to a total of nine atoms with 33 local levels. In order to define and describe this reduced problem we have to clarify some basic aspects of the physical characterization.

We choose the complex spherical harmonics as the one-particle basis. It is straightforward to rotate these functions around their z -axis. This property is useful in order to exploit the threefold symmetry of the $\text{Ca}_3\text{Co}_2\text{O}_6$ -chain. The disadvantage of using the spherical harmon-

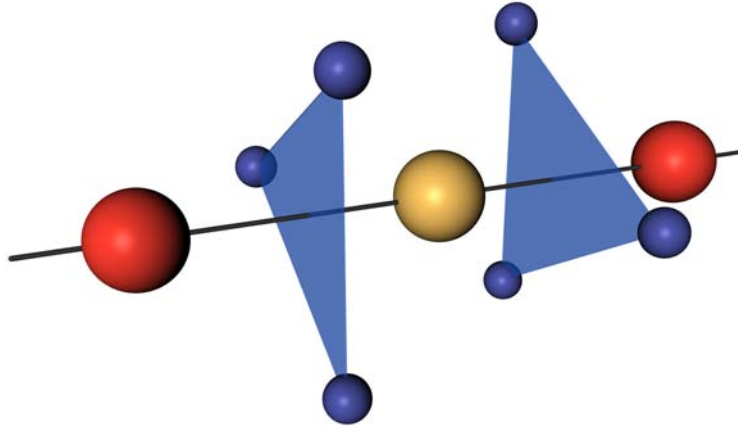


Fig. 6.1: Two Co2 (red), one Co1 (yellow), and six O (blue) atoms are the smallest cluster which is possibly sufficient to explain ferromagnetic coupling along the chain in a model that involves both superexchange and ring exchange processes.

ics is that we have to deal with complex matrix elements. But implementing the C_3 -symmetry in this system leads us to use complex characters anyway.

An obvious choice for a global coordinate system is to take the z -axis along the chain-axis and the point of origin on the Co1-site. We will call this global system Σ_{glob} . To define the x -axis of Σ_{glob} we use the direction vector to one of the oxygen atoms with positive z -coordinate. The projection of this vector on the plane perpendicular to z defines the x -axis. Σ_{glob} is our reference system for the different local systems. It will be useful for the calculation of the overlap integrals and the hopping matrix elements. On the other hand we need local systems in which the one-particle wave functions are defined.

A naming scheme for the oxygens is helpful for the definition of the local systems. The oxygen atoms are numbered counterclockwise starting with the one we used to define the global x -axis. Oxygen atom number four is the inversion of O_1 . We name a local system according to the atom it is attached to, e.g., Σ_{Co1} or Σ_{O1} . Of course all the local systems are centered at their respective atom site. For the Co2-atoms the choice is natural. One system will be parallel to the global system and the other rotated by an angle of 180° around the global z -axis. The local Co2-system is defined by the octahedral oxygen environment of the atom. Unfortunately this system is not aligned with the global system. Another problem arising in this local system is that the octahedral environment, as well as the trigonal prismatic, is distorted. It is therefore not possible to take exactly the oxygen positions to define the local system. We would like to cover the exact C_3 -symmetry of the single chain and be as close to the oxygen positions as possible. To achieve these goals we construct the unit vector \vec{o}_1 from Co1 to O_1 . The unit vector in the local system x' is then a weighted sum of the global z -vector and \vec{o}_1 , $\vec{e}_{x'} = \alpha(\vec{o}_1 + \beta\vec{e}_z)$. This construction pattern can be used again for y' with \vec{o}_2 , and z' with \vec{o}_3 . Because the result has to be threefold symmetric, the α and β values have to be the

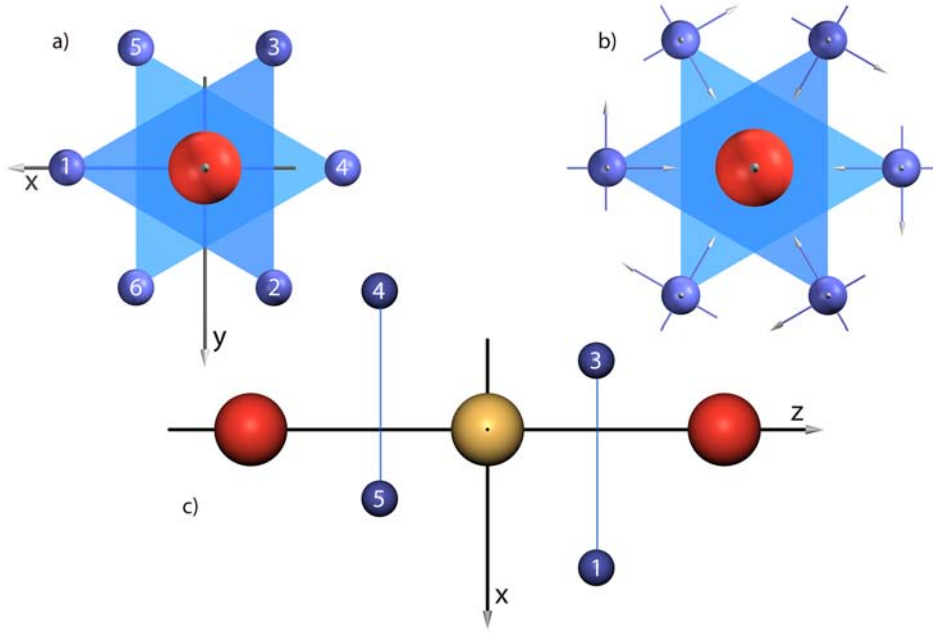


Fig. 6.2: Coordinate systems (colors as in 6.1) : a) Global coordinate system with the z -axis along the chain. The O atoms are numbered as explained in the text. b) Local O coordinate system with the x' -axis pointing towards the global z -axis. c) View in positive y -direction.

same for all three combinations. Cartesian coordinate vectors are orthonormal, which leads to the conditions:

$$\vec{e}_{x'} \cdot \vec{e}_{y'} = \alpha^2 (\vec{o}_1 \cdot \vec{o}_2 + \beta^2 + 2\beta o_z) = 0, \quad (6.1)$$

$$\vec{e}_{x'}^2 = \alpha^2 (1 + \beta^2 + 2\beta o_z) = 1. \quad (6.2)$$

In the above equations we take advantage of the threefold symmetry, that makes $\vec{e}_z \cdot \vec{o}_i$ independent of i , this value is called o_z . These equations yield $\alpha = 1/\sqrt{1 - \vec{o}_1 \cdot \vec{o}_2}$ together with $\beta = \sqrt{o_z^2 - \vec{o}_1 \cdot \vec{o}_2} - o_z$. There is also no unique choice for the local coordinate systems of the oxygen atoms. A reasonable choice should again reflect the threefold symmetry of the global structure. This can be attained in taking the z -axis of all oxygen systems parallel to the global z -axis and the local x -axis pointing to the global z -axis. Figure 6.2 gives a visual impression of all these definitions.

For the unperturbed \mathbf{H}_{loc} it is of no relevance that we use local coordinate systems which are rotated against each other. This becomes important when introducing the perturbation in the problem. Then we have to consider hopping processes which occur because of the finite overlap of the local wave functions on different sites. The overlap integrals have to be evaluated with the rotated wave functions. We will not do this exactly. Instead we use an approximation which was introduced by Koster and Slater. To use this approximation we

need to have a unique basis system for all sites and we have to express all local wave functions in terms of the global ones.

This turns out to be easy for most of our local systems. All local coordinate systems but that of Co1 share the z -axis with Σ_{glob} . To bring the local and global system in parallel it is sufficient to rotate the system about this z -axis. For the spherical harmonics this is equivalent to a simple multiplication with a complex number:

$$Y_l^m(\theta, \phi + \alpha) = c(l, m) P_l^m(\theta) \exp(i m (\phi + \alpha)) = Y_l^m(\theta, \phi) \exp(i m \alpha). \quad (6.3)$$

In the above equation $Y_l^m(\theta, \phi)$ is a spherical harmonic function, $P_l^m(\theta, \phi)$ is the associated Legendre polynomial. $c(l, m)$ is a constant only depending on l and m . In a physical context l is then typically the angular momentum and m the projection of the angular momentum on the z -axis.

For Σ_{Co1} we have to do the full expansion of the wave functions in Σ_{Co1} in terms of the wave functions in Σ_{glob} . Using the completeness of the spherical harmonics and the fact that a rotation does not change the total angular momentum, we get

$$|Y_l^{m'}(\theta', \phi')\rangle \equiv |\Psi(\theta, \phi)\rangle = \sum_{m=-l}^l \langle Y_l^m(\theta, \phi) | \Psi(\theta, \phi) \rangle |Y_l^m(\theta, \phi)\rangle. \quad (6.4)$$

Where primed quantities are defined in the local system. $\Psi(\theta, \phi)$ is the function one generates by expressing the local angles in terms of the global angles and inserting this in the local spherical harmonic. Doing this exercise for Σ_{Co1} yields a 5×5 transformation matrix M_{Oct} , which connects the wave functions of the Co1-system with the wave functions of the global system.

6.2 Anisotropic Spin Chains – Models

The basic building blocks for an effective magnetic model of $\text{Ca}_3\text{Co}_2\text{O}_6$ are chains of ferromagnetically coupled angular momenta. The simplest model Hamiltonian for an anisotropic magnetic interaction is the Ising model [123,124]. We will use this approach to get a first idea of the magnetic properties of the anisotropic high-spin chains in $\text{Ca}_3\text{Co}_2\text{O}_6$. For an extended study of the effects of the anisotropy, the Ising model will be compared to a Heisenberg model with an on-site anisotropy D . In these magnetic models the chains are only built of the sites, which carry a magnetic moment. Only ferromagnetic next-neighbor interaction is included, every magnetic site carries a spin S . The corresponding Ising Hamiltonian of a chain with length N has the form:

$$\mathbf{H}_{\text{SC,Is}} = -J_{\text{F}} \sum_{i=1}^{N_{\text{SC}}} \mathbf{S}_i^z \mathbf{S}_{i+1}^z - g \mu_{\text{B}} H^z \sum_{i=1}^{N_{\text{SC}}} \mathbf{S}_i^z. \quad (6.5)$$

The positive value J_F is the ferromagnetic coupling constant, S_i^z is a z -component of a local spin operator at site i , g is the Landé factor. The Bohr magneton is defined as $\mu_B = e\hbar/2m_e$, with the absolute value of the electron charge e and the electron mass m_e . Periodic boundary conditions are assumed in equation 6.5. The chain is N_{SC} sites long, where the subscript SC stands for “single chain”. The Ising Hamiltonian commutes with the individual spin operators S_i^z . Of course the z -component of the total spin $S^z = \sum_{i=1}^N S_i^z$ is conserved as well. A direct product of local S_i^z eigenstates is therefore an eigenstate of the Ising Hamiltonian. The one-dimensional Ising Hamiltonian can be solved analytically for an arbitrary number of sites N , for example with the transfer matrix method. This is a well understood textbook example [125]. In the present context the Ising model serves mainly as a reference system. Therefore we will restrict the analysis to appropriate system sizes, in order to compare results of the Ising chain with those of more complex spin models.

The Heisenberg chain, on the other hand, represents a much harder problem than a chain of Ising spins. An important difference is that the z -projection of an individual spin in the chain is no longer a conserved quantity for a Heisenberg Hamiltonian. As a consequence, there is in general neither an easy way to construct eigenstates of this Hamiltonian, besides the fully polarized ferromagnetic state, nor eigenvalues and the partition function. Despite of these complications it is still possible to find exact eigenstates and eigenenergies of the Heisenberg chain by using a special parameterization of the eigenstates, the famous Bethe ansatz [126] (for a nice introduction of the Bethe ansatz see [127, 128]). Like the Ising chain the Heisenberg chain serves as a reference system in the context of this work. We therefore restrict the discussion to chain lengths comparable to results of more complex situations. We will use the Heisenberg model with an additional on-site anisotropy D in the following form:

$$\mathbf{H}_{SC,Hb} = -J_F \sum_{i=1}^{N_{SC}} \vec{S}_i \cdot \vec{S}_{i+1} - D \sum_{i=1}^{N_{SC}} (S_i^z)^2 - g \mu_B H^z \sum_{i=1}^{N_{Ch}} S_i^z. \quad (6.6)$$

Again periodic boundary conditions are used. The anisotropy term favors high S_i^z states for $D > 0$. Spin chains with S larger than $\frac{1}{2}$ are not integrable models, the Bethe ansatz is not applicable. We solved both the Ising and the Heisenberg Hamiltonian for finite chain length with exact diagonalization. The exponential growth of the number of states with growing chain length N_{SC} restricts this method to small systems. A chain with 9 sites and $S = 2$ is characterized by $(2S + 1)^9 = 1953125$ states. To diagonalize a matrix of these dimensions is completely out of reach, even on the most advanced systems available today. It would need about 100 TB of memory and a prohibitively long computational time.

Fortunately it is possible to bring the Hamiltonian matrix in block diagonal form by employing the symmetries of the Hamiltonian. In the present case we have three symmetries that can be used: the rotational invariance for rotations about the z -axis leads to the conservation of the z -component of the total spin. This symmetry yields a decomposition of the Hamiltonian matrix into 37 blocks, the block with $S^z = 0$ having the highest dimension of 180325, closely followed by the blocks with $S^z = \pm 1$ with a size of 175725 states each. In the

subspace with $S^z = 0$ the Hamiltonian is invariant under the transformation $S_i^z \rightarrow -S_i^z$ at all sites simultaneously. Therefore we can use symmetric and antisymmetric states with respect to this transformation and split the biggest subspace into two smaller ones with 90 162 and accordingly 90 163 states. Finally the use of the translational symmetry brings another reduction of about a factor of 9. In the end the Hamiltonian matrix is block-diagonal with 363 blocks. The 12 blocks with $S^z = \pm 1$ have the highest block dimension of 19 525, a reduction of a factor of 100. For the calculation a computer with 16GB of main memory was used. This amount of memory restricts the calculation to 9 sites for spin 2 chains. Although it is possible to handle such an amount of states for this system size, the computation time is too long to be able to scan the parameter space, so we are effectively restricted to a chain length of 8 sites. In order to be able to discuss longer chains, systems with spin 1 have been additionally investigated. In this case it is possible to go up to a chain length of 12 sites.

6.3 Anisotropic Spin Chains – Results

The magnetic susceptibility, the specific heat and the magnetization of a single Ising chain and accordingly a single Heisenberg chain have been calculated. The results for the susceptibility of the Ising chain are depicted in figure 6.3. In the high temperature regime the inverse magnetic susceptibility shows a linear dependence in the temperature, in agreement with the Curie-Weiss law. The low temperature deviation from the pure linearity becomes more pronounced with increasing chain length, although the difference between the 12 and 15 site chains is already small. Both spin 1 and spin 2 chains show the Curie-Weiss behavior, however with two notable differences: first, the susceptibility for spin 2 deviates from Curie-Weiss at temperatures about four times higher than in the spin 1 case. The T^{-1} behavior of the susceptibility is approached if the spins are able to rotate nearly freely, undisturbed by their neighbors. The energy necessary to flip a spin completely scales with S^2 , thus explaining the factor four. Second, the slope of the straight line at high temperatures is lower in the spin 2 case. The inverse of this slope is the Curie-Weiss constant C_{CW} , which is proportional to $\mu_{\text{eff}} = g \mu_B \sqrt{S(S+1)}$. Therefore a lower slope is expected for larger spins.

The magnetic susceptibility results for the Heisenberg chain in figure 6.4 show the same qualitative behavior as the Ising chain. With the anisotropy energy D a second energy scale is present in the discussed Heisenberg Hamiltonian. If D is smaller or comparable to J_F , the main effect of the local anisotropy is to favor subspaces with high total $|S^z|$. As the magnetic susceptibility (at zero field) is proportional to the thermal average over $(S^z)^2$, the magnetic susceptibility grows with increasing anisotropy. The system behaves very differently for $D \gg J_F$. In this case a regime exists, where the temperature is smaller or comparable to D and considerably larger than J_F . Then it is easier to flip a single spin completely than to reduce its z -component only by one. Flipping a spin completely implies a stronger reduction of $|S^z|$. Therefore states with lower $|S^z|$ can be energetically more favorable than states with higher

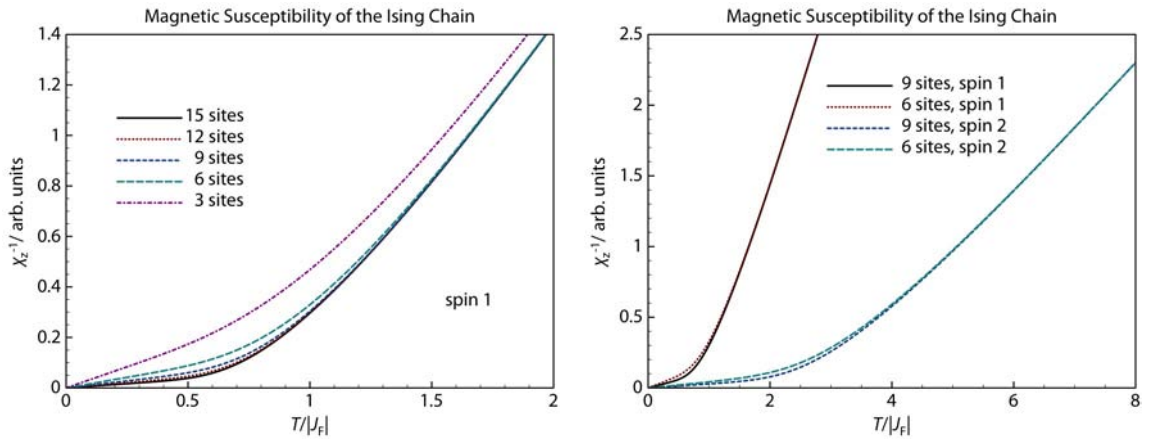


Fig. 6.3: Inverse magnetic susceptibility of the Ising chain. Left panel: several chain lengths are compared for a spin 1 chain. A Curie-Weiss behavior can be seen in all cases. Right panel: spin 1 and spin 2 data are compared. The higher effective magnetic moment in the spin 2 case is observed in the smaller slope.

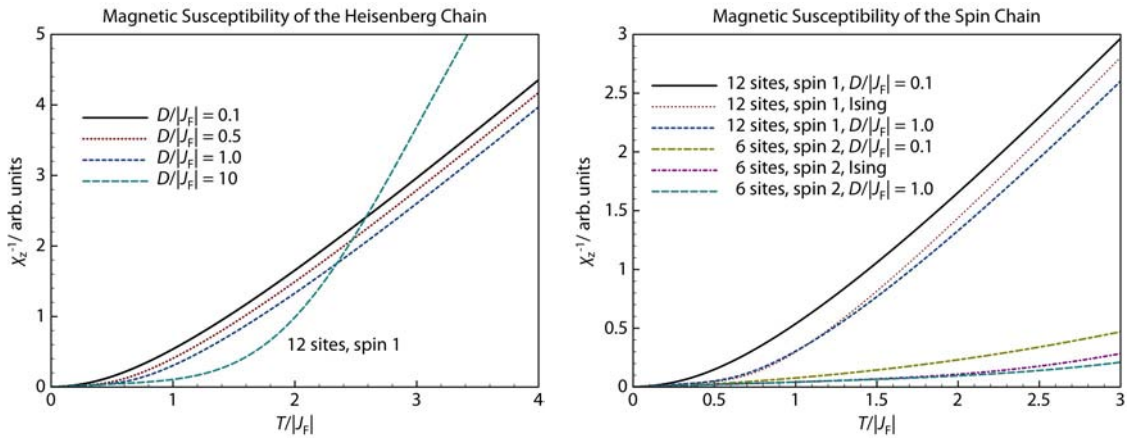


Fig. 6.4: Left panel: the curves show the inverse magnetic susceptibility for the Heisenberg chain with different on-site anisotropies D . Right panel: a direct comparison of the Ising chain with different anisotropies to the Heisenberg chain.

6 Magnetic Chains

S^z . This analysis suggests that the susceptibility is significantly suppressed for temperatures above the energy of a total local spin flip (compare with the curve for $D = 10$ in figure 6.4).

Besides we can directly compare the susceptibilities of the anisotropic Heisenberg and Ising Hamiltonians 6.4. This reveals that these two anisotropic models behave very differently, even for large D -values. In this limit the intermediate S_i^z states are suppressed, with the consequence that the anisotropic Heisenberg chain with large D is similar to a spin $\frac{1}{2}$ Ising chain.

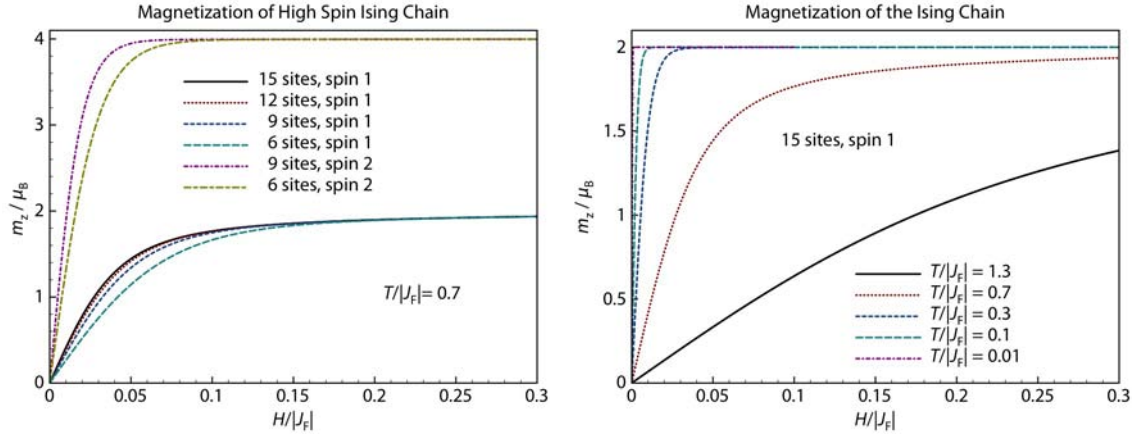


Fig. 6.5: Magnetization curves for the Ising chain with a g -factor of two. Left panel: the magnetization is plotted versus field for several numbers of sites and different spins. Right panel: the magnetization curves at various temperatures. Thermal fluctuations drive the system out of saturation.

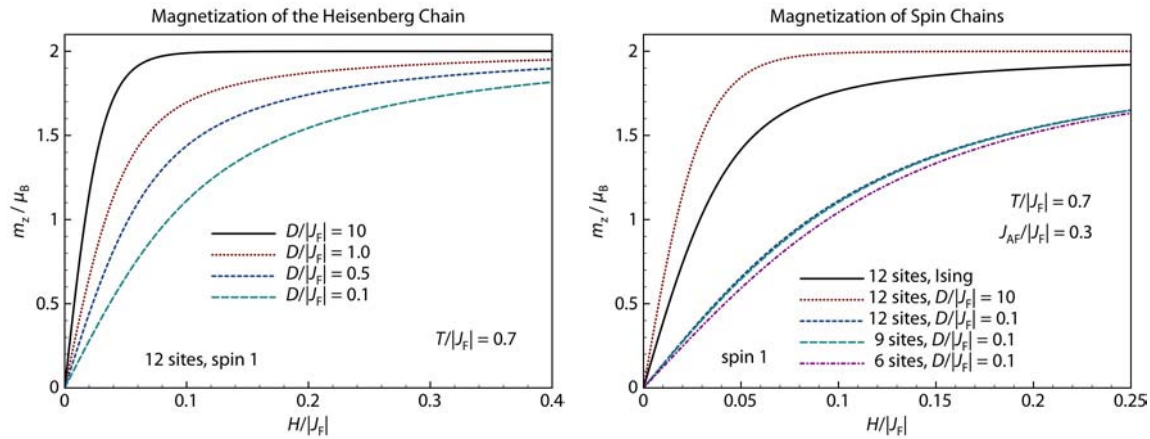


Fig. 6.6: Left panel: A high anisotropy stabilizes fully polarized states against thermal fluctuations. Right panel: the Ising chain is compared to different values of D for the Heisenberg chain. The Ising case falls into the intermediate anisotropy regime.

Figures 6.5 and 6.6 show magnetization data for the Ising and the Heisenberg case respectively. The symmetry of both Hamiltonians demands a vanishing magnetization at zero fields. For high fields the magnetization will eventually reach saturation. The two degenerate ferromagnetic ground states at $H = 0$ are both fully polarized, so at zero temperature applying an arbitrary small field results into full saturation. At higher temperatures the field has to overcome the thermal fluctuations in order to reach saturation. Longer chains are “more”

ferromagnetic in the sense that they show a steeper slope than shorter chains. The saturation magnetization is of course larger for chains with higher spins. In the figures a g -factor of 2 is assumed, thus the saturation magnetization is $2 \mu_B$ for spin 1 chains and $4 \mu_B$ for spin 2 chains. For higher spins the saturation is reached with smaller fields, because the energy to change a single spin from S_{\max}^z to $S_{\max}^z - 1$ scales linearly with S . Therefore the thermal fluctuations effect fewer excited states for larger spins. A higher anisotropy D has the same consequence as it lowers the energy of the fully polarized states compared to the excited states. In terms of the magnetization, the Ising chain compares to some intermediate anisotropy of the Heisenberg case.

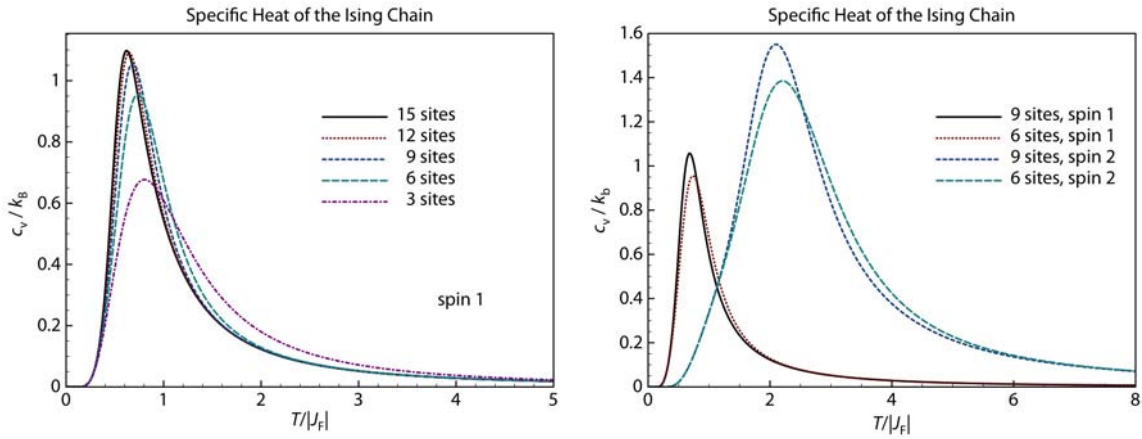


Fig. 6.7: Specific heat for the Ising chain. Left panel: The specific heat is plotted for different system sizes. The exponential growth at low temperatures is due to the gapped spectrum of the Ising chain. At high temperatures the specific heat vanishes like $1/T^2$. Right panel: the gap is more pronounced for spin 2.

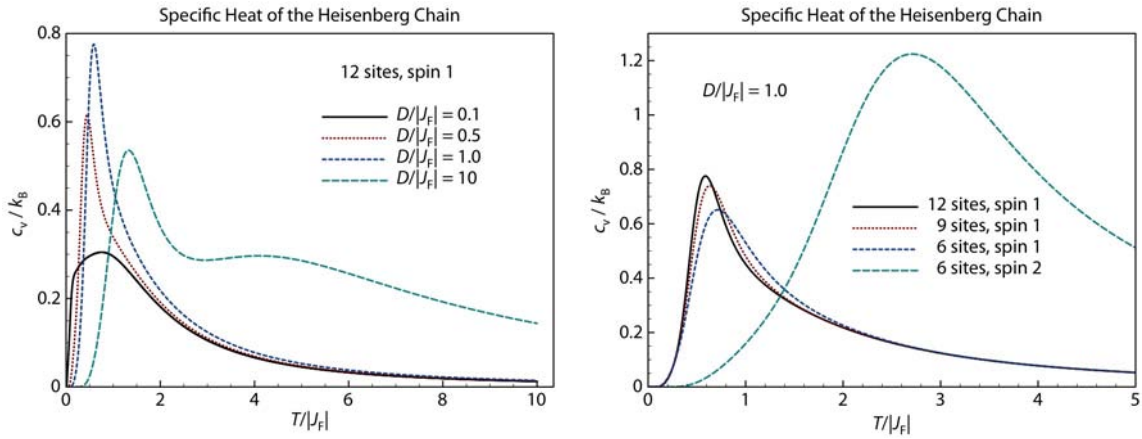


Fig. 6.8: Specific heat of the anisotropic Heisenberg chain. Left panel: the anisotropy affects the gap size. At low anisotropies the gap closes. Right panel: at intermediate anisotropies the overall behavior of the specific heat is comparable to the Ising case.

The specific heat data for the Ising chain shown in figure 6.7 result from a continuous crossover from the high temperature to the low temperature limit. For low temperatures the gapped nature of the spectrum leads to an exponential decrease. The width of this exponential

area depends on the size of the gap. The gap value is independent of the system size, hence the curves in the left plot of figure 6.7 exactly coincide at low temperatures. On the other hand the gap scales with the spin, which explains the wider exponential region for the spin 2 curve, compared to spin 1. For high temperatures the specific heat has to vanish as the entropy reaches a constant value $(2S+1)^{N_{sc}}$, where all states of the system can be accessed equally. The specific heat decays with $1/T^2$ in the high temperature limit. For intermediate anisotropies the shape of the specific anomaly is similar in the Heisenberg case (compare figures 6.7 and 6.8, right panels). The left side of figure 6.8 shows the dependence on the anisotropy. The gap closes with vanishing anisotropy term, and the isotropic Heisenberg model is gapless. For very high D -values, again an intermediate temperature region can be identified, showing a second maximum in the specific heat. This maximum occurs at energies of a complete flip of a single spin—compare the discussion at the beginning of this section—which is about $4J_F$ for a spin 1 chain.

Two lessons can be drawn from the above discussion: all results are consistent with known features of these systems. This assures the accuracy of the numerics. Second, the two types of anisotropy are rather different. In the range of intermediate on-site anisotropy both show similar physical properties but the Ising chain is not the limiting case of the Heisenberg Hamiltonian with high on-site anisotropies. This would only be true for the spin $\frac{1}{2}$ chain. Especially for anisotropies higher than the energy needed for a total flip of a single spin the differences become more pronounced.

6.4 Interacting Chains

A next step towards the understanding of the magnetic properties of $\text{Ca}_3\text{Co}_2\text{O}_6$ is to include more than one chain into the calculation. We need to include at least three chains in order to account for the frustration of the antiferromagnetic coupling. Again we will formulate an effective magnetic model, with next-neighbor interactions only. As in the case of a single chain, exclusively Co2 sites and the adjacent magnetic moments are relevant for the formulation of the problem. For the ferromagnetic interaction along the chain a next neighbor is uniquely defined, but to find the next neighbor of a Co2 site on another chain one has to examine the structure in more detail. If the criterion is just the shortest distance to the next Co2 site on a neighboring chain, then the situation is clear. Using the notation of figure 6.9, the distance $A - B_1$ is the shortest interchain Co2 distance. Nonetheless the antiferromagnetic interaction is most likely a result of exchange processes involving the oxygen environments of the Co2 sites. This means that the strongest coupling is probably rather related to the shortest O - O distance, than to the shortest Co2- Co2 distance.

Which next neighbor we choose has a strong impact on the topology of the model. The model is designed on an equilateral triangle of chains. Selecting B_1 as the next neighbor of site A results in a single helix (SH) structure, whereas choosing B_2 leads to a double helix

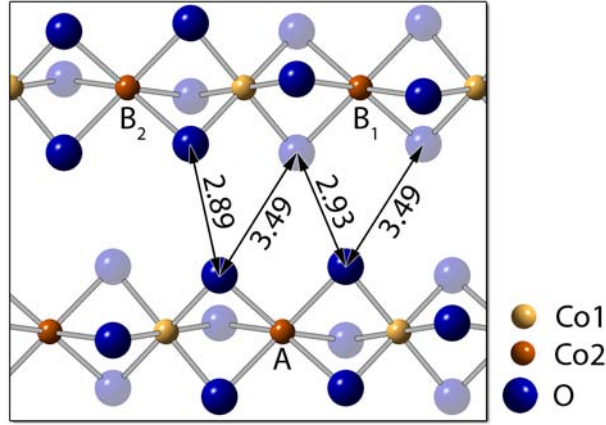


Fig. 6.9: Oxygen distances between two chains. The shortest Co2– Co2 distance is from A to B₁, but the shortest O – O distance occurs along A – B₂. All distances are given in Ångström. The brightness of the color indicates the distance to the viewer. Brighter blue spheres are further away.

(DH) geometry of the model. The single helix arrangement is depicted in figure 6.10. If one numbers the sites along the helix, a Heisenberg Hamiltonian can be formulated as:

$$\mathbf{H}_{\text{SH,iso}} = J_{\text{AF}} \sum_{j=0}^{3N_{\text{SH}}-1} \vec{\mathbf{S}}_j \vec{\mathbf{S}}_{j+1} - J_{\text{F}} \sum_{j=0}^{3N_{\text{SH}}-1} \sum_{n=0}^2 \vec{\mathbf{S}}_{3j+n} \vec{\mathbf{S}}_{3(j+1)+n} . \quad (6.7)$$

The system size is $3N_{\text{SH}}$, $J_{\text{AF}} > 0$ is the antiferromagnetic inter-chain coupling, and $J_{\text{F}} > 0$ the ferromagnetic intra-chain coupling. In this formulation the model is isotropic in spin space, which is denoted with the subscript “iso”. With cyclic boundary conditions the site $3N_{\text{SH}}$ is equivalent to the site 0. This boundary condition makes the Hamiltonian invariant under the transformation $\vec{\mathbf{S}}_k \rightarrow \vec{\mathbf{S}}_{k+1}$. Repeating this cyclic permutation $3N_{\text{SH}}$ times results in the identity operation. Therefore the cyclic group $C_{3N_{\text{SH}}}$ can be used to describe the symmetry of the Hamiltonian. A schematic drawing emphasizing the symmetry of $\mathbf{H}_{\text{SH,iso}}$ is given in figure 6.12 b).

For the double helix geometry the sites on one helix are indexed with odd numbers and the sites on the other helix are counted with even numbers. With this naming convention we present a Heisenberg Hamiltonian of the form:

$$\mathbf{H}_{\text{DH,iso}} = J_{\text{AF}} \sum_{j=0}^{3N_{\text{DH}}-1} \sum_{n=0}^1 \vec{\mathbf{S}}_{2j+n} \vec{\mathbf{S}}_{2(j+1)+n} - J_{\text{F}} \sum_{j=0}^{3N_{\text{DH}}-1} \sum_{n=0}^1 \vec{\mathbf{S}}_{2j+n} \vec{\mathbf{S}}_{2(j+2n)+1+n} . \quad (6.8)$$

An illustration of this structure is displayed in figure 6.11. The total Hamiltonian includes $6N_{\text{DH}}$ sites. Again, with cyclic boundary conditions the site $6N_{\text{DH}}$ is equivalent to the site 0. The symmetry of this Hamiltonian can also be described by a cyclic group but with reduced order. $\mathbf{H}_{\text{DH,iso}}$ is $C_{3N_{\text{DH}}}$ symmetric, so the order of the group is half the system size, in contrast to the case of the single helix, where the order of the group was the total number of sites. The

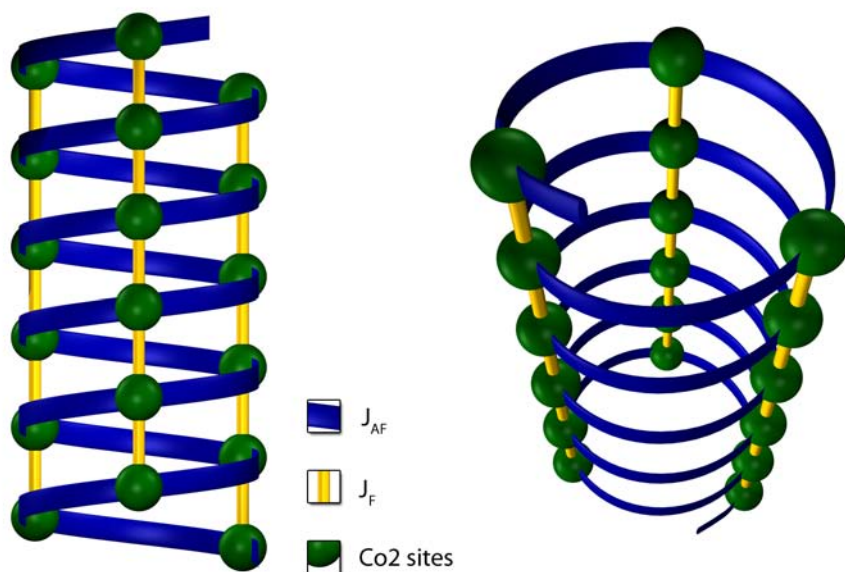


Fig. 6.10: Single helix: As the chains are shifted against each other in z -direction the antiferromagnetic coupling acts on a spiral. All sites (green spheres) are located on one helix, depicted as a blue ribbon. The ferromagnetic coupling is symbolized as yellow bars.

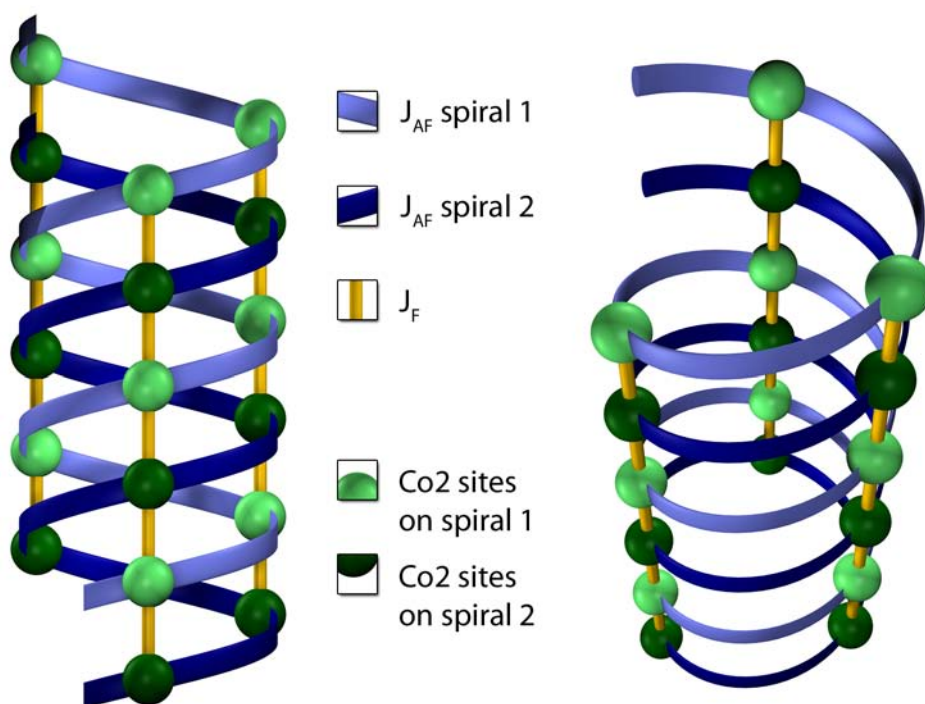


Fig. 6.11: Double helix: In this case the sites are located at two distinct spirals. Sites on one helix are antiferromagnetically coupled, whereas both helices are coupled ferromagnetically.

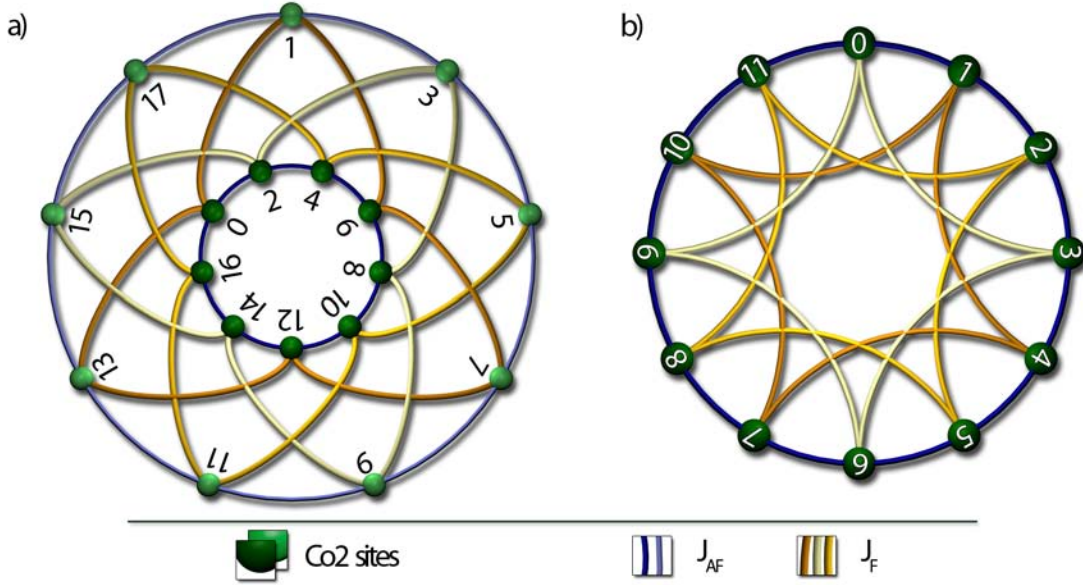


Fig. 6.12: The single and double helix Hamiltonian in a schematic drawing emphasizing the symmetry. The color code is the same as in figures 6.10 and 6.11. a) The double helix structure is disentangled and redrawn as two distinct circles. The sites on one circle interact antiferromagnetically. All connections between the two circles depict the ferromagnetic coupling J_F . The different shades of yellow are meant to emphasize the closed subsets of ferromagnetically coupled sites. The total number of sites is 18, $N_{DH} = 3$ and the symmetry group is C_9 . b) The single helix structure can be transformed into a circle of antiferromagnetically coupled sites. The connections in the area of the circle are again colored in different shades of yellow to show the groups of sites that are ferromagnetically connected, but they depict all the same ferromagnetic coupling. This example shows 12 sites with the symmetry C_{12} and $N_{SH} = 4$.

double helix structure grows in units of six sites. This property restricts the calculation for a spin 2 system to only one such unit, which is too short to build up real helices and hence is regarded as a pathologic case. The unfortunate consequence is that we have to restrict our discussion mainly to spin 1 chains.

For the calculations we will not use the isotropic Hamiltonians 6.7 and 6.8, but rather include an anisotropy term to them. For the Ising Hamiltonians all \vec{S}_i are replaced by S_i^z and for the anisotropic Heisenberg Hamiltonians the term $-D \sum_i (S_i^z)^2$ is simply added to the equations 6.8 and 6.7.

The magnetic susceptibility for the SH and DH structures in the Ising case is depicted in figure 6.13. A increasing antiferromagnetic coupling constant J_{AF} reduces the susceptibility. This is due to the fact that J_{AF} tends to anti-align neighboring spins and therefore favors states with low values of $|\mathbf{S}^z|$. The very same behavior is also seen for the anisotropic Heisenberg Hamiltonian (compare figure 6.14, right panel). At high temperatures the helices show the Curie-Weiss behavior as expected. The results for the Ising Hamiltonian of the SH and DH structure are surprisingly similar. In the Ising case we were able to calculate the physical properties for helices up to a length of 15 sites. The results for the 12 site helices are already close to the 15 sites for the SH structure, again indicating that finite size effects are moderate

6 Magnetic Chains

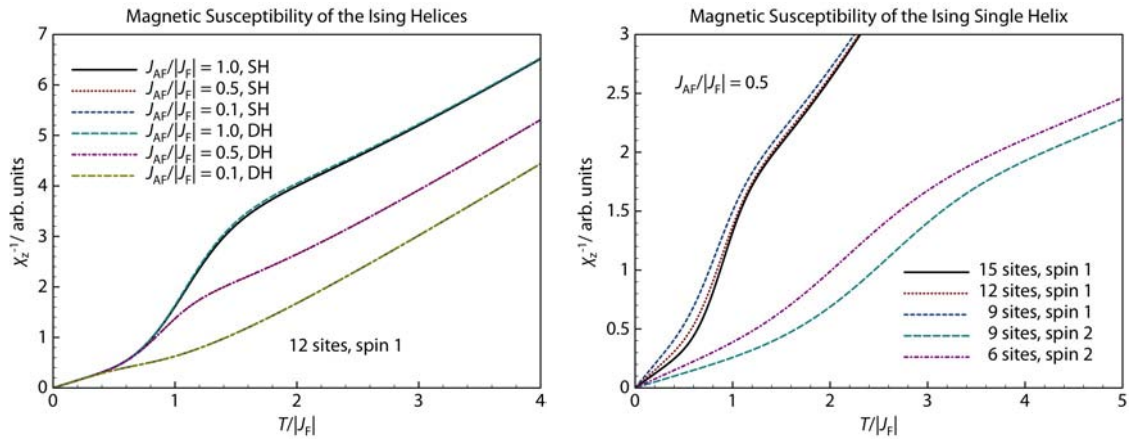


Fig. 6.13: Magnetic susceptibility for the Ising anisotropy. Left panel: the magnetic susceptibility of the single helix (SH) and double helix (DH) structure are compared for the Ising anisotropy. There is virtually no difference between SH and DH in this case. Right Panel: the susceptibility is depicted for several system lengths and for spin 1 and spin 2 helices.

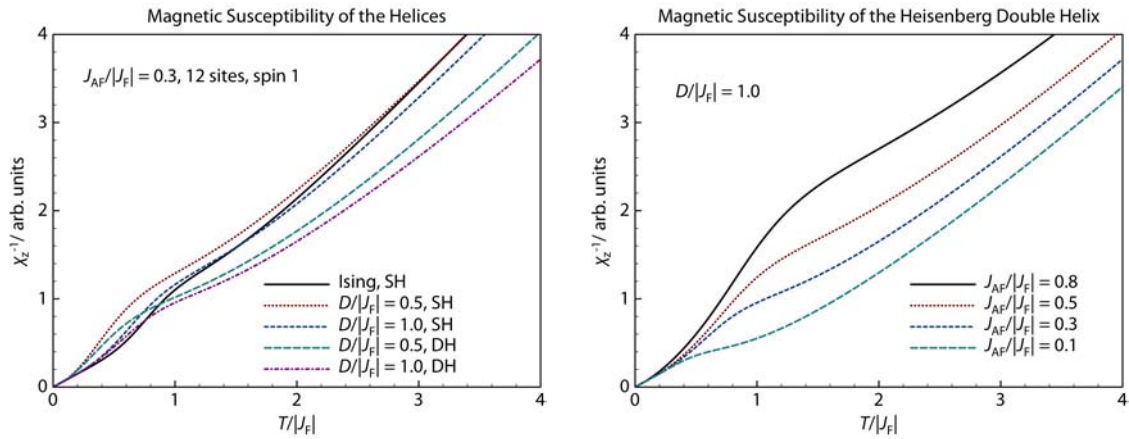


Fig. 6.14: Left panel: the picture shows the inverse magnetic susceptibility for various anisotropies including the Ising anisotropy. For the Heisenberg type Hamiltonian the SH and DH structure are compared at different anisotropies. Right Panel: the effect of a rising antiferromagnetic coupling is shown in the case of a Heisenberg Hamiltonian with intermediate anisotropy for the DH structure.

in this case. The discrepancies between spin 1 and spin 2 helices originate from the same physical properties as in the case of the single chain, namely the higher excitation energy and the higher effective magnetic moment for larger spins (compare figure 6.14, right side).

In contrast to the results for the Ising Hamiltonians, the evaluations for the Heisenberg models show a noticeable difference in the magnetic susceptibility for the SH and the DH structure. Figure 6.14 presents on the left panel the findings for the inverse susceptibility of the SH and DH configuration at different anisotropies. As in the case of the single chain, a moderate anisotropy tends to enhance the susceptibility. The DH structure shows a systematically higher susceptibility compared to the SH structure for the same D -values. A possible explanation for this behavior is provided by figure 6.12. The two structures show different mechanisms of frustration. For the SH structure on the right side of the figure the sites 1 and 4 are connected directly ferromagnetically. These two sites are on the other hand indirectly connected antiferromagnetically via the sites 2 and 3. In the DH configuration two directly ferromagnetically coupled sites, for example the sites 0 and 1, are not connected antiferromagnetically. The frustration is more complex in this case, e.g., the sites 0 and 6 are indirectly antiferromagnetically coupled via the sites 2 and 4 and are also indirectly coupled ferromagnetically via the site 1. One can expect this more indirect frustration to be weaker than the frustration in the single helix. A stronger frustration results into less pronounced ferromagnetic order, which in turn lowers the susceptibility.

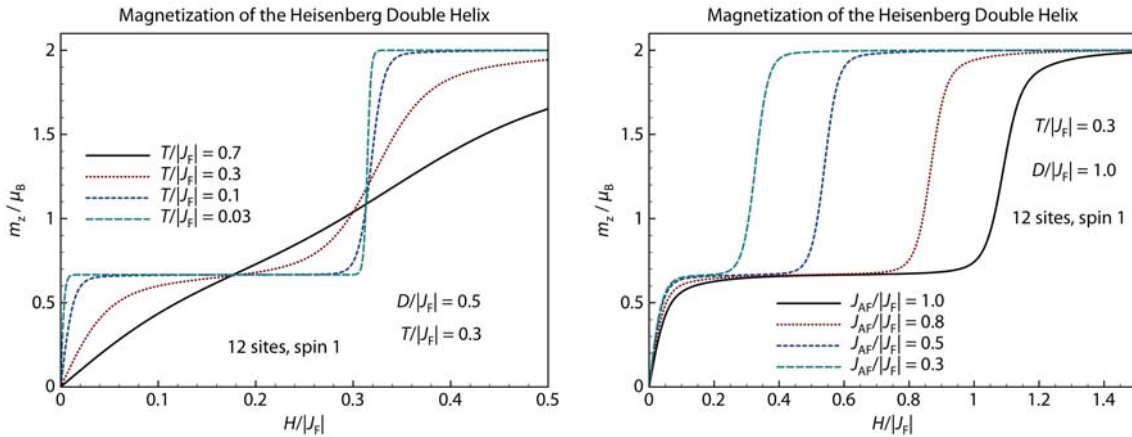


Fig. 6.15: Magnetization of the Heisenberg double helix. Left Panel: Magnetization curves for various temperatures. Right Panel: Influence of the antiferromagnetic coupling strength on the magnetization.

The magnetization of both helix structures shows steps at $\frac{1}{3}$ of the saturation magnetization (see figures 6.15 and 6.16). At temperatures well below J_F it is a sharp step that becomes less pronounced for higher temperatures. The magnetic field strength that is necessary to reach the saturation is of the order of the antiferromagnetic coupling. A simple picture that can explain these steps, for antiferromagnetic couplings weaker than the ferromagnetic coupling, is the following: the sites along the chains will order ferromagnetically at low fields and the chains as a whole will allow for the frustration by ordering antiferromagnetically, two of them up and the third down. The magnetization for this configuration is $\frac{1}{3}$ of the saturation

6 Magnetic Chains

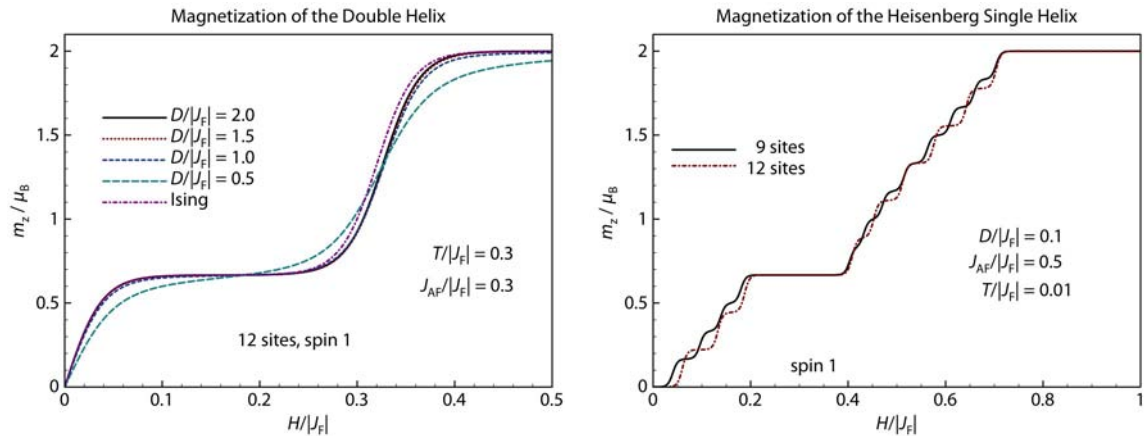


Fig. 6.16: Left Panel: the Dependence of the magnetization versus field curves on different anisotropy strengths, including the Ising anisotropy, is shown. Right Panel: at low temperatures the finite size effects become obvious in the magnetization.

magnetization. If the field is higher than J_{AF} , it can overcome the antiferromagnetic coupling energy and align all three chains. This argumentation implies some form of anisotropy as otherwise the strongly ferromagnetically coupled chains would act like a classical spin, as in the classical limit the spin can avoid frustration by gradually tilting. This is confirmed in the left panel of figure 6.16, where the magnetization step becomes more pronounced for stronger anisotropies.

By going to very low temperatures the magnetization depends more strongly on the size of the system. On the right panel of figure 6.16 the magnetization is depicted for 9 and 12 sites at a temperature of $0.01|J_F|$. The magnetization rises in 9 and 12 steps, the respective number of total S^z subspaces.

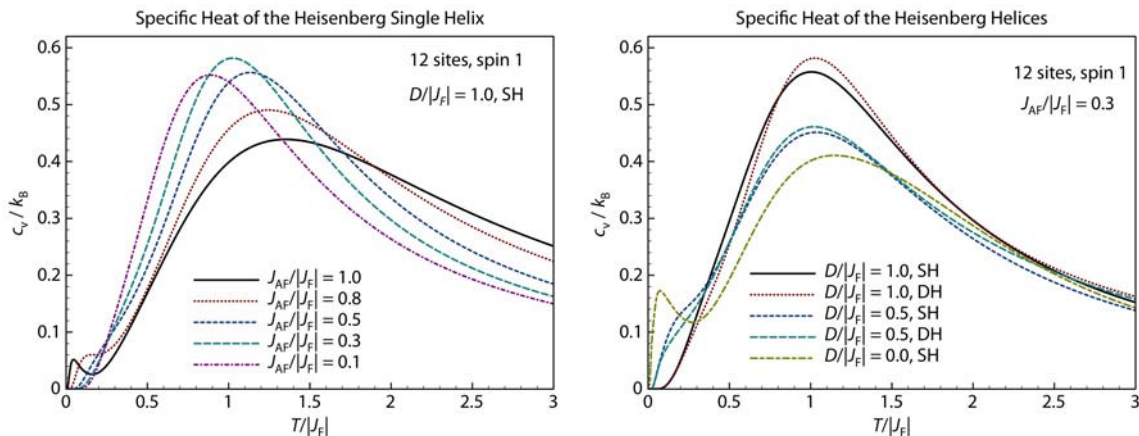


Fig. 6.17: Specific Heat of the Helices. Left Panel: the Heisenberg single helix shows a small additional feature at low temperatures and strong antiferromagnetic couplings. Right Panel: SH and DH structure curves differ slightly for various anisotropies. The additional feature becomes most pronounced for the isotropic case.

The specific heat for the Heisenberg helices shows an additional small low temperature feature due to the antiferromagnetic coupling, (see figure 6.17). For vanishing antiferromagnetic

coupling both helices evolve into three separate ferromagnetically coupled chains. Therefore the behavior for low J_{AF} is close to the case of the single chain. With rising antiferromagnetic coupling two notable changes occur: first, in the low energy regime the number of states becomes larger due to the antiferromagnetic coupling. This explains the small maximum of the specific heat at low temperatures and high antiferromagnetic coupling constants. Second, the total energy region, where energy levels occur, is broadened by the additional energy scale and therefore the main anomaly becomes less pronounced. For a fixed J_{AF} the low temperature feature gains weight for lower anisotropies, as the energy D shifts the excited states energetically away from the ground state. The difference between the SH and the DH results for the specific heat are shown in the right panel of figure 6.17. The general behavior is very similar and only slight differences are obtained.

7 Microscopic Ferromagnetic Coupling

The basis for the previous discussion of the effective magnetic models in section 6.4 was the experimentally determined magnetic interaction in $\text{Ca}_3\text{Co}_2\text{O}_6$. The magnetic moments on the Co2 atoms are coupled ferromagnetically along the chain direction and antiferromagnetically perpendicular to the chains. The resulting interplay of these two competing energy scales leads to a number of fascinating magnetic properties (a detailed discussion was given in chapter 2). However, the microscopic origin of precisely the ferromagnetic coupling remained a mystery. The common explanations for this type of effective interaction do not solve the problem, in particular because the complexity of the situation is immense. In order to gain a deeper understanding it is unavoidable to meet the challenge of the intricacy of the microscopic structure of $\text{Ca}_3\text{Co}_2\text{O}_6$.

7.1 Perturbative Treatment

In order to identify an effective coupling between next-neighbor magnetic moments, it is necessary to know the energy difference of the parallel and the anti-parallel orientation of the two magnetic moments. If the strong coupling limit is applicable, this goal can be achieved by a perturbation expansion in the hopping t . The lowest order of such an expansion that can possibly create an energy difference between singlet and triplet configurations has to correlate the two atoms that carry the magnetic moments. For $\text{Ca}_3\text{Co}_2\text{O}_6$ the first order that correlates two Co2 atoms is the fourth order. The topology of the Co – O_3 chains prohibit circular paths for even perturbation orders. To include circular paths in the discussion it is necessary to extend the discussion to the fifth order.

The principle approach is the following: the local Hamiltonians of Co1, Co2 and O are diagonalized exactly. The local description includes five d-orbitals on Co1 and Co2 and three p-orbitals on oxygen. The electron – electron interactions are taken into account via the Racah parameters A , B , and C (see Chapter 5). In addition the local Hamiltonian of Co1 and Co2 also include the spin-orbit coupling λ , and the crystal field splitting, in order to account for the observed anisotropies of the magnetic response. The largest local energy scale is A with

typical values of several electronvolt. The size of the crystal field splitting obviously varies strongly with the environment of an atom, in our case it varies between 1.3 eV on Co2 and 2.5 eV on Co1. The Racah parameters B and C are typically smaller than 1 eV. In the usually studied case C is several times larger than B . The smallest on-site energy scale is the energy scale of the spin-orbit coupling λ , for the Co atoms in $\text{Ca}_3\text{Co}_2\text{O}_6$ it is somewhere between 60 and 90 meV. The occupation of the local sites obviously changes with each hopping process. Therefore the diagonalization has to be performed in all necessary occupation subspaces for a fifth order expansion.

The total unperturbed Hamiltonian \mathbf{H}_0 is given by the sum of all local Hamiltonians, defined on the sites. \mathbf{H}_0 is diagonal in the basis of direct products of local solutions. These states are the basis for the perturbation expansion. A total of 9 atoms with 33 orbitals and 54 electrons (or 12 holes) is involved in this process. Only the conservation of the total number of electrons and the threefold symmetry of the chain can be used to reduce the size of the Hilbert space. Due to the inclusion of the spin-orbit coupling the number of up and down electrons is not conserved separately. Neither is the local total angular momentum, as the rotational invariance is broken by the crystal field splitting. Not even the z -component of the total angular momentum is a conserved quantum number, because of the hopping terms. But the latter can at least be used to classify the local and the global symmetry adapted eigenstates.

The number of states in the smallest subspace, namely the one with an occupation of six electrons on each atom, is $(210)^3 = 9\,261\,000$. The use of symmetry adapted eigenfunctions [129, 130] in order to exploit the threefold symmetry reduces the number of states by a factor of 3. Another observation can significantly lower the number of states that have to be taken into account. A fifth order process, that actually correlates the two Co2 sites never involves two intermediate-state holes on oxygen sites. This allows us to constrain the number of used occupation spaces significantly. Even then it is unavoidable to introduce an energy cut off in order to handle the Hilbert space. The presented results include 200 000 to 500 000 states. A naive implementation of the perturbation expansion would contain sums over more than $200\,000^4 = 16 \times 10^{20}$ intermediate states. With clock speeds of several GHz on modern processors this summation would still take more than 10^{10} seconds. Some care has to be taken in the implementation of the perturbation expansion in order to calculate the expansion terms as efficiently as possible [131].

The existence of a local energy scale such as λ , which is much smaller than the perturbation, additionally complicates the perturbative treatment. It lifts exact degeneracies and creates large subspaces of nearly degenerate states. The method to include nearly degenerate states in high-order perturbation theory was presented in chapter 3.

In general the problem is dominated by an overwhelming number of hopping paths. In order to treat the interference of all these paths correctly it is extremely important to take make shure that the fermionic commutation relations are treated exactly.

7.2 Determination of the Parameter Space

For an extended model calculation like the one presented in this work, the determination of the parameter space is an important task. We can differentiate two groups of parameters: first the local parameters, including the Racah parameters, the spin-orbit coupling, and the crystal field splitting. Second, the hopping parameters connecting the local orbitals of two nearest-neighbor atoms.

We obtain the hopping parameters from an approach developed by Koster and Slater [132]. This method is based on the LCAO description of molecular orbitals and uses the two-center approximation. A comprehensive discussion of the Koster-Slater hopping matrix elements and a semi-empirical extension to real systems is presented in Harrison's book [133]. The absolute value is finally adjusted by one overall constant that we take from our LDA data [64].

From the same LDA evaluation we obtain estimated values for the local orbital energies and the crystal field splittings. The LDA analysis of Eyert *et al.* is based on the augmented spherical wave method, which uses a set of basis functions that can be well interpreted in terms of local atomic wave functions. A spin-orbit coupling value of about 70 meV for $\text{Ca}_3\text{Co}_2\text{O}_6$ has been proposed by Wu *et al.* [65]. The local Racah parameters are well documented in the literature [118–122]. The solid state environment affects mainly the parameter A [119]. Therefore we will use the same values for the parameters B and C on Co1 and Co2.

7.3 Results for the Effective Coupling

Although we were able to fix most of the parameters in the problem, the parameter space is still spanned by several values: the Racah parameters A and B on the oxygen atoms (we assume them to be equal on all oxygen atoms), the Racah parameters A on Co1 and Co2 and the parameters B and C , that are both taken equal on the Co atoms. The parameter space is by our physical requirements necessarily very large, for which reason it is an extremely time consuming job to accomplish large scans over the parameter space. Therefore we concentrated on the Racah parameters A and C on the Co atoms.

Even in a physically reasonable range, the determined ground state will not adequately represent known experimental facts for a random choice of parameters. Especially if the state carries a significant magnetic moment on the Co1 site, it is not consistent with experimental findings. We will call such states “nasty” states. They are not allowed as ground states for the physical $\text{Ca}_3\text{Co}_2\text{O}_6$ system. On the other hand, states that conform with the condition of vanishing Co1 moment will be called “nice” states as they are welcome as possible ground states.

The left panel of figure 7.1 illustrates the dependence of the three lowest states on the Racah parameter A of the Co atoms. The three lowest states can be identified as a “nice” antiferromagnetic state, a “nice” ferromagnetic state and a “nasty” ferromagnetic state. At a value

7 Microscopic Ferromagnetic Coupling

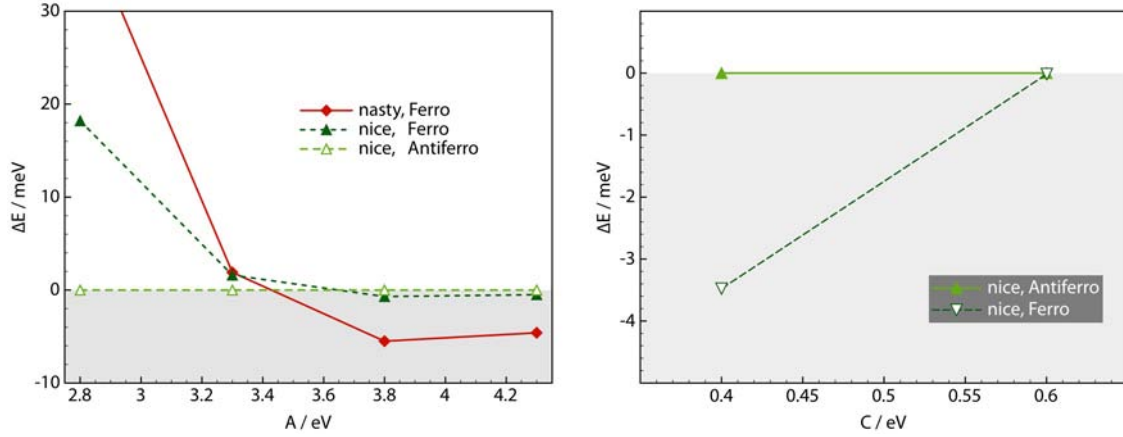


Fig. 7.1: Trend of the lowest energy states for varying Racah parameters A and C . Common parameters: $Co1, Co2$: $B = 0$ eV, $\lambda = 0.08$ eV, crystal field: $Co1: \Delta_{cf} = 2.5$ eV; $Co2: \Delta_{cf} = 1.3$ eV. Left panel: $C = 0.7$ eV; The lowest states of the hopping expansion are illustrated. Increasing values of A favor the ferromagnetic states but the “nasty” state, a state that does not have the desired property of vanishing moment on the $Co1$ site, gains more energy than the appropriate ferromagnetic state. Right panel: $A = 3.0$ eV; If the parameter C is lowered on the Co atoms the system realizes eventually the ferromagnetic ground state.

	“nice”, Ferro			“nice”, Antiferro			“nasty”, Ferro		
	$Co2_1$	$Co1$	$Co2_2$	$Co2_1$	$Co1$	$Co2_2$	$Co2_1$	$Co1$	$Co2_2$
S_z	-2	0	-2	-2	0	2	-2	-0.7	-2
L_z	-2	0	-2	-2	0	2	-2	-0.3	-2

Table 7.1: The expectation values of the z -components of local L and S on the cobalt atoms. The states are characterized by the term with the highest weight. The dominating terms of the presented states are direct products of fully polarized local $Co2$ eigenstates.

of 2.8 eV for A , the antiferromagnetic state is the ground state. Its energy is fixed at zero for all data sets in this figure. For increasing values of A , both the “nice” and the “nasty” ferromagnetic state are still excited states, but with significantly reduced excitation energies. For higher values of A the “nasty” state becomes the ground state. But even though the “nice” ferromagnetic state does not win the total competition, it outperforms the antiferromagnetic state. On the right panel of figure 7.1 the lowest states are shown for two values of the Racah C parameter on the Co atoms. In this case the ferromagnetic state becomes the real ground state of the system, hereby inducing an effective ferromagnetic coupling.

An estimate of the effect of the fourth order terms can be obtained, if we neglect the hopping paths over oxygens and neglect the e_g orbitals on $Co1$ because of the high crystal field splitting. It is then possible to rotate the remaining t_{2g} orbitals on $Co1$ in a way that only one of them has a significant overlap with the $Co2$ orbitals. With only one intermediate-state orbital on $Co1$ this scenario is very close to the superexchange of section 4.1 and should therefore create antiferromagnetic coupling. However this picture does not include the effects of the spin-orbit coupling.

At this point we identified a ferromagnetic regime in the configuration space, but the systematic analysis of the parameter space remains only at the beginning. The exact role of interfering fifth order cyclic paths has yet to be determined but there is already good evidence that these paths are able to stabilize a ferromagnetic ground state. To our knowledge $\text{Ca}_3\text{Co}_2\text{O}_6$ is the first system that realizes a ferromagnetic coupling due to cyclic exchange.

8 Summary and Outlook

This work is concerned with two important aspects of a theoretical understanding of the quasi one-dimensional compound $\text{Ca}_3\text{Co}_2\text{O}_6$. First, we developed and investigated effective magnetic models to describe the magnetic properties of $\text{Ca}_3\text{Co}_2\text{O}_6$. Second, we studied a possible theoretical explanation of the experimentally observed ferromagnetic coupling of Co2 moments along the chain.

In order to find an appropriate description for the complex magnetic structure of the compound we derived two magnetic models for a triangle of Co – O₃ chains. In one model the three chains are coupled antiferromagnetically by a single helix, that connects all sites on single line (single helix). In the other case two such helices, each connecting half of the sites antiferromagnetically are mediating the antiferromagnetic coupling between the chains (double helix). To incorporate the anisotropy in the design we investigated both an Ising Hamiltonian and an extension of the Heisenberg Hamiltonian with an on-site anisotropy term $-D(\mathbf{S}_i^z)^2$. We used diagonalized the Hamiltonians exactly to obtain the eigenenergies of the models and analyzed the magnetic susceptibility, the magnetization and the specific heat of the systems.

The analysis of the physical properties of the single helix and the double helix structure yield characteristic differences to the case of a single chain. The magnetic susceptibility showed a sizable suppression of the susceptibility at the temperatures around the antiferromagnetic coupling energy. A similar feature was reported in experimental results [19]. For temperatures below the ferromagnetic coupling energy a prominent step occurs in the magnetization curve for anisotropic single helix and double helix systems. The antiferromagnetic coupling generates an additional small peak at low temperatures for strong antiferromagnetic couplings and low anisotropies. Overall, the general behavior and the dependence on the parameters is very similar for the single helix and double helix structure. Indeed, there are virtually no differences in the case of an Ising anisotropy. The Ising anisotropy and the on-site Heisenberg anisotropy are very different in nature. The former is an anisotropy in the interaction of two spins, whereas the latter is a purely local anisotropy. Despite these conceptual differences their general effect on the investigated physical properties seems to be

comparable at intermediate strengths of the on-site anisotropy. But the differences in the details are significant even in the intermediate anisotropy range.

In order to investigate the ferromagnetic intrachain coupling we performed a Density Functional Theory calculation in a Local Density Approximation jointly with Volker Eyert [64]. This work gave us valuable insight in the local energy parameters and revealed a strong Co – O binding, which eventually led us to the extension of the superexchange scenario by cyclic exchange via the oxygen ligands. This class of spin-exchange processes is first generated in the fifth order of perturbation theory. Correspondingly, the next step was to setup a hopping expansion in order to identify the microscopic mechanisms that lead to the ferromagnetic coupling. It proved to be a much harder task than initially expected. There are two main reasons for the encountered complications. First, the structure of $\text{Ca}_3\text{Co}_2\text{O}_6$ is rather complex and the oxygen environments play obviously a crucial role [64]. Second, it is necessary to include an onsite spin-orbit coupling to account for the anisotropy of the magnetic response. From this low energy scale, large groups of nearly degenerate states emerge. The standard degenerate perturbation theory is not applicable in this case. To our knowledge such a situation is not investigated in the literature. We therefore had to develop a scheme to handle nearly degenerate states in a perturbation expansion to fourth order and above.

This scheme was adopted for the description of $\text{Ca}_3\text{Co}_2\text{O}_6$. The numerical implementation includes the full local Hubbard model with all relevant energy scales, the construction of symmetry adapted eigenstates in order to utilize the discrete rotational symmetry of the chains, the phase correct treatment of all paths up to fifth order, and the efficient accomplishment of the perturbation expansion. A first promising result of these efforts is the identification of a region in the physical configuration space that has a ferromagnetic ground state. This result suggests that, to our knowledge, $\text{Ca}_3\text{Co}_2\text{O}_6$ is the first realization of ferromagnetism that is stabilized through cyclic exchange.

With a deeper analysis of the parameter space for $\text{Ca}_3\text{Co}_2\text{O}_6$ it will be instructive to consider isostructural compounds like $\text{Ca}_3\text{FeRhO}_6$ or $\text{Ca}_3\text{CoRhO}_6$ that we already investigated by means of LDA. Despite their structural identity the magnetic response of the three differ significantly. $\text{Ca}_3\text{Co}_2\text{O}_6$ and $\text{Ca}_3\text{CoRhO}_6$ order ferromagnetically along the chains with $\text{Ca}_3\text{CoRhO}_6$ showing the higher ordering temperatures, whereas the intra-chain coupling along the chains in $\text{Ca}_3\text{FeRhO}_6$ is antiferromagnetic. The presented perturbation scheme could be of great importance to understand the different microscopic interactions in these compounds. This very same technique could also be applied to derive a more complete effective magnetic model of $\text{Ca}_3\text{Co}_2\text{O}_6$ through the investigation of the interaction paths and strengths between the chains.

The magnetic response of the single helix and the double helix structures shows anomalies with certain similarities to the experimental results. Nevertheless it is desirable to expand the models in order to overcome finite size effects. Specifically the explanation of the complex magnetic response of $\text{Ca}_3\text{Co}_2\text{O}_6$ at low temperatures and in particular the magnetization steps might demand the inclusion of more chains in the models. But this immediately

prohibits the use of exact diagonalization, due to the large system sizes needed for a comprehensive study of those systems. A more advanced technique that is possibly able to handle appropriate system sizes is the Density Matrix Renormalization Group (DMRG) method. Preliminary studies in cooperation with Peter Schmitteckert at the University of Karlsruhe confirmed the principle applicability of the method to these systems.

Finally a possible extension to the present discussion of $\text{Ca}_3\text{Co}_2\text{O}_6$ is the observation that Ca atoms can act as impurities in these systems and effectively cut the chains in shorter pieces. The finite size nature of the chain pieces of the induced disorder would add a new perspective to the understanding of $\text{Ca}_3\text{Co}_2\text{O}_6$.

“... at every title he discovered he let out exclamations of happiness, either because he knew the work, or because he had been seeking it for a long time, or finally because he had never heard it mentioned and was highly excited and titillated. In short, for him every book was like a fabulous animal that he was meeting in a strange land.”

Umberto Eco, *The Name of the Rose*

Bibliography

- [1] A. E. BRENNER, »The Computing Revolution and the Physics Community«, *Physics Today* **49** (10), 24 (1996).
- [2] H. H. GOLDSTINE, *The Computer: from Pascal to von Neumann* (Princeton University Press, 1972).
- [3] S. MCCARTNEY, *ENIAC: The Triumphs and Tragedies of the World's First Computer* (Walker and Co., New York, 1999).
- [4] J. BARDEEN and W. H. BRATTAIN, »The Transistor, A Semi-Conductor Triode«, *Physical Review* **74** (2), 230 (1948).
- [5] G. E. MOORE, »Cramming More Components onto Integrated Circuits«, *Electronic Magazin* **38** (8) (1965).
- [6] T. NOYES and W. E. DICKINSON, »The Random–Access Memory Accounting Machine«, *IBM Journal of Research and Development* **1**, 72 (1957).
- [7] J. M. HARKER, D. W. BREDE, R. E. PATTISON, G. R. SANTANA, and L. G. TAFT, »A Quater Century of Disk File Innovation«, *IBM Journal of Research and Development* **25** (5), 677 (1981).
- [8] D. A. THOMPSON and J. S. BEST, »The Future of Magnetic Data Storage Technology«, *IBM Journal of Research and Development* **44** (3), 311 (2000).
- [9] M. H. KRYDER and R. W. GUSTAFSON, »High-Density Perpendicular Recording–Advances, Issues, and Extensibility«, *Journal of Magnetism and Magnetic Materials* **287**, 449 (2005).
- [10] G. A. PRINZ, »Magnetoelectronic Applications«, *Journal of Magnetism and Magnetic Materials* **200** (1-3), 57 (1999).
- [11] T. MCGUIRE and R. POTTER, »Anisotropic Magnetoresistance in Ferromagnetic 3d Alloys«, *IEEE Transactions on Magnetics* **11** (4), 1018 (1975).
- [12] H. NAGURA, K. SAITO, K. TAKANASHI, and H. FUJIMORI, »Influence of Third Elements on the Anisotropic Magnetoresistance in Permalloy Films«,

Bibliography

- Journal of Magnetism and Magnetic Materials* **212** (1-2), 53 (2000).
- [13] M. N. BAIBICH, J. M. BROTO, A. FERT, F. N. VAN DAU, F. PETROFF, P. EITENNE, G. CREUZET, A. FRIEDERICH, and J. CHAZELAS, »Giant Magnetoresistance of (001)Fe/(001)Cr Magnetic Superlattices«, *Physical Review Letters* **61** (21), 2472 (1988).
- [14] K.-I. CHAHARA, T. OHNO, M. KASAI, and Y. KOZONO, »Magnetoresistance in Magnetic Manganese Oxide with Intrinsic Antiferromagnetic Spin Structure«, *Applied Physics Letters* **63** (14), 1990 (1993).
- [15] E. WOERMANN and A. MUAN, »Phase Equilibria in the System CaO-Cobalt Oxide in Air«, *Journal of Inorganic and Nuclear Chemistry* **32** (5), 1455 (1970).
- [16] H. FJELLVÅG, E. GULBRANDSEN, S. AASLAND, A. OLSEN, and B. C. HAUBACK, »Crystal Structure and Possible Charge Ordering in One-Dimensional $\text{Ca}_3\text{Co}_2\text{O}_6$ «, *Journal of Solid State Chemistry* **124**, 190 (1996).
- [17] S. AASLAND, H. FJELLVÅG, and H. B., »Magnetic Properties of the One-Dimensional $\text{Ca}_3\text{Co}_2\text{O}_6$ «, *Solid State Communications* **101** (3), 187 (1997).
- [18] K. E. STITZER, J. DARRIET, and H.-C. ZUR LOYE, »Advances in the Synthesis and Structural Description of 2H-Hexagonal Perovskite-Related Oxides«, *Current Opinion in Solid State and Materials Science* **5** (6), 535 (2001).
- [19] A. MAIGNAN, C. MICHEL, A. C. MASSET, C. MARTIN, and B. RAVEAU, »Single Crystal Study of the One Dimensional $\text{Ca}_3\text{Co}_2\text{O}_6$ Compound: Five Stable Configurations for the Ising Triangular Lattice«, *The European Physical Journal B* **15**, 657 (2000).
- [20] N. D. MERMIN and H. WAGNER, »Absence of Ferromagnetism or Antiferromagnetism in One- or Two-Dimensional Isotropic Heisenberg Models«, *Physical Review Letters* **17** (22), 1133 (1966).
- [21] P. BRUNO, »Absence of Spontaneous Magnetic Order at Nonzero Temperature in One- and Two-Dimensional Heisenberg and XY Systems with Long-Range Interactions«, *Physical Review Letters* **87** (13), 137203 (2001).
- [22] Y. B. KUDASOV, »Steplike Magnetization in a Spin-Chain System: $\text{Ca}_3\text{Co}_2\text{O}_6$ «, *Physical Review Letters* **96** (2), 027212 (2006).
- [23] A. MAIGNAN, V. HARDY, S. HÉBERT, M. DRILLON, M. R. LEES, O. PETRENKO, D. M. K. PAUL, and D. KHOMSKII, »Quantum Tunneling of the Magnetization in the Ising Chain Compound $\text{Ca}_3\text{Co}_2\text{O}_6$ «, *Journal of Material Chemistry* **14**, 1231 (2004).
- [24] B. BARBARA, W. WERNSDORFER, L. C. SAMPAIO, J. G. PARK, C. PAULSEN, M. A. NOVAK, R. FERRE, D. MAILLY, R. SESSOLI, and A. CANESCHI, »Mesoscopic Quantum Tunneling of the Magnetization«, *Journal of Magnetism and Magnetic Materials* **140-144** (Part 3), 1825 (1995).
- [25] J. R. FRIEDMAN, M. P. SARACHIK, J. TEJADA, and R. ZIOLO, »Macroscopic Measurement of Resonant Magnetization Tunneling in High-Spin Molecules«, *Physical Review Letters* **76** (20), 3830 (1996).

- [26] W. HEISENBERG, »Zur Theorie des Ferromagnetismus«, *Zeitschrift für Physik A* **49** (9-10), 619 (1928).
- [27] J. HUBBARD, »Electron Correlations in Narrow Energy Bands«, *Royal Society of London Proceedings Series A* **276** (1365), 238 (1963).
- [28] J. KANAMORI, »Electron Correlation and Ferromagnetism of Transition Metals«, *Progress of Theoretical Physics* **30** (3), 275 (1963).
- [29] R. STRACK and D. VOLLHARDT, »Rigorous Criteria for Ferromagnetism in Itinerant Electron Systems«, *Physical Review Letters* **72** (21), 3425 (1994).
- [30] J. WAHLE, N. BLÜMER, J. SCHLIPF, K. HELD, and D. VOLLHARDT, »Microscopic Conditions Favoring Itinerant Ferromagnetism«, *Physical Review B* **58** (19), 12749 (1998).
- [31] J. KANAMORI, »Superexchange Interaction and Symmetry Properties of Electron Orbitals«, *Journal of Physics and Chemistry of Solids* **10** (2-3), 87 (1959).
- [32] J. B. GOODENOUGH, »Theory of the Role of Covalence in the Perovskite-Type Manganites [La, M(II)]MnO₃«, *Physical Review* **100** (2), 564 (1955).
- [33] J. B. GOODENOUGH, »An Interpretation of the Magnetic Properties of the Perovskite-Type Mixed Crystals La_{1-x}Sr_xCoO_{3-λ}«, *Journal of Physics and Chemistry of Solids* **6**, 287 (1958).
- [34] A. GEORGES, G. KOTLIAR, W. KRAUTH, and M. J. ROZENBERG, »Dynamical Mean-Field Theory of Strongly Correlated Fermion Systems and the Limit of Infinite Dimensions«, *Reviews of Modern Physics* **68** (1), 13 (1996).
- [35] M. IMADA, A. FUJIMORI, and Y. TOKURA, »Metal-Insulator Transitions«, *Reviews of Modern Physics* **70** (4), 1039 (1998).
- [36] P. A. LEE, N. NAGAOSA, and X.-G. WEN, »Doping a Mott Insulator: Physics of High-Temperature Superconductivity«, *Reviews of Modern Physics* **78** (1), 17 (2006).
- [37] T. MAIER, M. JARRELL, T. PRUSCHKE, and M. H. HETTLER, »Quantum Cluster Theories«, *Reviews of Modern Physics* **77** (3), 1027 (2005).
- [38] A. SEKIYAMA, H. FUJIWARA, S. IMADA, S. SUGA, H. EISAKI, S. I. UCHIDA, K. TAKEGAHARA, H. HARIMA, Y. SAITOH, I. A. NEKRASOV, G. KELLER, D. E. KONDAKOV, A. V. KOZHEVNIKOV, T. PRUSCHKE, K. HELD, D. VOLLHARDT, and V. I. ANISIMOV, »Mutual Experimental and Theoretical Validation of Bulk Photoemission Spectra of Sr_{1-x}Ca_xVO₃«, *Physical Review Letters* **93** (15), 156402 (2004).
- [39] P. LOMBARDO, A.-M. DARE, and R. HAYN, »Effect of Hund's Exchange on the Spectral Function of a Triply Orbital Degenerate Correlated Metal«, *Physical Review B* **72** (24), 245115 (2005).
- [40] G. KOTLIAR, S. Y. SAVRASOV, K. HAULE, V. S. OUDOVENKO, O. PARCOLLET, and C. A. MARIANETTI, »Electronic Structure Calculations with Dynamical Mean-Field Theory«, *Reviews of Modern Physics* **78** (3), 865 (2006).

Bibliography

- [41] Y. TOKURA and Y. TOMIOKA, »Colossal Magnetoresistive Manganites«, *Journal of Magnetism and Magnetic Materials* **200** (1-3), 1 (1999).
- [42] B. RAQUET, M. N. BAIBICH, J. M. BROTO, H. RAKOTO, S. LAMBERT, and A. MAIGNAN, »Hopping Conductivity in One-Dimensional $\text{Ca}_3\text{Co}_2\text{O}_6$ Single Crystals«, *Physical Review B* **65** (10), 104442 (2002).
- [43] M. N. BAIBICH, J. M. BROTO, B. RAQUET, H. RAKOTO, M. COSTES, A. MAIGNAN, S. LAMBERT, and D. GREBILLE, »Electronic Conductivity in 1D Co Spin Chain Single Crystal«, *Physica B* **320** (1-4), 337 (2002).
- [44] A. MAIGNAN, S. HEBERT, C. MARTIN, and D. FLAHAUT, »One Dimensional Compounds with Large Thermoelectric Power: $\text{Ca}_3\text{Co}_2\text{O}_6$ and Ca_3CoMO_6 with $\text{M}=\text{Ir}^{4+}$ and Rh^{4+} «, *Materials Science and Engineering B* **104** (3), 121 (2003).
- [45] M. MIKAMI, R. FUNAHASHI, M. YOSHIMURA, Y. MORI, and T. SASAKI, »High-Temperature Thermoelectric Properties of Single-Crystal $\text{Ca}_3\text{Co}_2\text{O}_6$ «, *Journal of Applied Physics* **94** (10), 6579 (2003).
- [46] K. IWASAKI, H. YAMANE, S. KUBOTA, J. TAKAHASHI, and M. SHIMADA, »Power Factors of $\text{Ca}_3\text{Co}_2\text{O}_6$ and $\text{Ca}_3\text{Co}_2\text{O}_6$ -Based Solid Solutions«, *Journal of Alloys and Compounds* **358** (1-2), 210 (2003).
- [47] J. TAKAHASHI, H. YAMANE, and M. SHIMADA, »Thermoelectric Properties of $\text{Ca}_3\text{Co}_2\text{O}_6$ Single Crystal«, *Japanes Journal of Applied Physics* **43** (3a), L331 (2004).
- [48] N. V. NONG and M. OHTAKI, »Power Factors of Late Rare Earth-Doped $\text{Ca}_3\text{Co}_2\text{O}_6$ Oxides«, *Solid State Communications* **139**, 232 (2006).
- [49] J. G. BEDNORZ and K. A. MÜLLER, »Possible High T_c Superconductivity in the BaLaCuO System«, *Zeitschrift für Physik B* **64** (2), 189 (1986).
- [50] S. NIITAKA, H. KAGEYAMA, M. KATO, K. YOSHIMURA, and K. KOSUGE, »Synthesis, Crystal Structure, and Magnetic Properties of New One-Dimensional Oxides $\text{Ca}_3\text{CoRhO}_6$ and $\text{Ca}_3\text{FeRhO}_6$ «, *Journal of Solid State Chemistry* **146** (1), 137 (1999).
- [51] T. N. NGUYEN and H.-C. ZUR LOYE, »A Family of One-Dimensional Oxides: Sr_3MIR_6 ($\text{M} = \text{Ni}, \text{Cu}, \text{Zn}$): Structure and Magnetic Properties«, *Journal of Solid State Chemistry* **117** (2), 300 (1995).
- [52] H. KAGEYAMA, K. YOSHIMURA, and K. KOSUGE, »Synthesis and Magnetic Properties of New Series of One-Dimensional Oxides $\text{Ca}_3\text{Co}_{1+x}\text{B}_{1-x}\text{O}_6$ ($\text{B} = \text{Ir}, \text{Ru}$)«, *Journal of Solid State Chemistry* **140**, 14 (1998).
- [53] H. KAGEYAMA, K. YOSHIMURA, K. KOSUGE, H. MITAMURA, and T. GOTO, »Field-Induced Magnetic Transitions in the One-Dimensional Compound $\text{Ca}_3\text{Co}_2\text{O}_6$ «, *Journal of the Physical Society of Japan* **66** (6), 1607 (1997).
- [54] H. KAGEYAMA, K. YOSHIMURA, K. KOSUGE, M. AZUMA, M. TAKANO, H. MITAMURA, and T. GOTO, »Magnetic Anisotropy of $\text{Ca}_3\text{Co}_2\text{O}_6$ with Ferromagnetic Ising Chains«, *Journal of the Physical Society of Japan* **66** (12), 3996 (1997).

- [55] V. HARDY, S. LAMBERT, M. R. LEES, and D. M. PAUL, »Specific Heat and Magnetization Study on Single Crystals of the Frustrated Quasi-One-Dimensional Oxide $\text{Ca}_3\text{Co}_2\text{O}_6$ «, *Physical Review B* **68** (1), 014424 (2003).
- [56] E. V. SAMPATHKUMARAN, Z. HIROI, S. RAYAPROL, and Y. UWATOKO, »Heat-Capacity Anomalies in the Presence of High-Magnetic Fields in the Spin-Chain Compound, $\text{Ca}_3\text{Co}_2\text{O}_6$ «, *Journal of Magnetism and Magnetic Materials* **284**, L7 (2004).
- [57] X. Y. YAO, S. DONG, and J.-M. LIU, »Steplike Magnetization of Spin Chains in a Triangular Lattice: Monte Carlo Simulations«, *Physical Review B* **73** (21), 212415 (2006).
- [58] J. SUGIYAMA, H. NOZAKI, J. H. BREWER, E. J. ANSALDO, T. TAKAMI, H. IKUTA, and U. MIZUTANI, »Appearance of a Two-Dimensional Antiferromagnetic Order in Quasi-One-Dimensional Cobalt Oxides«, *Physical Review B* **72** (6), 064418 (2005).
- [59] M. M. FOGLER, S. TEBER, and B. I. SHKLOVSKII, »Variable-Range Hopping in Quasi-One-Dimensional Electron Crystals«, *Physical Review B* **69** (3), 035413 (2004).
- [60] A. L. EFROS and B. I. SHKLOVSKII, »Coulomb Gap and Low Temperature Conductivity of Disordered Systems«, *Journal of Physics C* **8** (4), L49 (1975).
- [61] S. RAYAPROL, K. SENGUPTA, and E. V. SAMPATHKUMARAN, »Magnetic Frustration in the Stoichiometric Spin-Chain Compound $\text{Ca}_3\text{CoIrO}_6$ «, *Physical Review B* **67** (18), 180404 (2003).
- [62] V. HARDY, D. FLAHAUT, M. R. LEES, and O. A. PETRENKO, »Magnetic Quantum Tunneling in $\text{Ca}_3\text{Co}_2\text{O}_6$ Studied by ac Susceptibility: Temperature and Magnetic-Field Dependence of the Spin-Relaxation Time«, *Physical Review B* **70** (21), 214439 (2004).
- [63] M.-H. WHANGBO, D. DAI, H.-J. KOO, and S. JOBIC, »Investigations of the Oxidation States and Spin Distributions in $\text{Ca}_3\text{Co}_2\text{O}_6$ and $\text{Ca}_3\text{CoRhO}_6$ by Spin-Polarized Electronic Band Structure Calculations«, *Solid State Communications* **125** (7-8), 413 (2003).
- [64] V. EYERT, C. LASCHINGER, T. KOPP, and R. FRÉSARD, »Extended Moment Formation and Magnetic Ordering in the Trigonal Chain Compound $\text{Ca}_3\text{Co}_2\text{O}_6$ «, *Chemical Physics Letters* **385**, 249 (2004).
- [65] H. WU, M. W. HAVERKORT, Z. HU, D. I. KHOMSKII, and L. H. TJENG, »Nature of Magnetism in $\text{Ca}_3\text{Co}_2\text{O}_6$ «, *Physical Review Letters* **95** (18), 186401 (2005).
- [66] R. VIDYA, P. RAVINDRAN, H. FJELLVG, A. KJEKSHUS, and O. ERIKSSON, »Tailor-Made Electronic and Magnetic Properties in One-Dimensional Pure and Y-Substituted $\text{Ca}_3\text{Co}_2\text{O}_6$ «, *Physical Review Letters* **91** (18), 186404 (2003).
- [67] E. V. SAMPATHKUMARAN, N. FUJIWARA, S. RAYAPROL, P. K. MADHU, and Y. UWATOKO, »Magnetic Behavior of Co Ions in the Exotic Spin-Chain Compound $\text{Ca}_3\text{Co}_2\text{O}_6$ from ^{59}Co NMR Studies«, *Physical Review B* **70** (1), 014437 (2004).

Bibliography

- [68] D. DAI and M.-H. WHANGBO, »Analysis of the Uniaxial Magnetic Properties of High-Spin D^6 Ions at Trigonal Prism and Linear Two-Coordinate Sites: Uniaxial Magnetic Properties of $\text{Ca}_3\text{Co}_2\text{O}_6$ and $\text{Fe}[\text{C}(\text{SiMe}_3)_3]_2$ «, *Inorganic Chemistry* **44** (12), 4407 (2005).
- [69] B. MARTINEZ, V. LAUKHIN, M. HERNANDO, J. FONTCUBERTA, M. PARRAS, and J. M. GONZALEZ-CALBET, »Enhancement of Antiferromagnetic Coupling in the Quasi-One-Dimensional $\text{Ca}_3\text{Co}_2\text{O}_6$ Ferrimagnet«, *Physical Review B* **64** (1), 012417 (2001).
- [70] M. HERNANDO, B. MARTINEZ, V. LAUKHIN, J. FONTCUBERTA, M. PARRAS, and J. M. GONZALEZ-CALBET, »Magnetic Properties and Pressure Effects in $\text{Ca}_3\text{Co}_2\text{O}_6$ Ferrimagnet«, *Journal of Magnetism and Magnetic Materials* **242-245** (Part 2), 757 (2002).
- [71] T. GOKO, N. NOMURA, S. TAKESHITA, and J. ARAI, »Pressure Effect on Magnetic Transitions in One-Dimensional $\text{Ca}_3\text{Co}_2\text{O}_6$ «, *Journal of Magnetism and Magnetic Materials* **272** (2004).
- [72] C. MARTIN, private communication.
- [73] T. SEKIMOTO, S. NOGUCHI, and T. ISHIDA, »Electron Doping Effect on the Magnetic and Electric Properties of $\text{Ca}_{3-x}\text{Y}_x\text{Co}_2\text{O}_6$ «, *Journal of the Physical Society of Japan* **73** (11), 3217 (2004).
- [74] V. G. ZUBKOV, G. V. BAZUEV, A. P. TYUTYUNNIK, and I. F. BERGER, »Synthesis, Crystal Structure, and Magnetic Properties of Quasi-One-Dimensional Oxides $\text{Ca}_3\text{CuMnO}_6$ and $\text{Ca}_3\text{Co}_{1+x}\text{Mn}_{1-x}\text{O}_6$ «, *Journal of Solid State Chemistry* **160** (2), 293 (2001).
- [75] S. RAYAPROL, K. SENGUPTA, and E. V. SAMPATHKUMARAN, »Magnetic Behaviour of Quasi-One-Dimensional Oxides, $\text{Ca}_3\text{Co}_{1+x}\text{Mn}_{1-x}\text{O}_6$ «, *Solid State Communications* **128**, 79 (2003).
- [76] D. FLAHAUT, A. MAIGNAN, S. HÉBERT, C. MARTIN, R. RETOUX, and V. HARDY, »Chromium Site Selective Substitution in $\text{Ca}_3\text{Co}_2\text{O}_6$: Influence on the Magnetic Properties of an Ising-like Triangular Lattice«, *Physical Review B* **70**, 094418 (2004).
- [77] H. KAGEYAMA, S. KAWASAKI, K. MIBU, M. TAKANO, K. YOSHIMURA, and K. KOSUGE, »Mössbauer Observation of the Quantum Levels of Fe^{3+} Ions Doped in 1D Ising Ferromagnet $\text{Ca}_3\text{Co}_2\text{O}_6$ «, *Physical Review Letters* **79** (17), 3258 (1997).
- [78] J. ARAI, H. SHINMEND, S. TAKESHITA, and T. GOKO, »Mössbauer Study of Impurity Effect on Ferrimagnet $\text{Ca}_3\text{Co}_2\text{O}_6$ with 1-D Ferromagnetic Chains«, *Journal of Magnetism and Magnetic Materials* **272-276**, 809 (2004).
- [79] A. MAIGNAN, private communication.
- [80] J. K. H. ISHII and T. NAKAMURA, »Localized Spin Waves in Ferromagnets with an Antiferromagnetic Impurity«, *Progress of Theoretical Physics* **33** (5), 795 (1965).

- [81] S. NIITAKA, H. KAGEYAMA, K. YOSHIMURA, K. KOSUGE, S. KAWANO, N. ASO, A. MITSUDA, H. MITAMURA, and T. GOTO, »High-Field Magnetization and Neutron Diffraction Studies of One-Dimensional Compound $\text{Ca}_3\text{CoRhO}_6$ «, *Journal of the Physical Society of Japan* **70** (5), 1222 (2001).
- [82] S. NIITAKA, K. YOSHIMURA, K. KOSUGE, A. MITSUDA, H. MITAMURA, and T. GOTO, »Pulsed High Field Study of New Partially Disordered Antiferromagnetic Phase in $\text{Ca}_3\text{CoRhO}_6$ «, *Journal of Physics and Chemistry of Solids* **63**, 999 (2002).
- [83] K. E. STITZER, W. H. HENLEY, C. J. B., H.-C. ZUR LOYE, and R. C. LAYLAND, » $\text{Sr}_3\text{NiRhO}_6$ and $\text{Sr}_3\text{CuRhO}_6$ – Two New One-Dimensional Oxides. Magnetic Behaviour as a Function of Structure: Commensurate vs Incommensurate«, *Journal of Solid State Chemistry* **164**, 220 (2002).
- [84] M. J. DAVIS, M. D. SMITH, and H.-C. ZUR LOYE, »Crystal Growth, Structural Characterization and Magnetic Properties of $\text{Ca}_3\text{CoRhO}_6$, $\text{Ca}_3\text{Co}_{1.34}\text{Rh}_{0.66}\text{O}_6$ and $\text{Ca}_3\text{FeRhO}_6$ «, *Journal of Solid State Chemistry* **173**, 122 (2003).
- [85] S. NIITAKA, K. YOSHIMURA, K. KOSUGE, K. MIBU, H. MITAMURA, and T. GOTO, »Magnetic and ^{57}Fe Mossbauer Studies of $\text{Ca}_3\text{FeRhO}_6$ «, *Journal of Magnetism and Magnetic Materials* **260** (1-2), 48 (2003).
- [86] E. V. SAMPATHKUMARAN and A. NIAZI, »Superparamagnetic-Like ac Susceptibility Behavior in the Partially Disordered Antiferromagnetic Compound $\text{Ca}_3\text{CoRhO}_6$ «, *Physical Review B* **65** (18), 180401 (2002).
- [87] M. COSTES, J. M. BROTO, B. RAQUET, H. RAKOTO, M. A. NOVAK, J. P. SINNECKER, S. SORIANO, W. S. D. FOLLY, A. MAIGNAN, and V. HARDY, »Dynamic Effects in One-Dimensional A_3ABO_6 «, *Journal of Magnetism and Magnetic Materials* **294** (2), e123 (2005).
- [88] V. HARDY, C. MARTIN, G. MARTINET, and G. ANDRE, »Magnetism of the Geometrically Frustrated Spin-Chain Compound $\text{Sr}_3\text{HoCrO}_6$: Magnetic and Heat Capacity Measurements and Neutron Powder Diffraction«, *Physical Review B* **74** (6), 064413 (2006).
- [89] V. EYERT, U. SCHWINGENSCHLÖGL, C. HACKENBERGER, T. KOPP, R. FRÉSARD, and U. ECKERN, »Magnetic Ordering in Trigonal Chain Compounds«, *Progress of Solid State Chemistry* **35** (2007).
- [90] S. NIITAKA, K. YOSHIMURA, K. KOSUGE, M. NISHI, and K. KAKURAI, »Partially Disordered Antiferromagnetic Phase in $\text{Ca}_3\text{CoRhO}_6$ «, *Physical Review Letters* **87** (17), 177202 (2001).
- [91] J. AN and C.-W. NAN, »Electronic Structure and Transport of $\text{Ca}_3\text{Co}_2\text{O}_6$ and $\text{Ca}_3\text{CoNiO}_6$ «, *Solid State Communications* **129**, 51 (2004).
- [92] J. P. PERDEW and A. ZUNGER, »Self-Interaction Correction to Density-Functional Approximations for Many-Electron Systems to Density-Functional Approximations for Many-Electron Systems«, *Physical Review B* **23** (10), 5048 (1981).

Bibliography

- [93] V. EYERT, K.-H. HÖCK, and P. S. RISEBOROUGH, »The Electronic Structure of $\text{La}_2\text{BaCuO}_5$: A Magnetic Insulator«, *Europhysics Letters* **31**, 385 (1995).
- [94] R. WEHT and W. E. PICKETT, »Extended Moment Formation and Second Neighbor Coupling in Li_2CuO_2 «, *Physical Review Letters* **81** (12), 2502 (1998).
- [95] G. H. WANNIER, »Antiferromagnetism. The Triangular Ising Net«, *Physical Review* **79** (2), 357 (1950).
- [96] M. S., »Magnetic Properties of Ising-Like Heisenberg Antiferromagnets on the Triangular Lattice«, *Journal of the Physical Society of Japan* **55** (10), 3605 (1986).
- [97] M. N. LEUENBERGER and D. LOSS, »Spin Tunneling and Phonon-Assisted Relaxation in Mn_{12} -Acetate«, *Physical Review B* **61** (2), 1286 (2000).
- [98] T. LIS, »Preparation, Structure, and Magnetic Properties of a Dodecanuclear Mixed-Valence Manganese Carboxylate«, *Acta Crystallographica Section B* **36** (9), 2042 (1980).
- [99] W. NOLTING, *Grundkurs Theoretische Physik 7: Viel-Teilchen-Theorie*, Springer-Lehrbuch (Spinger-Verlag, 2002), 5th edition.
- [100] J. H. VAN VLECK, »A Survey of the Theory of Ferromagnetism«, *Reviews of Modern Physics* **17** (1), 27 (1945).
- [101] P. W. ANDERSON, »Antiferromagnetism. Theory of Superexchange Interaction«, *Physical Review* **79** (2), 350 (1950).
- [102] J. YAMASHITA and J. KONDO, »Superexchange Interaction«, *Physical Review* **109** (3), 730 (1958).
- [103] P. W. ANDERSON, »New Approach to the Theory of Superexchange Interactions«, *Physical Review* **115** (1) (1959).
- [104] H. ESKES and J. H. JEFFERSON, »Superexchange in the Cuprates«, *Physical Review B* **48** (13), 48 (1993).
- [105] S. FELDKEMPER, W. WEBER, J. SCHULENBURG, and J. RICHTER, »Ferromagnetic Coupling in Nonmetallic Cu^{2+} Compounds«, *Physical Review B* **52** (1), 313 (1995).
- [106] T. HOTTA and E. DAGOTTO, »Orbital Ordering, New Phases, and Stripe Formation in Doped Layered Nickelates«, *Physical Review Letters* **92** (22), 227201 (2004).
- [107] A. M. O. . RAYMOND FRÉSARD, MARCIN RACZKOWSKI, »Interplay of Orbitally Polarized and Magnetically Ordered Phases in Doped Transition Metal Oxides«, *Physica Status Solidi B* **242** (2), 370 (2005).
- [108] M. RACZKOWSKI, R. FRÉSARD, and A. M. OLEŚ, »Magnetic and Orbital Correlations in a Two-Site Molecule«, *Journal of Physics: Condensed Matter* **18** (31), 7449 (2006).
- [109] H. TASAKI, »Ferromagnetism in Hubbard Models«, *Physical Review Letters* **75** (25), 4678 (1995).

- [110] H. TASAKI, »The Hubbard Model - An Introduction and Selected Rigorous Results«, *Journal of Physics* **10** (20), 4353 (1998).
- [111] K. PENC, H. SHIBA, F. MILA, and T. TSUKAGOSHI, »Ferromagnetism in Multiband Hubbard Models: From Weak to Strong Coulomb Repulsion«, *Physical Review B* **54** (6), 4056 (1996).
- [112] H. TASAKI, »Ferromagnetism in the Hubbard Models with Degenerate Single-Electron Ground States«, *Physical Review Letters* **69** (10), 1608 (1992).
- [113] A. MIELKE, »Ferromagnetism in the Hubbard Model and Hund's Rule«, *Physics Letters A* **174** (5-6), 443 (1993).
- [114] S. FELDKEMPER and W. WEBER, »Generalized Calculation of Magnetic Coupling Constants for Mott-Hubbard Insulators: Application to Ferromagnetic Cr Compounds«, *Physical Review B* **57** (13), 7755 (1998).
- [115] P. FASZEKAS, *Lecture Notes on Electron Correlation and Magnetism*, volume 5 of *Series in Modern Condensed Matter Physics* (World Scientific Publishing, 1999).
- [116] G. RACAH, »Theory of Complex Spectra. II«, *Physical Review* **62** (9-10), 438 (1942).
- [117] G. RACAH, »Theory of Complex Spectra. I«, *Physical Review* **61** (3-4), 186 (1942).
- [118] J. VAN ELP, J. L. WIELAND, H. ESKES, P. KUIPER, G. A. SAWATZKY, DE F. M. F. GROOT, and T. S. TURNER, »Electronic Structure of CoO, Li-doped CoO, and LiCoO₂«, *Physical Review B* **44** (12), 6090 (1991).
- [119] M. ABBATE, R. POTZE, G. A. SAWATZKY, and A. FUJIMORI, »Band-Structure and Cluster-Model Calculations of LaCoO₃ in the Low-Spin Phase«, *Physical Review B* **49** (11), 7210 (1994).
- [120] A. TANAKA and T. JO, »Resonant 3d, 3p and 3s Photoemission in Transition Metal Oxides Predicted at 2p Threshold«, *Journal of the Physical Society of Japan* **63** (7), 2788 (1994).
- [121] T. SAITOH, A. E. BOCQUET, T. MIZOKAWA, and A. FUJIMORI, »Systematic Variation of the Electronic Structure of 3d Transition-Metal Compounds«, *Physical Review B* **52** (11), 7934 (1995).
- [122] S. SUGANO, Y. TANABE, and H. KAMIMURA, *Multiplets of Transition-Metal Ions in Crystals* (Academic, New York, 1970).
- [123] E. ISING, »The Theory of Ferromagnetism«, *Zeitschrift für Physik* **31**, 253 (1925).
- [124] G. F. NEWELL and E. W. MONTROLL, »On the Theory of the Ising Model of Ferromagnetism«, *Reviews of Modern Physics* **25** (2), 353 (1953).
- [125] W. NOLTING, *Grundkurs Theoretische Physik 6: Statistische Physik*, Springer-Lehrbuch (Springer-Verlag, 2002), 4th edition.
- [126] H. BETHE, »Zur Theorie der Metalle«, *Zeitschrift für Physik A* **V71** (3), 205 (1931).

- [127] M. KARBACH and G. MÜLLER, »Introduction to the Bethe Ansatz I«, *Computers in Physics* **11**, 36 (1997).
- [128] M. KARBACH, K. HU, and G. MÜLLER, »Introduction to the Bethe Ansatz II«, *Computers in Physics* **12**, 565 (1998).
- [129] W. LUDWIG and C. FALTER, *Symmetries in Physics*, volume 64 of *Springer Series in Solid-State Sciences* (Springer-Verlag, 1996).
- [130] R. L. CARTER, *Molecular Symmetry and Group Theory* (John Wiley & Sons, Inc., 1998).
- [131] R. CHANDRA, L. DAGUM, D. KOHR, D. MAYDAN, J. McDONALD, and R. MENON, *Parallel Programming in OpenMP* (Morgan Kaufmann Publishers, 2001).
- [132] J. C. SLATER and G. F. KOSTER, »Simplified LCAO Method for the Periodic Potential Problem«, *Physical Review* **94** (6), 1498 (1954).
- [133] W. A. HARRISON, *Electronic Structure and the Properties of Solids – The Physics of the Chemical Bond* (Dover Publications, Inc., New York, 1989).

Lebenslauf

<i>Zur Person</i>	Name	Christian Hackenberger geb. Laschinger
	Geburtstag	6. September 1974
	Familienstand	verheiratet, 1 Kind
<i>Schulbildung</i>	9/1986 – 7/1990	Realschule Pfarrkirchen
	9/1990 – 7/1992	Fachoberschule Pfarrkirchen
	7/1992	Abschluß: Fachhochschulreife
<i>Studium</i>	11/1992 – 7/1993	Studium Physikalische Technik an der Fachhochschule München
	7/1993	Abschluß: Fachgebundene Hochschulreife
<i>Zivildienst</i>	8/1993 – 10/1994	Rotes Kreuz Pfarrkirchen
<i>Studium</i>	11/1994 – 7/2001	Studium Allgemeine Physik an der Technischen Universität München
	7/2001	Vorlage Diplomarbeit mit dem Thema: <i>“Theoretische und Experimentelle Untersuchungen zu den Grenzen des Auflösungsvermögens der Rasterkraftmikroskopie”</i>
	7/2001	Abschluß: Diplom-Physiker (Univ.)
<i>Promotion</i>	seit 7/2001	Wissenschaftlicher Angestellter und Promotion am Lehrstuhl für Experimentalphysik VI der Universität Augsburg
92	12/2006	Abschluß: Dr. rer. nat.